EFFECT OF ACTIVE PHASES IN PDMS-BASED COMPOSITE FOR PIEZOELECTRIC NANOGENARATOR

KANJANA MALIWAL

WASANA KRAJANGCHANG

A SPECIAL PROJECT SUBMITTED IN PARTIAL FULFILLMENT OF

THE REQUIREMENT FOR

THE DEGREE OF BACHELOR OF SCIENCE (INDUSTRIAL CHEMISTRY)

DEPARTMENT OF CHEMISTRY, FACULTY OF SCIENCE

KING MONGKUT'S INSTITUTE OF TECHNOLOGY LADKRABANG

ACADEMIC YEAR 2018

Title	Effect of active phases in PDMS-based composite for piezoelectric nanogenerator
Students	Miss Kanjana Maliwal Student ID 58050440
	Miss Wasana Krajangchang Student ID 58050542
Degree	Bachelor of Science (Industrial Chemistry)
Department	Chemistry
Year	2018
Advisor	Assoc. Prof. Naratip Vittayakorn

Faculty of science, King Mongkut's Institute of technology Ladkrabang, has approved this special project submitted in partial fulfillment of the requirement for the degree of Master of Science in academic year 2018.

Committee	Signatures
Asst. Prof. Dr. Panpailin Seeharaj (Committee, Chairperson)	
Dr. Chaval Sriwong (Committee)	
Assoc. Prof. Dr. Naratip Vittayakorn (Adviser)	

Title	Effect of active phases in PDMS-based composite for piezoelectric nanogenerator
Students	Miss Kanjana Maliwal Student ID 58050440
	Miss Wasana Krajangchang Student ID 58050542
Degree	Bachelor of Science (Industrial Chemistry)
Department	Chemistry
Faculty	Science
University	King Mongkut's Institute of Technology Ladkrabang (KMITL)
Academic Year	2018
Advisor	Assoc. Prof. Naratip Vittayakorn

ABSTRACT

This work focus on the effect of active phases on the electrical output performance of flexible piezo-composite. The composite consisted of PDMS, and piezoelectric active phase was fabricated in this work by casting method. The Polydimethylsiloxane (PDMS) is used as a matrix phase, and an active phase is a piezoelectric compound. The impact of morphology and different type of piezoelectric compounds were considered in this work. Several piezoelectric compounds such as $BaTiO_3$, Hydroxyapatite, $NaNbO_3$, and ZnO were used as a piezoelectric phase. A plate-like $NaNbO_3$ particle was synthesized successfully by topochemical microcrystal conversion. Flower-like hydroxyapatite ($Ca_5(PO_3)_4(OH)$; flower-like HA and coral-like hydroxyapatite ($Ca_5(PO_3)_4(OH)$; Coral-like HA) were synthesized by hydrothermal and microwave irradiation method respectively. The XRD, FI-TR, and Raman are the basic techniques to characterize the crystal structure and confirm the purity phase of the synthetic compound. The active phase was deposited on the surface of the PDMS, and the thickness of the active layer was varied by the curing time.

The results show that the thickness of the active oxide layer decreased with increasing the curing time. The width of the active oxide layer can be controlled by

curing time and morphology of the active phase. Our fabricated composite exhibited flexible, stretchable, and deformable. The composite with different piezoelectric active oxide powders provide a varying of the electrical output performance, which is related to the amount of the active filler on the PDMS surface. The composite with the most top thickness performs the highest output performance. And the BT/PDMS composite exhibits the highest output performance when compared with the others active phase. Besides, the effect of different particle shapes with different electrical outputs as well. Coral-like HA/PDMS composite provide higher voltage/current output than flower-like HA/PDMS composite.

Keywords: Piezoelectric, nanogenerator, PDMS, flexible composite

ACKNOWLEDGEMENT

This special project has been successfully completed. Due to kindness and the cooperation of everyone, which the researcher must thank here.

Firstly, we would like to thank our thesis consultant, Assoc. Prof. Dr. Naratip Vittayakorn, for the topic assigned to our group as well as waiting for close supervision, provide good advice to improve problems, helping to check this special project thesis to be more complete and accurate in special projects. And honor is a special project professor consultant, so thank you very much here.

We would like to thank the special project consultant, Post. Dr. Thitirat Charoonsuk, to provide knowledge and practice about the project and suggestion and helping to check this special project thesis to be more complete and accurate.

We would like to thank the special project consultant, Post. Dr. Saichon Sriphan to provide knowledge and practice about measure electrical output and suggestion and helping to check this special project thesis to be more complete and accurate.

We would like to thank our supervisory committee members, Asst. Prof. Dr. Panpailin Seeharaj and Dr. Chaval Sriwong, for their questions and recommend during the test.

We would like to thank the professor of chemistry, Faculty of Science, King Mongkut's Institute of Technology Ladkrabang, All of you who help to improve the knowledge of the subject and consultation.

We are thankful to the chemical laboratory staff, administrative staff of the department of chemistry and staff of the instrumental science center for help and convenient in the field of chemical equipment and tools for accomplishing special projects.

We are thankful to all graduate and doctoral students in advance materials research to help this special project until making this special project successful.

Finally, we are grateful to our family that provides educational opportunities as well as training and as a force to complete this special project successfully and including our friends and other people not mentioned the project preparer would like to thank you very much for their support.

Kanjana Maliwal

Wasana Krajangchang

TABLE OF CONTENTS

TABLE OF CONTENTS

(Continued)

TABLE OF CONTENTS

(Continued)

TABLE OF CONTENTS

(Continued)

TABLE OF CONTENTS

(Continued)

TABLE OF CONTENTS

(Continued)

LIST OF TABLES

Table No. **Page**

LIST OF FIGURES

Figure No. **Page**

LIST OF FIGURES

(Continued)

Figure No. **Page**

LIST OF FIGURES

(Continued)

Figure No. **Page**

LIST OF FIGURES

(Continued)

Figure No. **Page**

LIST OF FIGURES

(Continued)

LIST OF FIGURES

(Continued)

Figure No. **Page**

LIST OF FIGURES

(Continued)

Figure No. **Page**

LIST OF FIGURES

(Continued)

Figure No. **Page**

ABBREVIATIONS/SYMBOLS

Abbreviations/Symbols	Explanation
BT	Barium titanate
HA	Hydroxyapatite
NN	Sosium niobate
ZnO	Zinc oxide
PDMS	Polydimethylsiloxane
XRD	X-ray Diffraction
FT-IR	Fourier Transform Infrared Spectroscopy
SEM	Scanning Electron Microscope
μA	Micro ampere
hr.	Hour
M	Molar

CHAPTER 1

INTRODUCTION

1.1 Overview

Piezoelectric nanogenerators transform mechanical energy into electrical energy. They use mechanical force to change asymmetric unit cells to alter the electric dipole in piezoelectric materials. Mechanical energy can be easily found from human daily routines such as walking, finger typing, even blood flow. It provides relatively small energy. Previously, it was not common. However, in the future, many scholars believe that small electrical devices will reduce energy use. Now, mechanical energy may be appropriate for use. Small electrical devices need nanogenerators to drive them, are not wasteful and able to generate electrical energy for continuous use in electrical equipment [1].

Piezoelectric energy harvesting techniques were reported by 2006 by Zhong and Song, who studied the piezoelectric properties of zinc oxide (ZnO) [2]. Lead Zirconate Titanate (PZT) was discovered which very effective piezoelectric material [3] is. However, PZT contains lead [3] and is not accepted by many countries and banned in waste from electrical and electronic equipment which restricts certain hazardous substances (RoHS) directive [4, 5]. Therefore, other piezoelectric materials were developed to replace PZT, such as barium titanate (BT), although it does not provide as high output electrical power as PZT, but it has a high dielectric constant and no hazardous components. There are many researchers seeing the importance of different crystal structure characteristics, that effect to the electrical output of the piezoelectric materials such as BT nanoparticles and BT nanowire [6-10]. Sodium niobate and hydroxyapatite are other materials that have piezoelectric properties. However, no researcher has yet fabricated it as a nanogenerator [11, 12]. Importantly, material flexibility and durability are necessary for actual use, because the input is a mechanical force. Most piezoelectric powders are mixed with polymers, such as polydimethylsiloxane (PDMS), for increased flexibility and durability [13]. However, the mixing abovementioned is a common technique. No research has yet fabricated

the piezoelectric nanocomposite by dispersing of oxide powders on PDMS that may be increase surface charge of them [14, 15].

We propose to prepare piezoelectric nanocomposite materials between PDMS and oxide powders dispersive on PDMS, including pure plate-like sodium niobate nanostructures (NN), pure flower-like hydroxyapatite nanostructures (flower-like HA), pure coral-like hydroxyapatite nanostructure (coral-like HA), Barium titanate nanoparticles (BT) and Zinc oxide nanoparticles (ZnO) [16-17]. Nontoxic NN, flower-like HA, and coral-like HA will be synthesized first. The appropriate ratio of them to PDMS will be determined by dispersing it on setting PDMS over various times, from 3 to 5 hours. Then the voltage and current output of each type will be measured by the compression machine.

1.2 Objectives of this work

1.2.1 To study the synthesis of pure plate-like sodium niobate nanostructures (NN) from molten salt, pure flower-like hydroxyapatite nanostructures (flower-like HA) via hydrothermal method and pure coral-like hydroxyapatite nanostructure (coral-like HA) via microwave irradiation.

1.2.2 To study the dispersion of four types of oxide powders on top of PDMS and measure output voltages and currents as a piezoelectric nanogenerator. The systems will include:

1.2.2.1 $BaTiO_3$ / PDMS

1.2.2.2 ZnO / PDMS

1.2.2.3 NN / PDMS

1.2.2.4 Flower-like HA / PDMS

1.2.2.5 Coral-like HA / PDMS

1.2.3 To study the influence of curing time on these systems.

1.3 Research scopes

1.3.1 Characterization the systems synthesized in section 1.2.2.1-1.2.2.5 with

1.3.1.1 X-ray powder diffraction (XRD) analysis.

1.3.1.2 Fourier transform infrared spectroscopy (FTIR) analysis.

1.3.1.3 Scanning electron microscope (SEM) analysis.

1.3.2 Assessment the effect of curing times.

1.4 Expected benefits

1.4.1 Understanding the synthesis of NN, flower-like HA and coral-like HA.

1.4.2 Understanding the influence of different types of their curing times on PDMS substrates on output voltage and current as piezoelectric nanogenerators.

1.4.3 Understanding the influence of different types of oxide powders on PDMS substrates on output voltage and current as piezoelectric nanogenerators.

1.5 REFERENCES

[1] Wang, X. (2012). "Piezoelectric nanogenerators-harvesting ambient mechanical energy at the nanometer scale." Nano Energy 1(1): 13-24.

[2] Zhong Lin Wang and J Song. (2006). Piezoelectric Nanogenerators Based on Zinc Oxide Nanowire Arrays. Science, American Association for the Advancement of Science, Apr 14; 312, 242-6.

[3] Kozielski, A.Lisińska-Czekaj and D.Czekaj. (2007). "Graded PZT ceramics for piezoelectric transformers." Progress in Solid State Chemistry 35(2): 521-530.

[4] Toffolet, R. (2016). Chapter 1 - WEEE Management. WEEE Recycling. A. Chagnes, G. Cote, C. Ekberg, M. Nilsson and T. Retegan, Elsevier: 1-30.

[5] Stewart, R. (2012). 2 - EU legislation relating to electronic waste: the WEEE and RoHS Directives and the REACH regulations. Waste Electrical and Electronic Equipment (WEEE) Handbook. V. Goodship and A. Stevels, Woodhead Publishing: 17-52.

[6] Choi, H. Y. and Y. G. Jeong (2019). "Microstructures and piezoelectric performance of eco-friendly composite films based on nanocellulose and barium titanate nanoparticle." Composites Part B: Engineering 168: 58-65.

[7] Zhang, M., Tao Gao, Jian Shu Wang and Jian Jun Liao (2015). "Single $BaTiO_3$ nanowires-polymer fiber based nanogenerator." Nano Energy 11: 510-517.

[8] Rahman, W., Wahida Rahman, Samiran Garain, Ayesha Sultana, Tapas Ranjan Middya and Dipankar Mandal.(2018). "Self-Powered Piezoelectric Nanogenerator Based on Wurtzite ZnO Nanoparticles for Energy Harvesting Application." Materials Today: Proceedings 5(3, Part 3): 9826-9830.

[9] Jiao, H., Hua Jiao,Kang Zhao, Lining Ma, Tierong Bian, Yongmei Ma and Yufei Tang. (2018). "Preparation, electrical property and periodic DFT calculation of barium titanate/hydroxyapatite rod-like nanocomposite materials." Materials Science and Engineering: B 229: 184-192.

[10] Rodriguez, R., Rogelio Rodriguez, Domingo Rangel, Gerardo Fonseca, Maykel Gonzalez and Susana Vargas (2016). "Piezoelectric properties of synthetic hydroxyapatite-based organic-inorganic hydrated materials." Results in Physics 6: 925-932.

[11] Wang, Y., Yuan Yu Wang, Qilong Zhang, Liang Hu, Enjie Yu and Hui Yang. (2016). "Synthesis of alkalis niobate nanorods and their enhanced piezoelectric properties." Journal of Alloys and Compounds 685: 1-7.

[12] Su, X., Xinghua Su, Ge Bai, Yongjie Jia, Zhenjun Wang, Yuwei Hu, Xin Yan and Jing Xie. (2019). "Flash sintering of sodium niobate ceramics." Materials Letters 235: 15-18.

[13] Owen, M. J. (2001). Elastomers: Siloxane. Encyclopedia of Materials: Science and Technology.
[14] Yan, J., Jing Yan, Min Liu, Young Gyu Jeong, Weimin Kang, Lan Li, Yixia Zhao, Nanping Deng, Bowen Cheng and Guang Yang. (2019). "Performance enhancements in poly (vinylidene fluoride)-based piezoelectric nanogenerators for efficient energy harvesting." Nano Energy 56: 662-692.
[15] Ji, J., Minghao Gu, Jun Zhang, Xiaolin Wang, Haijun Tao and Litian Ge. (2015). "Poly (vinylidene fluoride) (PVDF) membranes for fluid separation." Reactive and Functional Polymers 86: 134-153.
[16] Chang, Y., Yunfei Chang, Zupei Yang, Xiaolian Chao, Zonghuai Liu and Zenglin Wang. (2008). "Synthesis and morphology of anisotropic $NaNbO_3$ seed crystals." Materials Chemistry and Physics 111(2): 195-200.
[17] Kumar, G. S., G. Suresh Kumar, A.Thamizhavel and E.K.Girija. (2012). "Microwave conversion of eggshells into flower-like hydroxyapatite nanostructure for biomedical applications." Materials Letters 76: 198-200.

CHAPTER 2

BACKGROUND INFORMATION AND LITERATURE REVIEW

2.1 Composites

A composite can be defined as a combination of two or more materials in macroscopic scale that results in preferable properties than those of the individual components used alone [1]. A composite material has two main components, which are a reinforcing phase and matrix phases. The schematic diagram of the composite is shown in Figure 2.1. A reinforcing phase can be used in the form of particles, sheet laminate, short fibers or continuous fibers. A particulate composite in all directions have approximately equal particle size, rigid and inexpensive. And another important component in composite is a matrix phase that acts as the main phase and a phase for distribution. The matrix (continuous phase) performs numerous important functions, including maintaining the distance and proper direction of the fiber, also protects them from the environment and scratches [2]. In most instances, the reinforcement phase is stronger, harder, and stiffer than the matrix phase [1].

The properties of composite materials are depended on the phase distribution and the ratio of material. Therefore, it can be improved from mixing of substrate materials with different in chemical compositions or structure distributed within a continuous phase. For the properties of composite materials such as strength, stiffness, fatigue, corrosion resistance, wear resistance, temperature dependent behavior, thermal conductivity or insulation, electrical conductivity, acoustic insulation, vibration damping, weight, self-healing, fracture toughness, health monitoring, shape morphing, etc. [3].

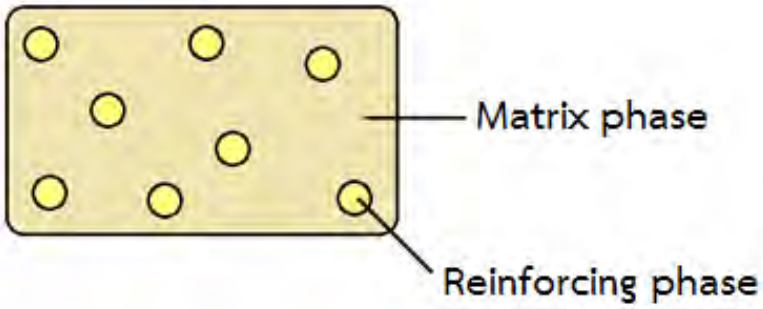

Figure 2.1 The schematic diagram of the composite [3].

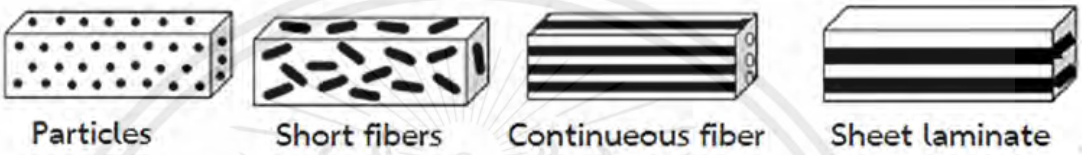

Figure 2.2 Types of composite materials based on reinforcement patterns in the classification of composite materials according to the modified matrix material [2].

2.2 Piezoelectric materials

The piezoelectric properties were discovered in 1880 by Jacques and Pierre Curie, both have experimented with the effect of pressure on the generation of electric charge of crystals such as quartz, tourmaline, cane sugar, topaz and Rochelle salt, for the charge is proportional to the stress. Therefore, they called this effect as "Piezo". The word "Piezo" comes from the Greek language means pressing. Mentioned piezoelectric properties afterward being called piezoelectricity [4].

2.2.1 Piezoelectric effect

Piezoelectricity of substance can be divided into two characteristics is the direct piezoelectric effect and the converse piezoelectric effect as shown in Figure 2.3 [4].

2.2.1.1 Direct piezoelectric effect

The polarization in asymmetry crystal is induced with mechanical stress be formed voltage in the crystal.

2.2.1.2 Converse piezoelectric effect

The crystal is induced with electric field be formed mechanical strain. Both effect these can be explained with the relationship equation as follows.

$$D = dT + \varepsilon^{T} + E \qquad \textbf{(Direct piezoelectric effect)} \qquad (2.1)$$

$$E = S^{E}T + dE \qquad \textbf{(Converse piezoelectric effect)} \qquad (2.2)$$

D is dielectric displacement

E is electric field (N/C)

T is stress (N/m^2)

d is piezoelectric constant (or piezoelectric coefficient) of substance (C/N)

ε^{T} is dielectric constant by the superscript symbol T instead the stress is constant

S^{E} is compliance by the superscript symbol E instead the electric filed is constant [4]

Superscript is a symbol that indicates conditions that are defined to have constant such as ε^{T} means dielectric of materials when the stress is constant. In the case of S^{E} means compliance of materials when the electric field is constant. But the piezoelectric properties of materials depend on directions of stress or electric field.

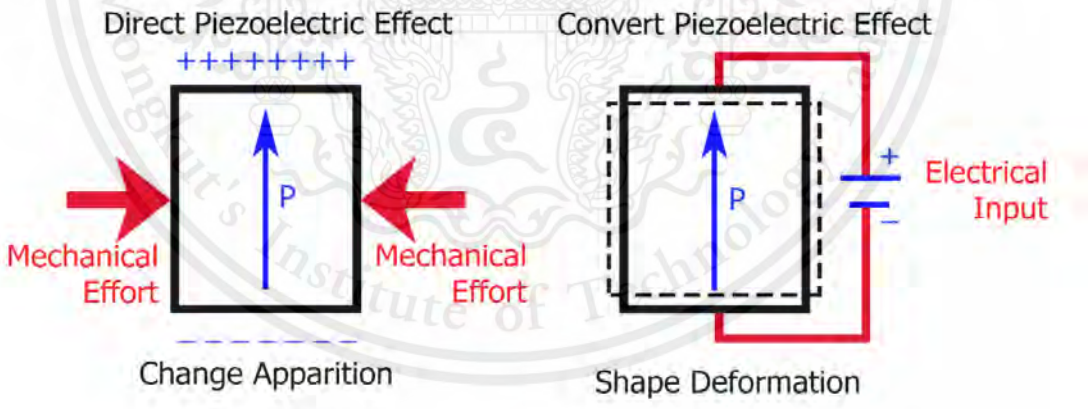

Figure 2.3 Direct piezoelectric and Converse piezoelectric effect of a piezoelectric element responding to external force element and external electric field [5].

2.3 Piezoelectric composites

Piezoelectric composites is a material that has been designed to achieve integration between piezoelectric ceramics and polymer, formed a new material with

the piezoelectric properties as required. The connection between phases that is a composition of the piezoelectric composite were extremely effecting the piezoelectric composite [6].

The possibility connecting of piezoelectric composites between ceramic and polymer, there are 10 types can be written as a symbol as follows 0-0, 0-1, 0-2, 0-3, 1-1, 1-2, 2-2, 1-3, 2-3, and 3-3, which the first number means piezoelectric ceramic phase and the second number means polymer phase as shown in Figure 2.5 [6].

Nowadays, the piezoelectric composite design is mostly 1-3 connectivity by the piezoelectric ceramic is continuously connected in along the length or one direction, while the polymer has continuous connection in all directions, which the changes ceramic volume ratio in 1-3 connectivity piezoelectric composite affecting the properties that are important to the performance of the device. Therefore, the design and determination of the volume ratio between ceramics and composites in 1-3 connectivity piezoelectric composite imperative to consider the equilibrium, that makes the composite have electromechanical/piezoelectric coupling factor (k) is high valuable and acoustic impedance (Z) low value. If the volume of ceramics has a ratio less than the volume of polymer resulting in acoustic impedance value is decrease, meanwhile electromechanical / piezoelectric coupling factor also decreases [6].

The advantages of piezoelectric composite are: (1) Replacing some of the stiff and dense ceramic with a less dense and less flexibility, (2) Piezoelectric composite materials are preferably useful for medical diagnostic ultrasonic transducer and underwater sonar applications, (3) Piezo-passive-dampers consist piezoelectric ceramic particle, polymer, and a carbon black, Which inhibits the vibration of the sound more effectively than the traditional rubber, etc. [6].

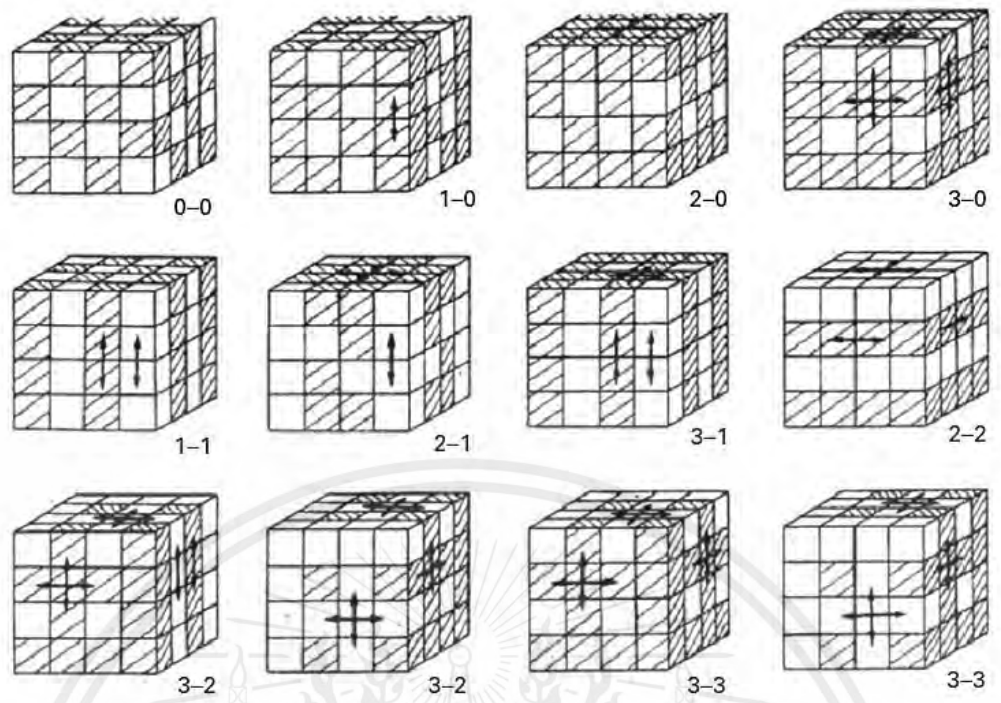

Figure 2.4 Classification of two-phase composites with respect to connectivity [6].

In this research interesting 5 type of piezoelectric materials which were found form synthesize. Include; BT, ZnO, plate-like NN, flower-like HA and coral-like HA. Especially HA also find in naturals. Piezoelectric composites were fabricated between polydimethylsiloxane (PDMS) and as above piezoelectric materials.

2.3.1 Barium titanate ($BaTiO_3$, BT)

Barium titanate is ferroelectric oxide with a perovskite structure. This ceramic has a relatively high electromechanical coupling factor, and a piezoelectric strain constant, and has been partially used for piezoelectric applications such as sonars. However, the working temperature range of the BT is narrow for actual piezoelectric applications because the BT has a low Curie temperature, T_c (=120–135°C) [7].

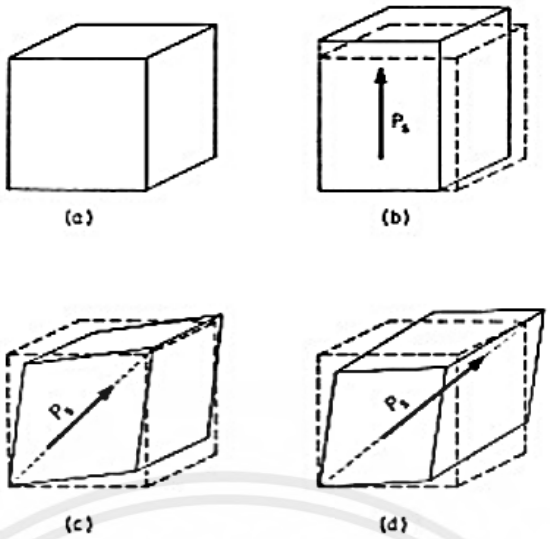

Figure 2.5 Unit cells of the four phases of BT: (a) Cubic, stable above 120 °C, (b) Tetragonal, stable between 120 °C and 5 °C, (c) Orthorhombic, stable between 5 °C and -90 °C, (d) Rhombohedral, stable below -90 °C [7].

2.3.2 Zinc oxide (ZnO)

Zinc oxide is semiconductor compound. Its crystal structure is rocksalt, zinc blende, and wurtzite. The schematic diagram of these shown in Figure 2.6. In neutral, stabilized structure is wurtzite. Zinc blende stabled when it grew in only cubic substrates and rocksalt structure acquired relatively high pressure for stabilized structure [8].

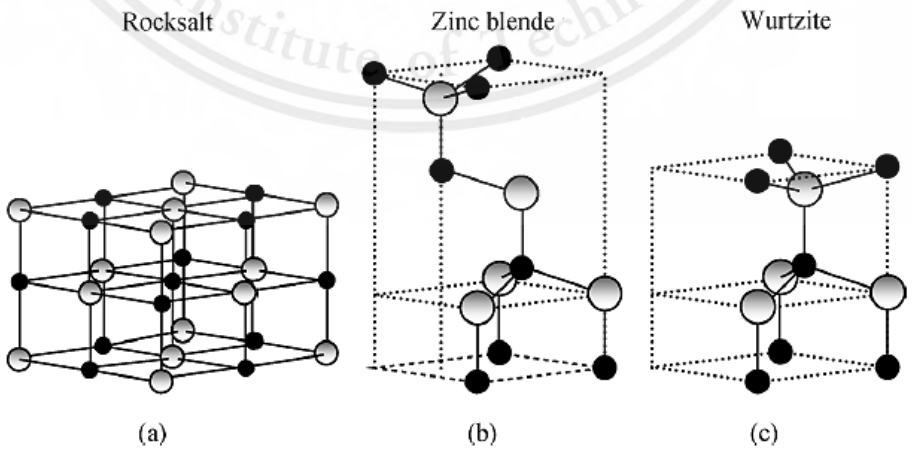

Figure 2.6 The schematic diagram of ZnO crystal structure include; rocksalt, zinc blende and wurtzite respectively [8].

ZnO is one of the piezoelectric materials. Its direct effect was used several applications such as small medical equipment device. Mechanical energy input was harvest from body movement of patients such as muscle movement or blood flow [9].

2.3.3 Plate-like sodium niobate ($NaNbO_3$, NN) nanostructure

Sodium niobate is an oxide powder that has interesting electrical properties include; antiferroelectric, ferroelectric and piezoelectric properties. Its crystal structure is orthorhombic structure. The schematic diagram of the crystal structure shown in Figure 2.6. Yunfei Chang and group synthesis plate-like NN nanostructure in 2008 [10].

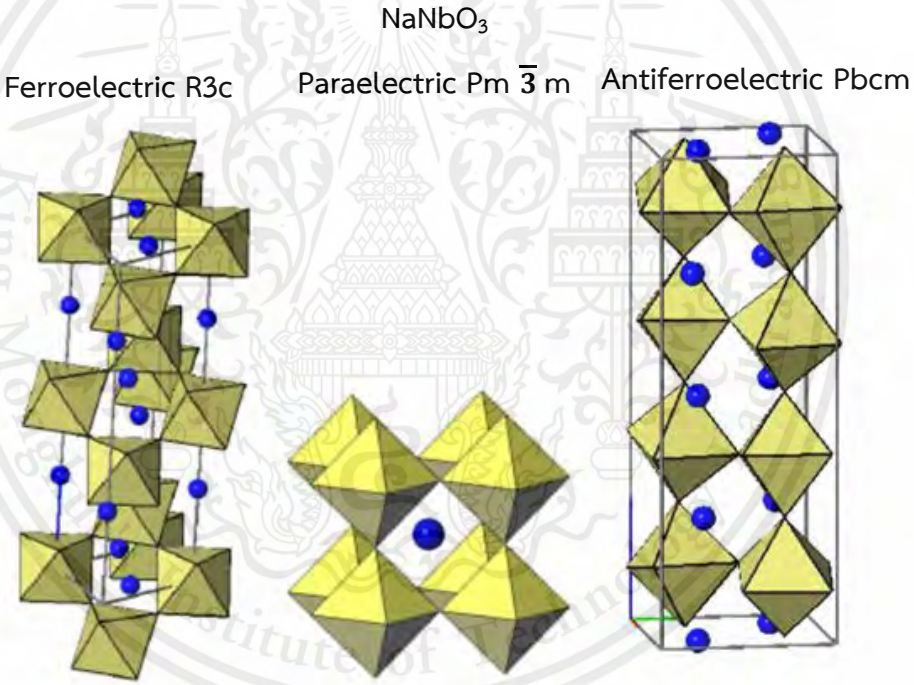

Figure 2.7 The schematic diagram of NN crystal structure (orthorhombic structure) [10].

2.3.4 Flower – like hydroxyapatite ($Ca_5(PO_4)_3(OH)$, HA) nanostructure

Hydroxyapatite is an inorganic compound in bone and teeth. The empirical formula is $Ca_5(PO_4)_3(OH)$. Therefore, HA can be biocompatibility with human tissue. It crystallizes in the hexagonal crystal system. In 2008 Aidin Lak and group

discovered flower-like HA nanostructure rapid hydrothermal method. SEM images of flower-like HA nanostructure shown in Figure 2.8 [12] Flower-like HA nanostructures have high specific surface area, which is a relevant property for catalysts and molecular sieves. [12].

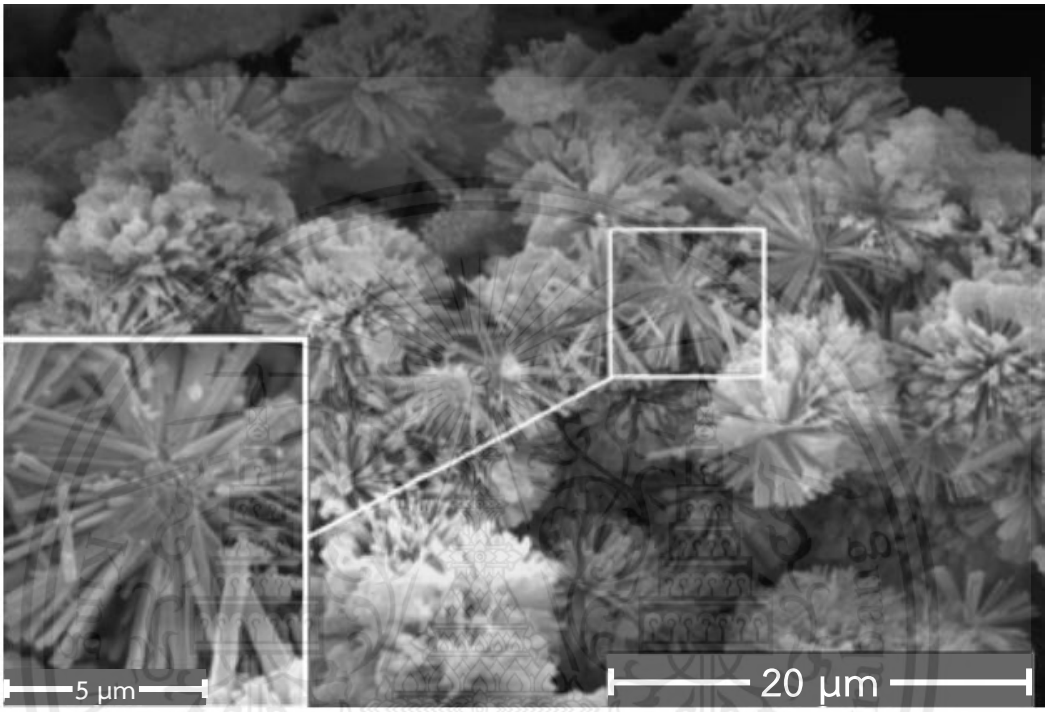

Figure 2.8 SEM images of flower-like HA nanostructure [12].

2.3.5 Coral – like hydroxyapatite ($Ca_5(PO_4)_3(OH)$, HA) nanostructure

Coral – like hydroxyapatite is an inorganic compound in bone and teeth. The empirical formula, crystal structure and biocompatibility property seem flower-like HA. In 2012 G. Suresh Kumar and group discovered coral-like HA nanostructure rapid microwave irradiation method. SEM images of coral-like HA nanostructure shown in Figure 2.9 [13]. Coral-like HA has piezoelectric properties. There are several application were mostly used about biomedical [13].

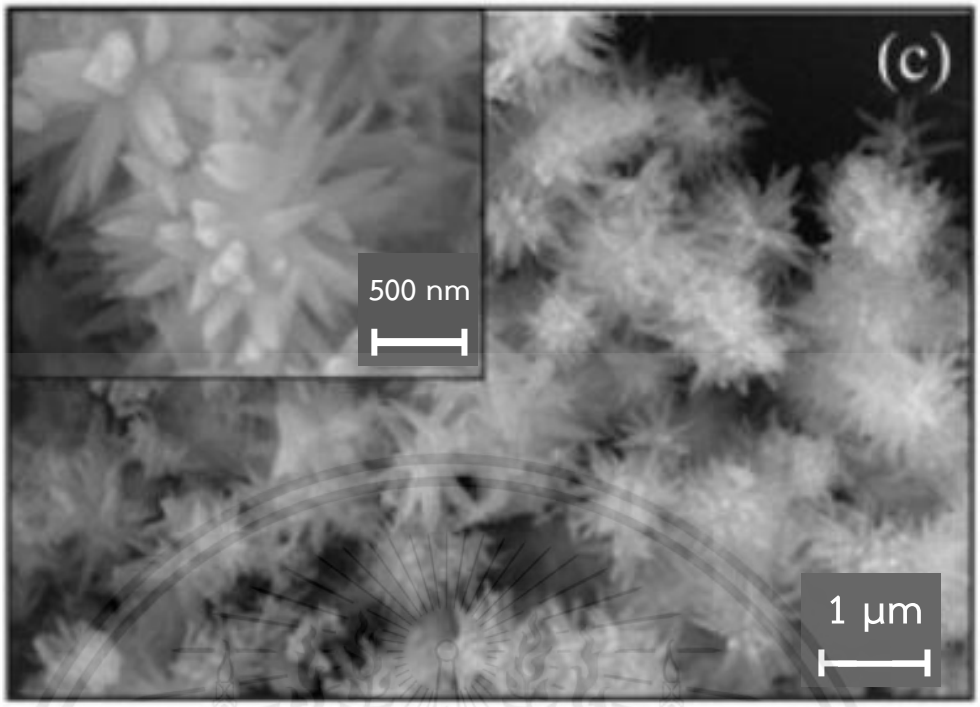

Figure 2.9 SEM images of coral-like HA nanostructure [13].

2.3.6 Polydimethylsiloxane (PDMS)

Polydimethylsiloxane is an inorganic polymes. This polymer is a good dielectric that it has also good physical property. The chemical formula for PDMS is $CH_3[Si(CH_3)_2O]nSi(CH_3)_3$ and chemical struture show in Figure 2.10 [14].

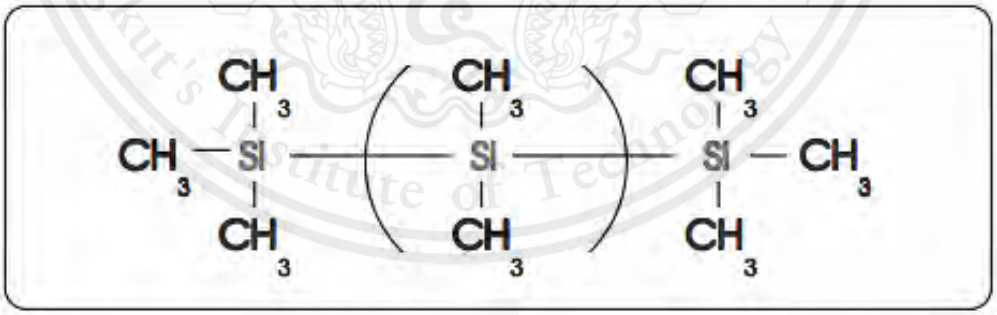

Figure 2.10 Polydimethylsiloxane structure [15].

In piezoelectric composites, PDMS has used to been matrix phase of ceramics oxide. Because there are appropriate properties such as flexible, impact strange, hydrophobic, transparent, easy to forming, and thermoset polymer type [14].

2.4 Literature reviews

In 2012, Kwi-Il Park and co-workers [16] reported nanocomposite generator (NCG) reaching a simple, low cost and large area fabrication with BT nanoparticle (BT NPs) synthesized from the hydrothermal method and universal graphitic carbons such as reduced graphene oxide (RGO), single-walled and multi-walled carbon nanotubes (SW/MWCNTs). The BT NPs and carbon nanoparticles are dispersed in PDMS by mechanical agitation to produce a piezoelectric nanocomposite (p-NC). Under periodic external mechanical deformation by biomechanical movements or bending stage from a human body and others. The electric signals are generated from the NCG device and used to drive a commercial red LED. For the schematic diagram of the fabrication process of NCG device as shown in Figure 2.11.

When a measurement instrument is forward connected to the device. The NCG device generates a positive voltage and current upon the bending states. In the case of the reverse connection, the negative output pulses are measured. The results found that the measured outputs are the true signals generated from our NCGs strained by bending motions. Under the continual bending and unbending cycles, the NCG device repeatedly generates an open-circuit voltage (V_{oc}) about 3.2 V and a short-circuit current (I_{sc}) signal about 250 to 350 nA as shown in Figure 2.12.

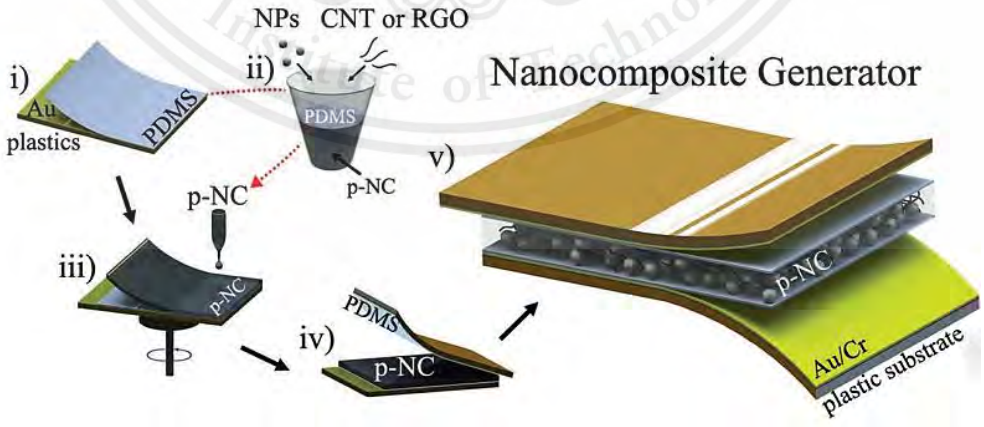

Figure 2.11 Schematic diagrams illustration of the fabrication process for the NCG device [15].

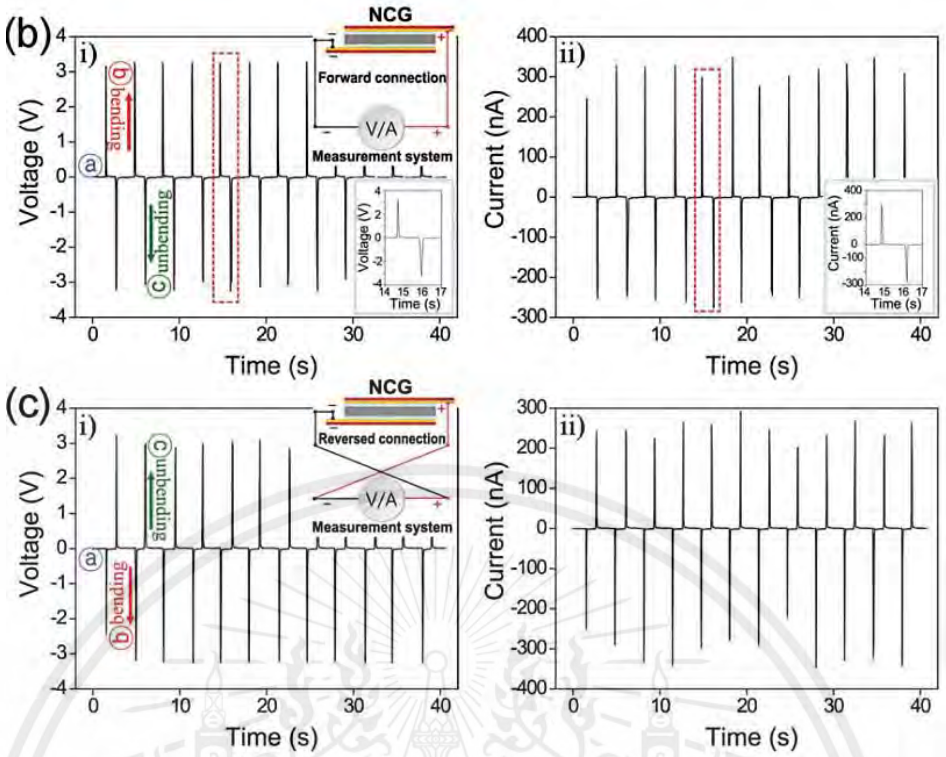

Figure 2.12 The measured output voltage and current signals of the NCG device in the forward connection during the periodic bending and unbending motions, (c) The open-circuit voltage and short-circuit current signals generated in the reverse connection [15].

In 2012, Zong-Hong Lin and co-workers [17] fabricated the piezoelectric nanogenerator (NG) with BT nanotubes were synthesized via a hydrothermal method. BT nanotubes are dispersed in PDMS to create the piezoelectric NG. The NG consist of five layers as schematically shown in Figure 2.13. Under periodic external mechanical deformation, they obtained a high output piezoelectric signals, that is an open-circuit voltage (V_{OC}) of 5.5 V and short-circuit current (I_{SC}) exceeding 350 nA and measured the output of the NG with a reverse connection to confirm the obtained signal from piezoelectricity of BT nanotubes as shown in Figure 2.14. The NG can continuously drive a commercial LCD under the biomechanical movements.

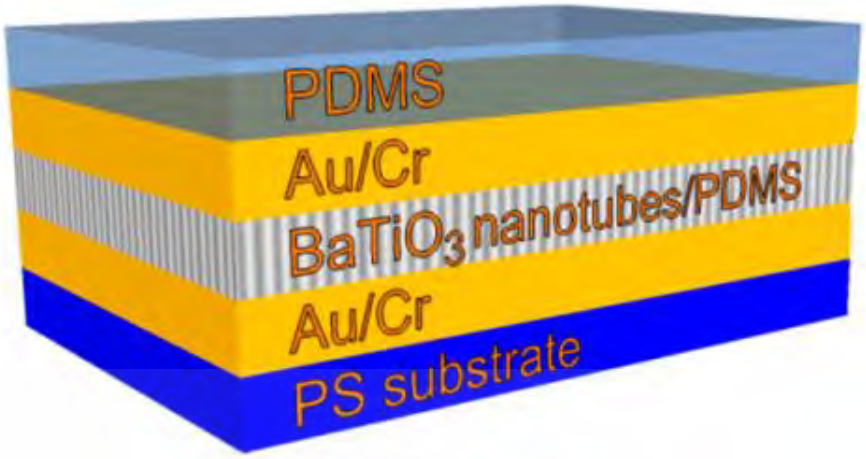

Figure 2.13 Scheme of the as developed NG [17].

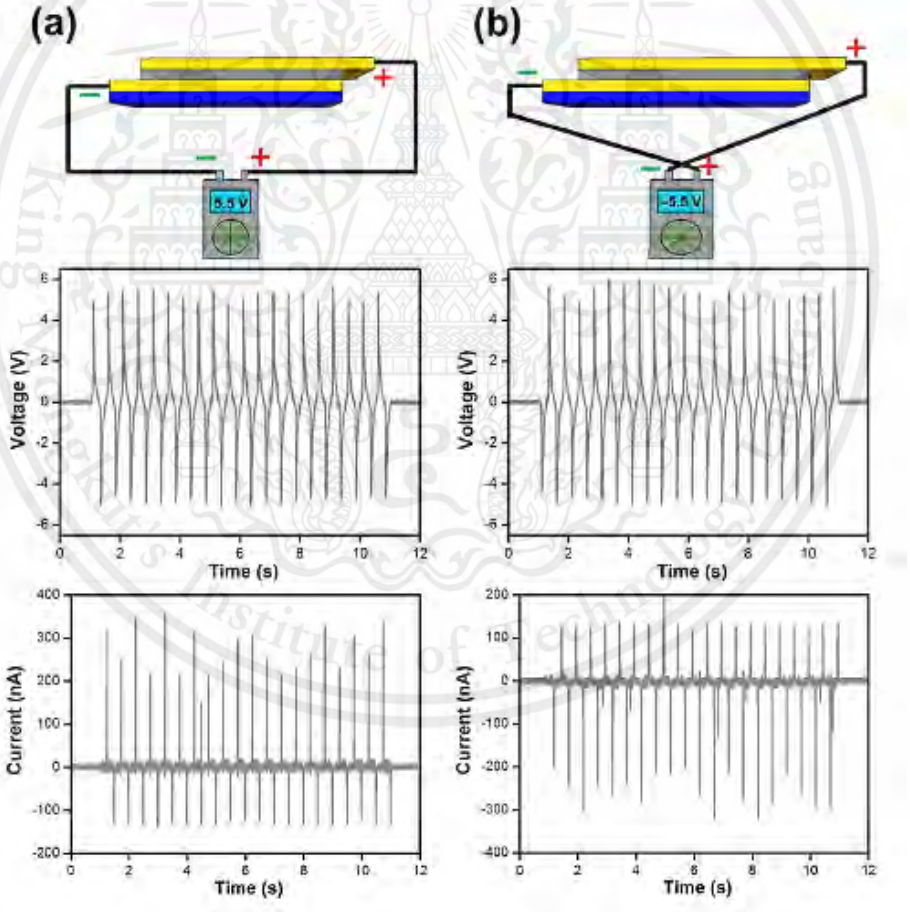

Figure 2.14 Electrical output for V_{oc} and I_{sc} of the as-developed NG under a compress stress of 1 MPa at forward connection (a) and reversed connection (b) to the measurement system [17].

In 2013, Kwi-Il Park and co-workers [18] fabricated a large-area NCG device with the size 30 cm × 30 cm from a bar-coating technique to scale-up previously reported NCG device. The PZT particles as an energy generation source and multiwalled carbon nanotubes (MW-CNTs) as an improver are dispersed in a PDMS matrix to build a piezoelectric nanocomposite (p-NC). For the schematic diagram of the fabrication process of NCG device as shown in Figure 2.15. During the mechanical bending and unbending deformation, the output voltage and the output current signals of a large-area NCG device (30 cm × 30 cm) are ≈100 V and 10 μA, respectively as shown in Figure 2.16. A large-area NCG device are used to drive LED without external circuits.

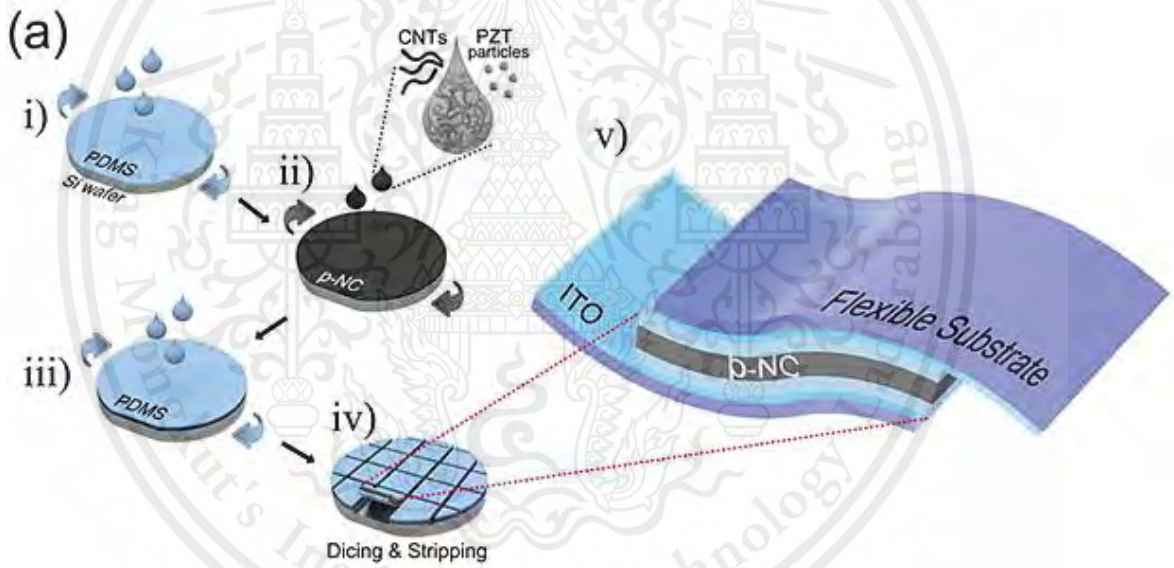

Figure 2.15 Schematic illustration of the process for fabricating flexible a large-area NCG device [18].

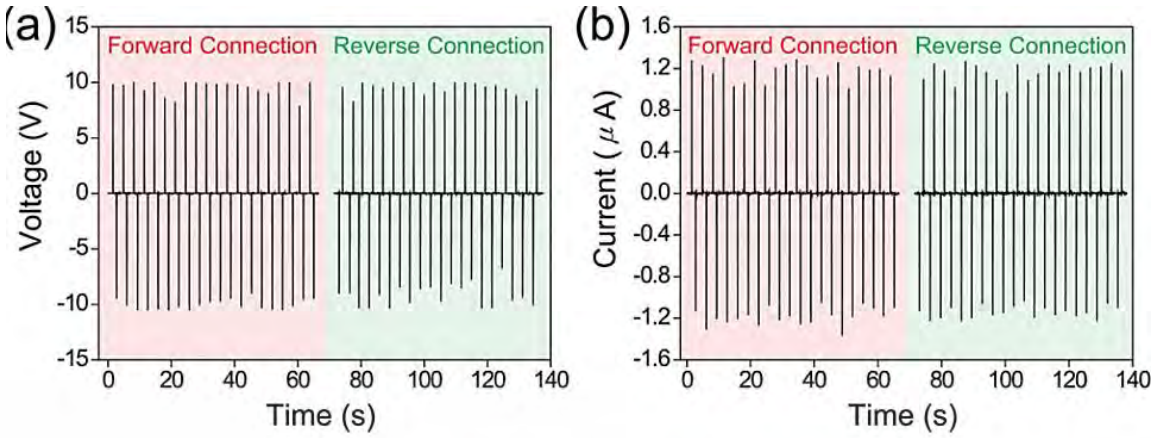

Figure 2.16 Shows electrical output (a) output voltage and (b) output current of the NCG device in the forward and reverse connection [18].

In 2014, Chang Kyu Jeong and co-workers [19] demonstrate a high-performance of lead-free NCG device using the intrinsically excellent piezoelectric KNLN particles and copper nanorods (Cu NRs). The KNLN particles as power generation sources and Cu NRs as energy enhancers, dispersant and conducting agents. The KNLN particles and Cu NRs are embedded in a PDMS elastomeric matrix to create a piezoelectric nanocomposite (p-NC). The spin-casted p-NC layer is placed between two indium tin oxide (ITO)-deposited polyethylene terephthalate (PET) substrates. For the schematic of the NCG structure with KNLN particles and Cu NRs, which assemble a well-distributed p-NC layer in the device as shown in Figure 2.17. During periodical bending deformation, the KNLN-based flexible NCG device (3 cm × 3 cm) produced a maximum output voltage of ≈12 V and output current of ≈1.2 μA as shown in Figure 2.18. This p-NC device is four times higher than those of a previous lead-free BTO/carbon nanotube (CNT)-based NCG device.

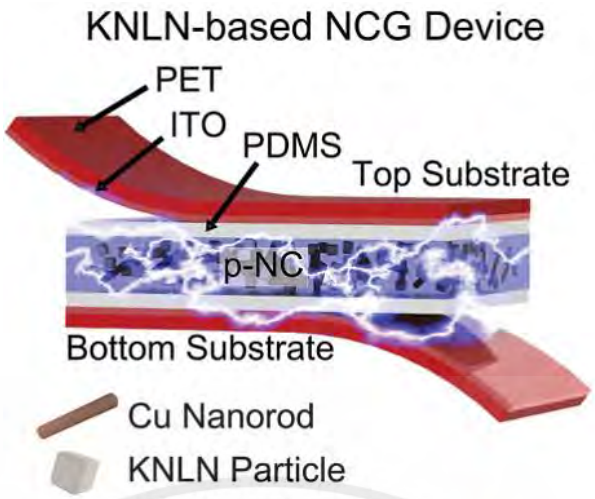

Figure 2.17 Schematic of an NCG device using KNLN particles and Cu NRs [19].

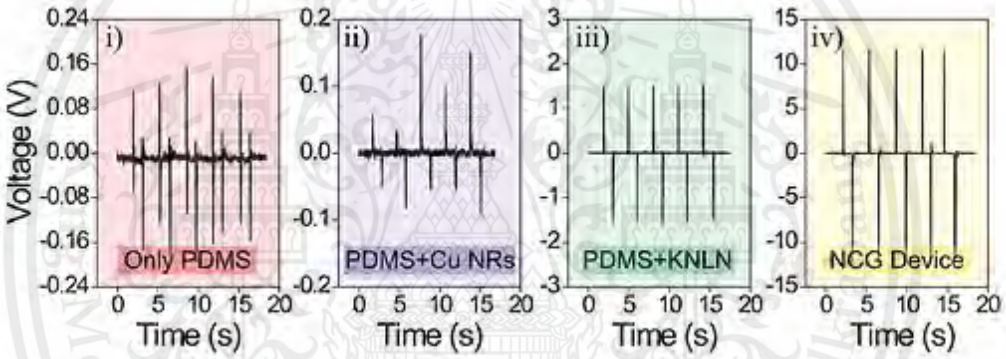

Figure 2.18 (i) Output voltage generated from the devices fabricated using only a PDMS layer, (ii) a Cu NRs-PDMS composite, (iii) a composite with only KNLN particles, and (iv) an NCG device [19].

In 2017, Cuixian and co-workers [20] fabricated a flexible and highly effective piezoelectric nanogenerator (PNG). The composite film obtained from dispersing BT NPs and BT/C in a PDMS matrix. For the schematics of the flexible PNG fabricating process are shown in Figure 2.19. Measured and analyzed the output voltage and current of the fabricated PNG. Under external mechanical deformation by beating from mechanical vibrator, the electric output are repeatedly generated from the PNGs device and stored to drive a commercial red LED. Flexible PNGs have an

output voltage of ~7.43 V and the maximum power can reach up to ~7.92 μW as shown in Figure 2.20. The voltage and the current of BT/PDMS composite PNGs enhance from 0.61 V to 6.02 V and 0.41 μA - 4.03 μA with the concentration ratio of commercial BT NPs that are different from 10 wt.% to 40 wt.% and output voltages about 3.05, 3.49, 5.01, 7.43, 3.67 and 0.33 V from the PNGs, for C fractions of 0, 1.6, 2.4, 3.2, 4.0 and 4.8 wt %, respectively as shown in Figure 2.21.

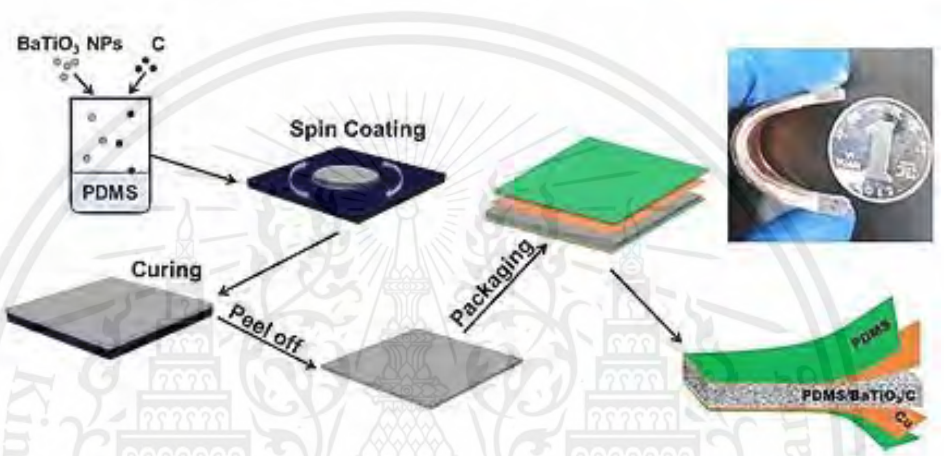

Figure 2.19 Schematic diagrams of the BT/PDMS/C composite nanogenerators fabricating process [20].

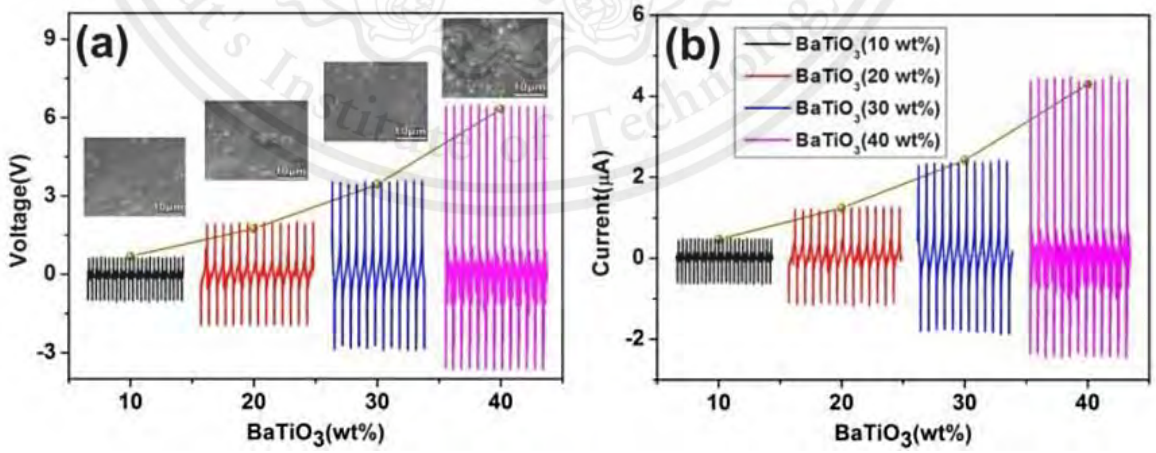

Figure 2.20 The output performance for BT/PDMS composite PNGs: (a) The output voltage for PNGs with 10, 20, 30 and 40 wt.% BT NPs concentration; (b) The output current for PNGs with different concentration of BT NPs (10, 20, 30 and 40 wt.%) [20].

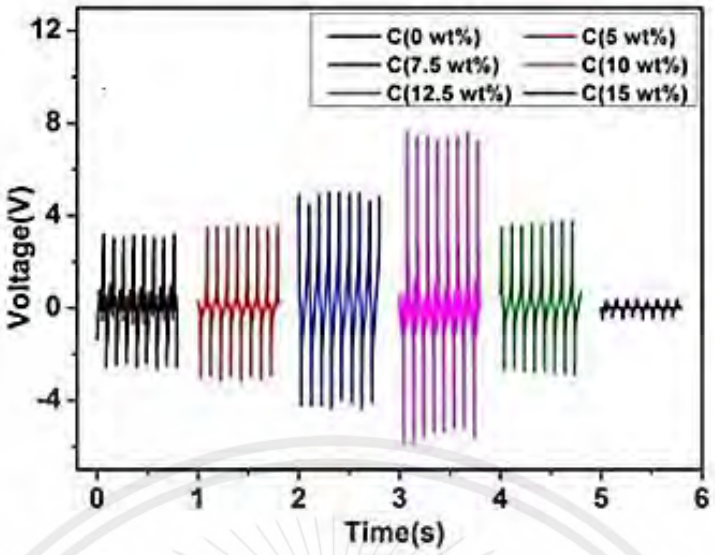

Figure 2.21 The output performance for BT/PDMS/C composite PNGs: (a) The output voltage for PNGs with different C contents (0, 1.6, 2.4, 3.2, 4.0 and 4.8 wt.%) [20].

In 2017, Xiaoliang Chen and co-workers [21] fabricated a high performance flexible piezoelectric nanogenerator that exhibits increase voltage of 13.2 V and a current density of 0.33 μA cm^{-2}. Under mechanical stress, electricity is generated from the nanogenerator and used to drive many electronic devices to work. The flexible nanocomposite micropillar based piezoelectric device was successfully fabricated as shown in Figure 2.22. The P(VDF-TrFE)/BT nanocomposite micropillar array structure in vertically well-aligned as a result with a maximum force of 50 N at 1 Hz as show in Figure 2.23 (a-c). They measured the outputs voltage and current from nanocomposite micropillar array based sample and original P(VDF-TrFE) film for comparison.

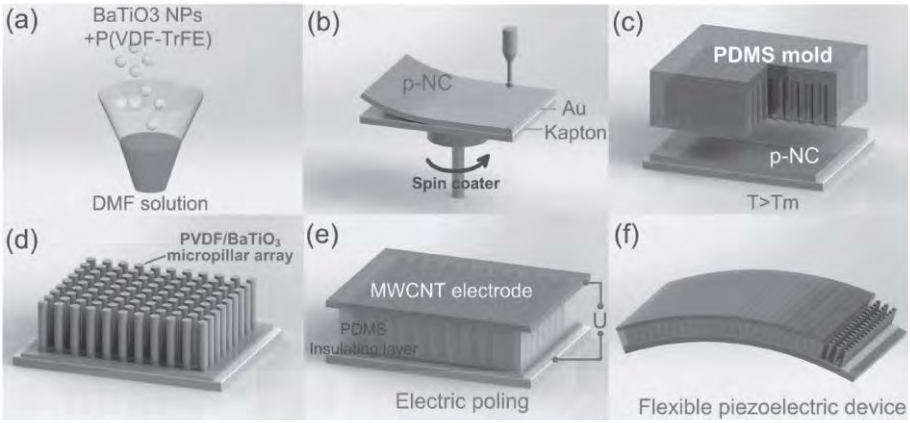

Figure 2.22 (a–e) Experimental methods for fabricating the high-performance piezoelectric nanogenerator based on P(VDF-TrFE)/BT nanocomposite micropillar array, f) A schematic of the flexible piezoelectric device [21]

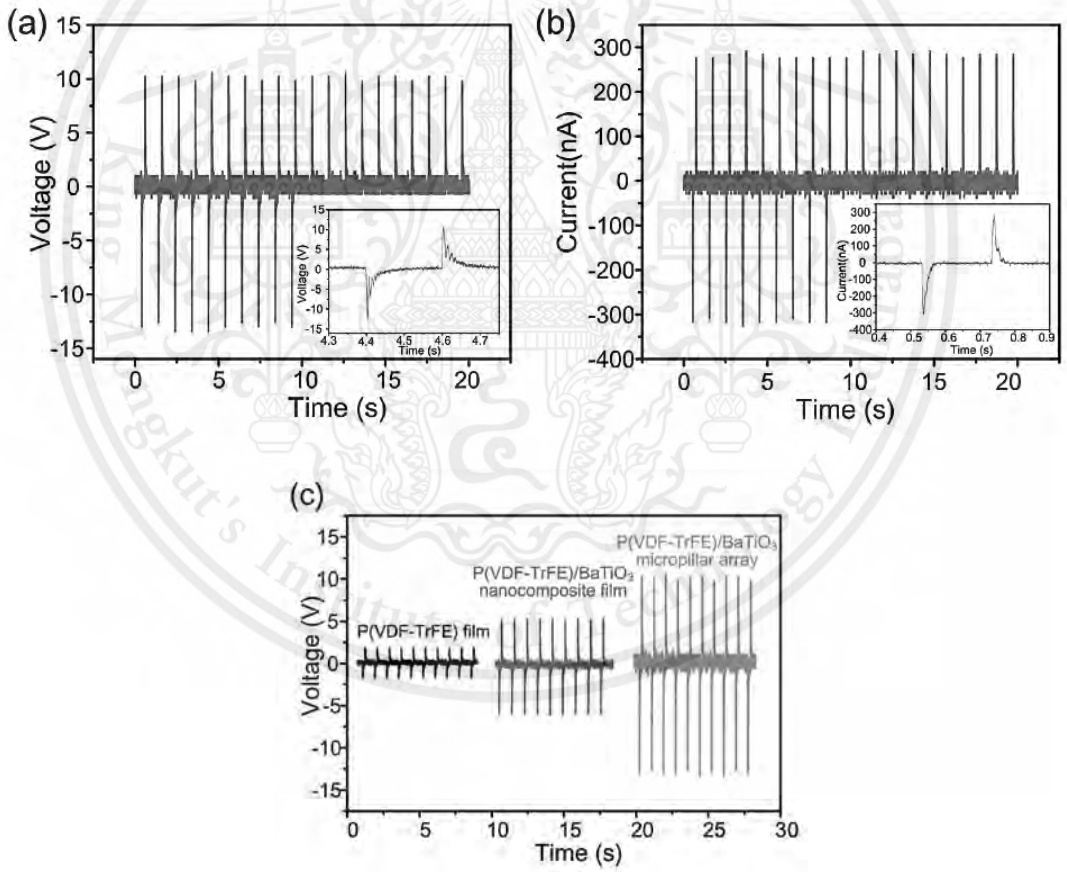

Figure 2.23 (a),(b) Measured output voltage and current signals of the PENM-NG under continuous compress, respectively. c) A comparison of output voltages for the piezoelectric devices based on P(VDF-TrFE)/BT micropillar array, P(VDF-TrFE)/BT nanocomposite film and for a bulk P(VDFTrFE) film [21].

In 2017, Seong-Ho Baek and Il-Kyu Park [22] reported the fabrication of flexible composites consisting of ZnO nanorods (NRs) and Si micro-pillar (MP) arrays from a transfer technique for use in flexible PNGs as show in Figure 2.24. By providing an enlarged surface area and forming a heterojunction structure to modify the electron energy band structure cause many good effects, such as flexible support to connect the ZnO NRs mechanically and electrically and enhancing the piezoelectric output performances by providing an enlarged surface area and forming a heterojunction structure to modify the electron energy band structure. In Figure 2.25 shows the output voltage measured from the flexible PNGs that have different lengths of the Si MP arrays of 5 to 20 μm. The flexible PNGs show voltage and current output and show negative and positive voltage and current peaks, when stressed and relieved, respectively.

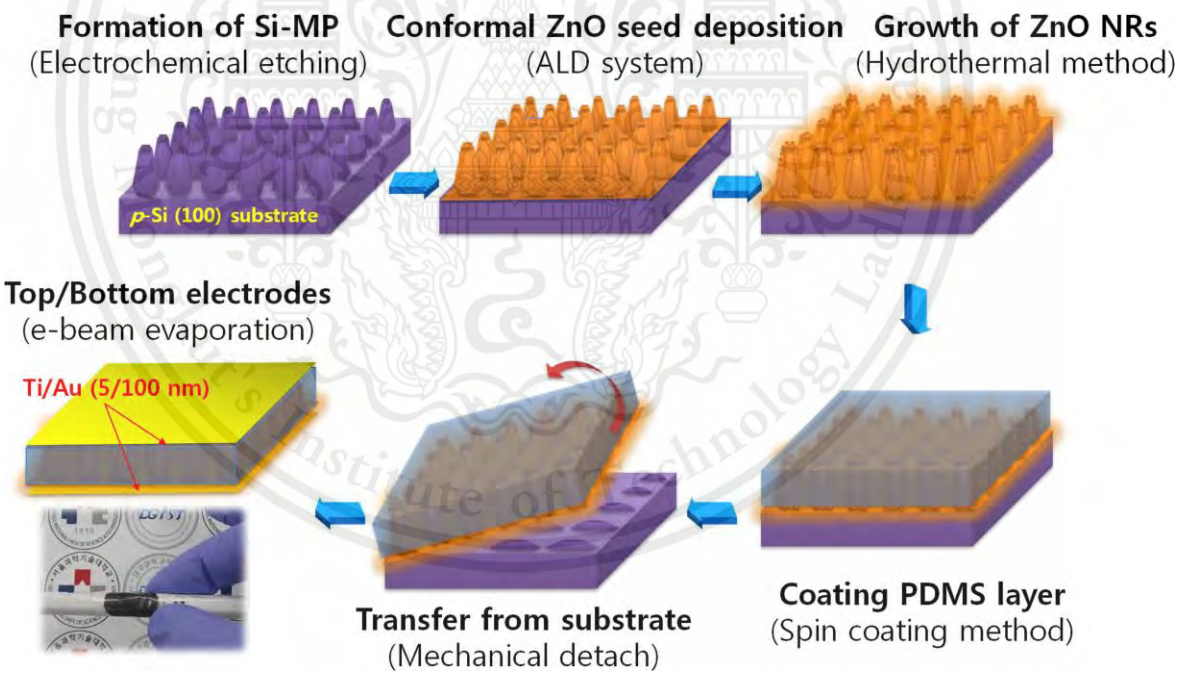

Figure 2.24 Experimental methods for fabricating the high-performance piezoelectric nanogenerator based on transferred ZnO nanorod/Si micropillar array [22].

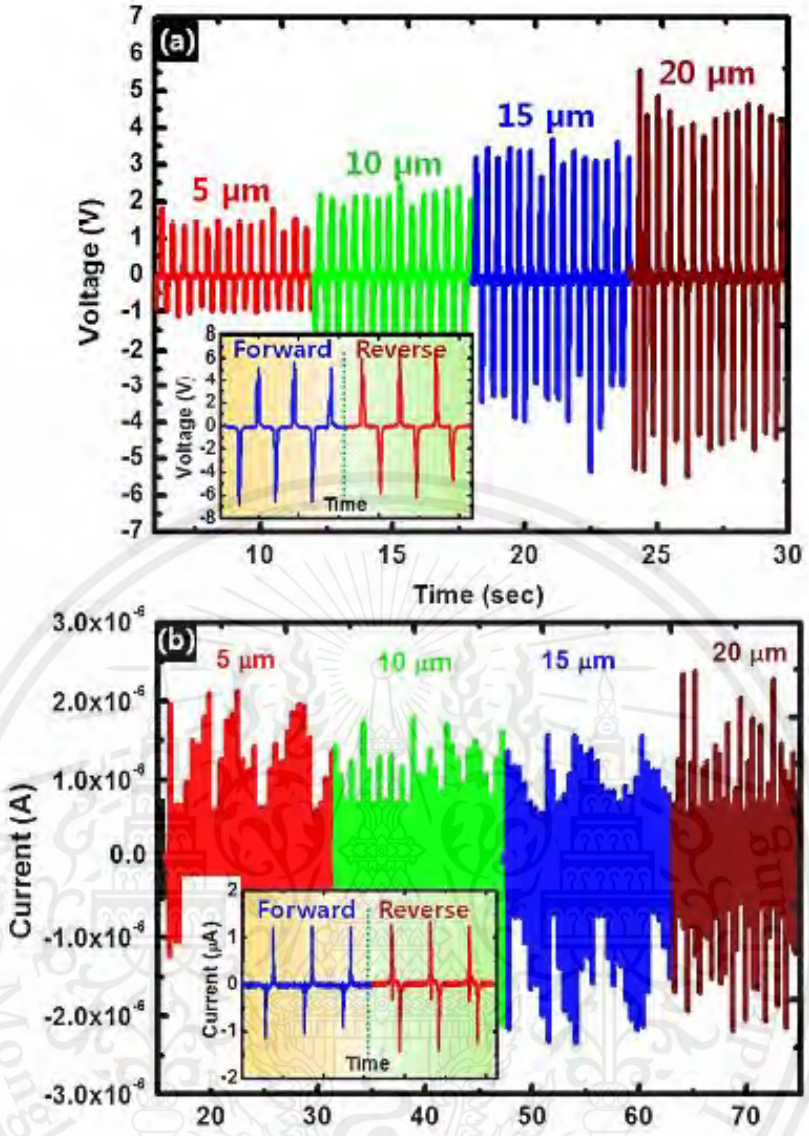

Figure 2.25 (a) Output voltage and (b) current measured from flexible PNGs with Si MP arrays with lengths of 5, 10, 15 and 20 μm. The insets show the polarity-dependent output voltage and current for forward and reverse connections which were measured from the flexible PNG on a Si MP array with a length of 20 μm [22].

In 2018, Chen Zhang and co-workers [23] developed an easy and facile route to a fully rollable lead-free PVDF-niobate-based nanocomposite-based nanogenertor (NCG) with high performance, which a compositionally modified NKN-based piezoelectric material with nominal composition of $0.915(Na_{0.5}K_{0.5})(Nb_{0.94}Sb_{0.06})O_3$-$0.045LiTaO_3$-$0.04BaZrO_3$ (NKNS-LT-BZ) is adopted. The thin-film nanocomposite made

of well distributed NKNS-LT-BZ NPs and PVDF polymer matrix is integrated with the nanocomposite so as to be conscious rollability for the NCG. A schematic the structure of the flexible PVDF-niobate based NCG is illustrated in Figure 2.26 (a). Under periodical agitation at a compressive force of 50 N and 1 Hz, the area size for NCG is 2 × 2 cm^2 can generate an open-circuit voltage (V_{OC}) of 18 V and a short-circuit current (I_{SC}) of 2.6 μA. For under the force of 50 N at a frequency of 1 Hz, the open-circuit voltage (V_{OC}) and short circuit current (I_{SC}) were recorded from the NCGs with different NKNS-LT-BZ NPs content as shown in Figure 2.24 (b),(c).

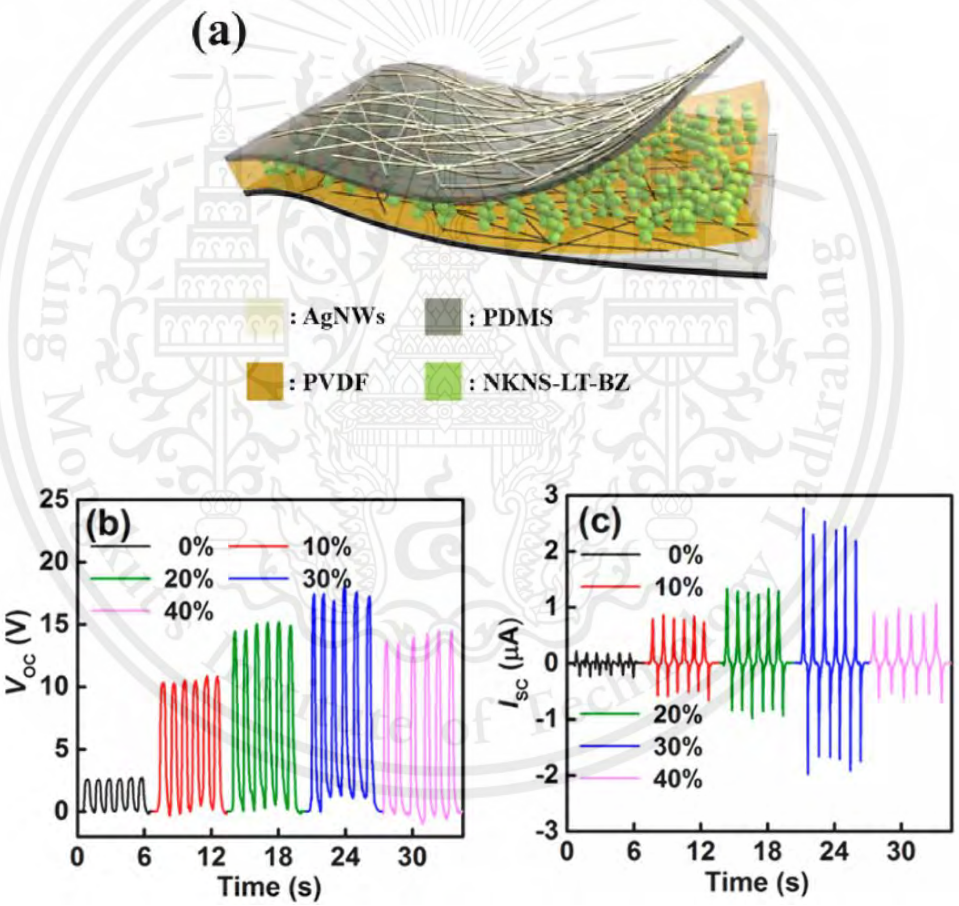

Figure 2.26 (a) Schematic illustration presenting the structure of the PVDF-niobate-based NCG with the Ag NW-based electrodes, (b) V_{OC} and (c) I_{SC} of the NCGs with different NKNS-LT-BZ NPs content from 0 to 40% [23].

In 2018, Hemalatha Parangusan and co-workers [24] investigated the structure, morphology and piezoelectric performances of neat polyvinylidene fluoride hexafluoropropylene (PVDF-HFP) and PVDF-HFP/Co-ZnO nanofibers, fabricated by electrospinning and Co-doped ZnO nanofiller concentration in the PVDF-HFP matrix. The flexible nanogenerator manipulated from the polymer nanocomposite (PVDF-HFP/Co-ZnO) exhibits an output voltage as high as 2.8 V compared with the neat PVDF-HFP sample (~120 mV). A schematic of the PVDF-HFP composite nanofiber based energy harvester is shown in Figure 17 (a) and the experiment setup as show in Figure 2.27 (b). In Figure 2.28 displays the piezoelectric properties of PVDF-HFP nanocomposite films. Piezoelectric output voltages of 2 V, 2.4 V and 2.8 V were respectively obtained from the nanogenerator containing filler loadings of 0.5, 1 and 2 wt% of Co-ZnO.

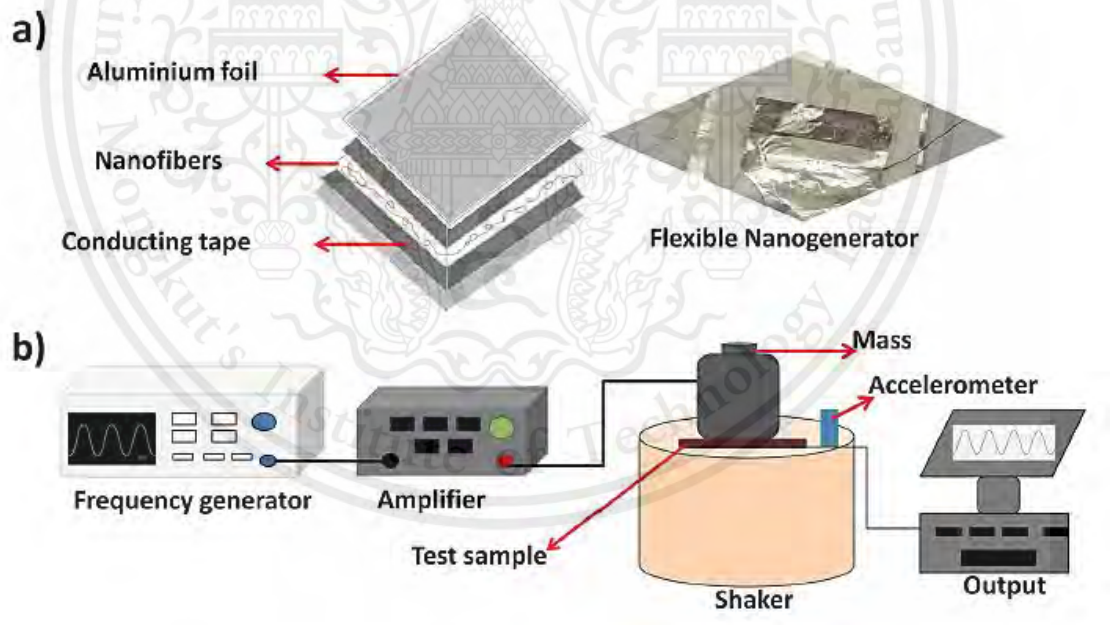

Figure 2.27 Schematic representation of (a) PVDF-HFP fiber nanogenerator and (b) piezoelectric experimental setup [24].

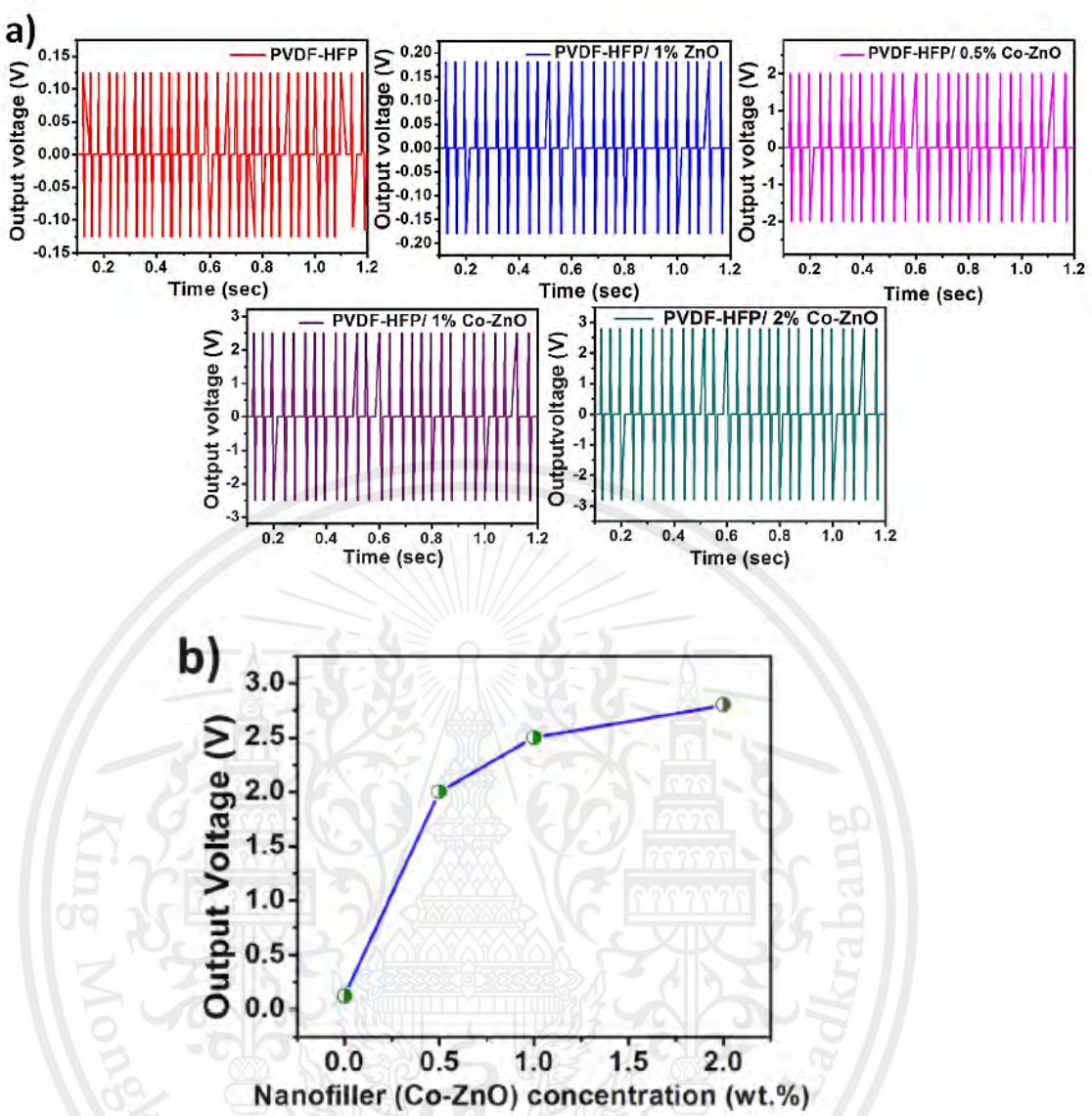

Figure 2.28 (a) Generation of output voltages from neat PVDF-HFP and its nanocomposites, (b) the output voltages as a function of the Co-doped ZnO filler loading [24].

In 2018, Changyeon Baek and co-workers [25] incorporated one-dimensional of BT nanoparticles to the nanogenerator (NCG) device to achieve a homogeneous distribution of piezoelectric materials and enhanced performance. BT spherical nanoparticles (SPs) and BT nanowires (NWs) were synthesized via hydrothermal reaction. The morphology and the microstructures of prepared piezoelectric nanomaterials as shown in Figure 2.29. The various p-NC layers with a different

weight ratio of BT SPs and NWs were prepared the NCG device to find the optimal ratio to maximize the output performance of the NCG device. For a schematic illustration of lead-free NCG as shown in Figure 2.30. Under external mechanical, the output voltage and current obtained from the NCG devices with various BT SPs and NWs weight ratios reached the highest output values for V_{OC}～ 60 V and I_{SC}～ 1.1 μA at a ratio of 4:1 as shown in Figure 2.31.

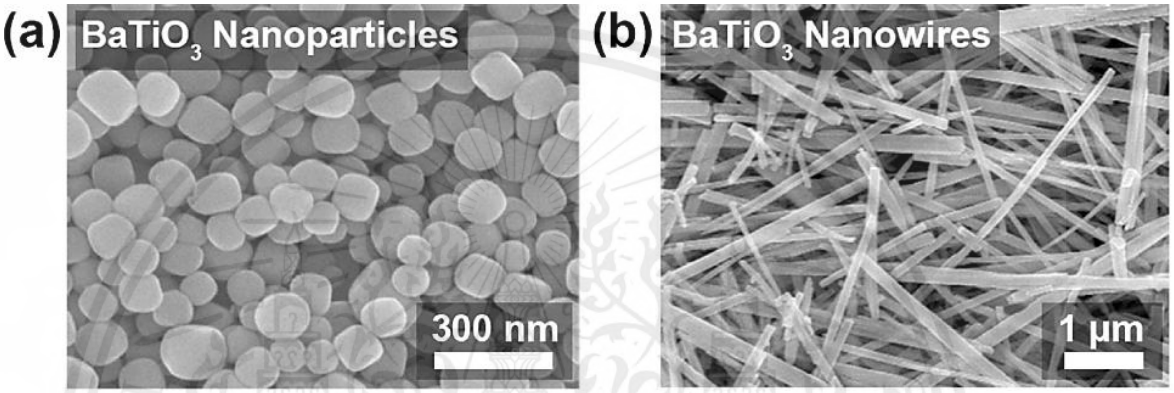

Figure 2.29 Hydrothermally synthesized BT (a) spherical nanoparticles (SPs) and (b) nanowires (NWs) [25].

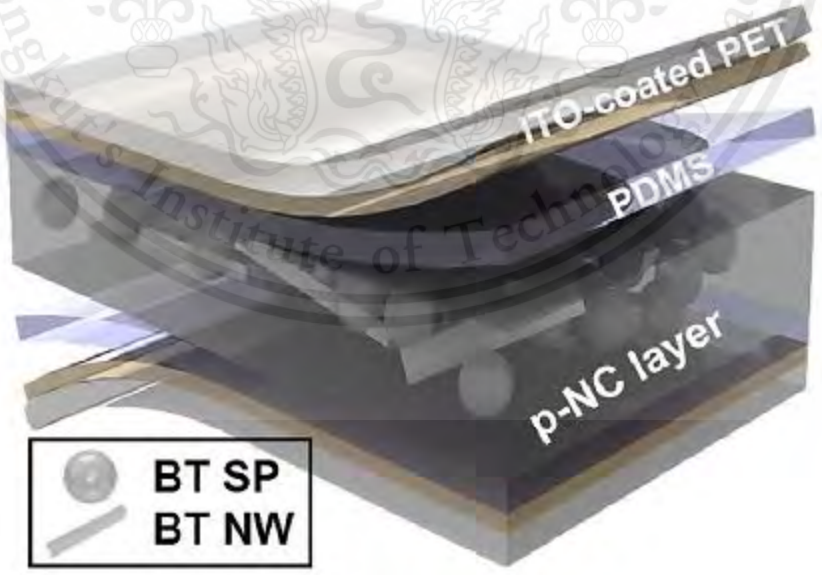

Figure 2.30 Schematic illustration of the BT SPs and NWs embedded NCG [25].

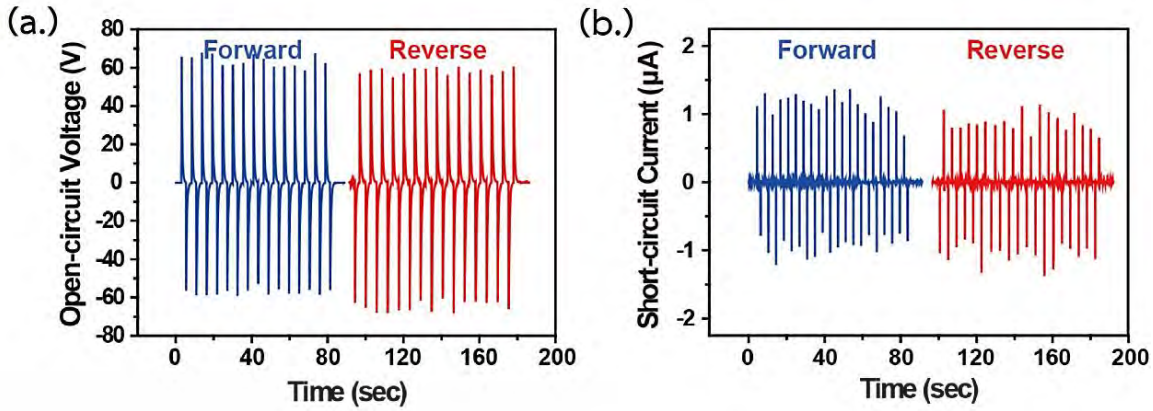

Figure 2.31 The electrical output (a.) open-circuit voltage and (b.) short-circuit current from the NCG at a BT SP and NW weight ratio of 4:1 when the device is connected forwardly and reversely to the measurement kit [25].

2.5 REFERENCES

[1] Campbell, F. C. (2010). Introduction to Composite Materials, ASM International, 2010.

[2] WANISA KHUMPEERA, S. C., SUTASINEE NAKSUK (2017). The study of Phase Dispersion Effect on The Electrical Output Performance for The Composite-Based Flexible, KING MONGKUT'S INSTITUTE OF TECHNOLOGY LADKRABANG.

[3] ผศ.ดร.สินติพีร์ เอมมณี, "วัสดุคอมโพสิตหรือวัสดุผสม (Composite Materials)." [Online]. Available: http://auto.kmutt.ac.th/custom/uploads/files/1533012166.pdf.

[4] Uthaisar, C. (2013). INFLUENT OF TANTALUM DOPANT ON ELECTRICAL FATIGUEBEHAVIOROFLEAD-FREEFERROELECTRIC CERAMIC ($K_{0.50}Na_{0.46}Li_{0.04}$)($Nb_{(0.96-x)}Sb_{0.04}Ta_x$)$O_3$), Suranaree University of Technology. Degree of Master of Engineering in Ceramic Engineering.

[5] Kokkinopoulos, Kokkinopoulos, A.Vokas, Georgios Papageorgas, Panagiotis. (2013). Energy Harvesting Implementing Embedded Piezoelectric Generators – The Potential for the Attiki Odos Traffic Grid.

[6] Uchino, K. (2017). Chapter 9 - Piezoelectric Composite Materials. Advanced Piezoelectric Materials (Second Edition). K. Uchino, Woodhead Publishing: 353-382.

[7] Bobiæ, M.M. Stojanoviæ , J.D. Vijatoviæ , B.D. 2008. "History and Challenges of Barium Titanate I". Science of sintering.40 : 155-165.

[8] Hadis Morkoç and Ümit Özgur. (2009). Zinc Oxide: Fundamentals, Materials and Device Technology.

[9] ดร.ศุภมาส ด่านวิทยากุล, (เมษายน - มิถุนายน 2556). "ซิงค์ออกไซด์ วัสดุอเนกประสงค์." [Online].Available: https://www2.mtec.or.th/th/e-magazine/admin/upload/286_13-22.pdf.

[10] Mishra, S. K.Choudhury, N.Chaplot, S. L.Krishna, P. S. R.Mittal, R. (2007). "Competing antiferroelectric and ferroelectric interactions in $NaNbO_3$: Neutron diffraction and theoretical studies." Physical Review B 76(2): 024110.

[11] Rujitanapanich, Sawittree Kumpapan, Pitoon Wanjanoi, Panthong. (2014). "Synthesis of Hydroxyapatite from Oyster Shell via Precipitation." Energy Procedia 56: 112-117.

[12] Aidin Lak, Mahyar Mazloumi, Matin Mohajerani, Amir Kajbafvala, Saeid Zanganeh, Hamed Arami, S. K. Sadrnezhaadw. (2008). "Self-Assembly of Dandelion-Like Hydroxyapatite Nanostructures Via Hydrothermal Method" 91: 3292–3297

[13] Kumar, G. Suresh Thamizhavel, A.Girija, E. K. (2012). "Microwave conversion of eggshells into flower-like hydroxyapatite nanostructure for biomedical applications." Materials Letters 76: 198-200.

[14] H. C. Hilborg. 2001. "Loss and recovery of hydrophobicity of polydimetylsiloxaneafter exposure to electrical discharges". Department of polymer technology,Royal institute of technology, Stockholm, Sweden.

[15] ดร.ธนาวลี ลี้จากภัย, (2545). "ซิลิโคน : วัสดุจากเม็ดทราย." Moment of discovery & invention. [Online]. Available: https://www2.mtec.or.th/th/e-magazine/admin/upload/284_24.pdf.

[16] Park, Kwi-Il Lee, Nuri Liu, Ying Moon, San Hwang, Geon Zhu, Guang Kim, Ji Eun Kim, Sang Kim, Do Kyung Wang, Zhong Lee, J. (2012). Flexible Nanocomposite Generator Made of $BaTiO_3$ Nanoparticles and Graphitic Carbons.

[17] Lin, Zong-Hong Yang, Ya Wu, Jyh Ming Liu, Ying Zhang, Fang Wang, Zhong Lin. (2012). "$BaTiO_3$ Nanotubes-Based Flexible and Transparent Nanogenerators." The Journal of Physical Chemistry Letters 3(23): 3599-3604.

[18] Kwi-Il Park , Chang Kyu Jeong , Jungho Ryu , Geon-Tae Hwang , and Keon Jae Lee. (2013). Flexible and Large-Area Nanocomposite Generators Based on Lead Zirconate Titanate Particles and Carbon Nanotubes.

[19] Chang Kyu Jeong , Kwi-Il Park , Jungho Ryu , Geon-Tae Hwang , and Keon Jae Lee. (2014). Large-Area and Flexible Lead-Free Nanocomposite Generator Using Alkaline Niobate Particles and Metal Nanorod Filler.

[20] Cuixian Luo, Sihuan Hu, Mengjie Xia, Pengwei Li, Jie Hu, Gang Li, Huabei Jiang, and Wendong Zhang, (2017). “A Flexible Lead-Free $BaTiO_3$/PDMS/C Composite Nanogenerator as a Piezoelectric Energy Harvester” Energy Technology.

[21] Chen, Xiaoliang Li, Xiangming Shao, Jinyou An, Ningli Tian, Hongmiao Wang, Chao Han, Tianyi Wang, li Lu and Bingheng (2017). High-Performance Piezoelectric Nanogenerators with Imprinted P(VDF-TrFE)/$BaTiO_3$ Nanocomposite Micropillars for Self-Powered Flexible Sensors.

[22] Baek, S.-H. and I.-K. Park (2017). "Flexible piezoelectric nanogenerators based on a transferred ZnO nanorod/Si micro-pillar array." Nanotechnology 28(9): 095401.

[23] Zhang, Chen Fan, Youjun Li, Huayang Li, Yayuan Zhang, Lei Cao, Shubo Kuang, Shuangyang Zhao, Yongbin Chen, Aihua Zhu, Guang Wang and Zhong Lin. (2018). "Fully Rollable Lead-Free Poly(vinylidene fluoride)-Niobate-Based Nanogenerator with Ultra-Flexible Nano-Network Electrodes." ACS Nano 12(5): 4803-4811.

[24] Parangusan, Hemalatha Ponnamma, Deepalekshmi Al-Maadeed and Mariam Al Ali. (2018). "Stretchable Electrospun PVDF-HFP/Co-ZnO Nanofibers as Piezoelectric Nanogenerators." Scientific Reports 8(1): 754.

[25] Baek, Changyeon Yun, Jong Hyuk Wang, Hee Seung Wang, Ji Eun Park, Hyeonbin Park, Kwi-Il Kim and Do Kyung. (2018). "Enhanced output performance of a lead-free nanocomposite generator using $BaTiO_3$ nanoparticles and nanowires filler." Applied Surface Science 4(29): 164-170.

CHAPTER 3

RESEARCH METHODOLOGY

This chapter describes the experiment details for the synthesis of plate-like $NaNbO_3$ nanostructure from the molten salt method, pure flower-like hydroxyapatite nanostructure via the hydrothermal method and pure coral-like hydroxyapatite nanostructure via microwave irradiation. Characterization of powders the fabrication of piezoelectric materials and Measurement electrical output.

3.1 Glasswares and equipments

- Beakers 10 ml, 25 ml and 600 ml.
- Mould 30 × 30 mm.
- Cylinders 100 ml and 250 ml.
- Filler paper no. 2
- Foils
- Magnetic bar
- Microwave oven
- Oven
- Pestle mortar
- Petri dishes
- Planetary milling machine
- Spatula
- Spoon
- Stainless steel Teflon-lined autoclave
- Universal indicator papers
- Vacuum filter

3.2 Synthesis of pure plate-like $NaNbO_3$ nanostructure from molten salts

3.2.1 Reagents

- Bismuth oxide (Bi_2O_3), > Quality Reagent Chemical Company, Ltd., Thailand, 99.5% purity.
- Niobium oxide (Nb_2O_5), > Inframat Advanced Materials Company, Ltd., U.S.A, 99.9% purity.
- Sodium carbonate (Na_2CO_3), > Riedel-de Haen, France, 99.8% purity.
- Sodium chloride (NaCl), > Xi'an Chemical Reagent Co., Ltd., Shaanxi, China, 99.5% purity.
- De-ionized water
- Nitric acid 65% (HNO_3), > CARLO ERBA reagents Company, Ltd., U.S.A, 64–66%wt.

3.2.2 Experimental producers

3.2.2.1 Synthesis of Bismuth sodium niobium oxide ($Bi_{2.5}Na_{3.5}Nb_5O_{18}$; BNN) via molten salt method.

3.2.2.1.1 Starting materials of Na_2CO_3, Bi_2O_3, and Nb_2O_5 weighed according to the stoichiometric ratios

3.2.2.1.2 NaCl salt was added in the ratio 1:1.5 and ball-milled together in ethanol for 30 minutes.

3.2.2.1.3 Evaporate solvent by using magnetic stirred and dried at 90°C overnight.

3.2.2.1.4 Transferred to the alumina crucibles.

3.2.2.1.5 Then, they were calcine at 1125°C for 4 hours.

3.2.2.1.6 At the end of the calcination, the remaining salt was washed using hot de-ionized water several times and Chloride ions content measured by titration with 0.01M $AgNo_3$ solution.

3.2.2.1.7 BNN particles were obtained. The experimental steps are illustrated in Figure 3.1.

$$1.75Na_2CO_{3\,(s)} + 1.25Bi_2O_{3\,(s)} + 2.5Nb_2O_{5\,(s)} \longrightarrow Bi2.5Na_{3.5}Nb_5O_{18\,(s)} + 1.75CO_{2\,(g)} \quad (1)$$

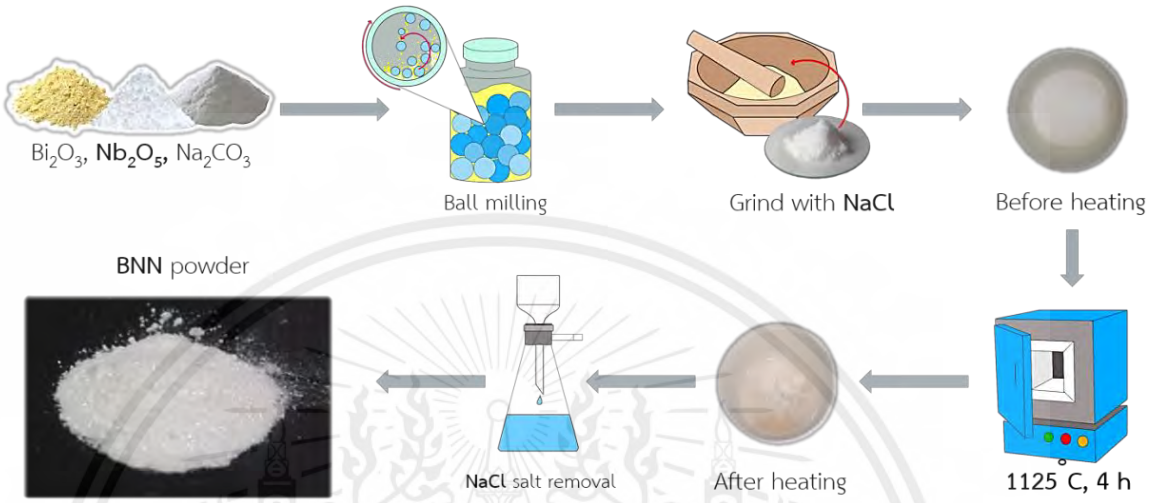

Figure 3.1 Experimental step for the synthesis of Bismuth sodium niobium oxide ($Bi_{2.5}Na_{3.5}Nb_5O_{18}$; BNN) via molten salt method.

3.2.2.2 Synthesis of pure plate-like $NaNbO_3$ (NN) nanostructure via molten salt

3.2.2.2.1 $Bi_{2.5}Na_{3.5}Nb_5O_{18}$ precursor was ground with Na_2CO_3 by pestle mortar in the ratio 1:1.5 by weight.

3.2.2.2.2 Mixed with mixed powder and NaCl salt by pestle and mortar in the ratio 1:1.5 by weight.

3.2.2.2.3 Calcined at 1000°C for 4 hours.

3.2.2.2.4 Washed using hot de-ionized water to remove NaCl.

3.2.2.2.5 Soaked in 30% HNO_3 for 2 hours to remove Bi_2O_3.

3.2.2.2.6 Washed using hot de-ionized water to remove HNO_3 and $NaNbO_3$ particles were obtained. The experimental step are illustrated in Figure 3.2.

$$Bi_{2.5}Na_{3.5}Nb_5O_{18\,(s)} + 0.75Na_2CO_{3\,(s)} \longrightarrow 5NaNbO_{3\,(s)} + 1.25Bi_2O_{3\,(s)} + 0.75CO_{2\,(g)} \quad (2)$$

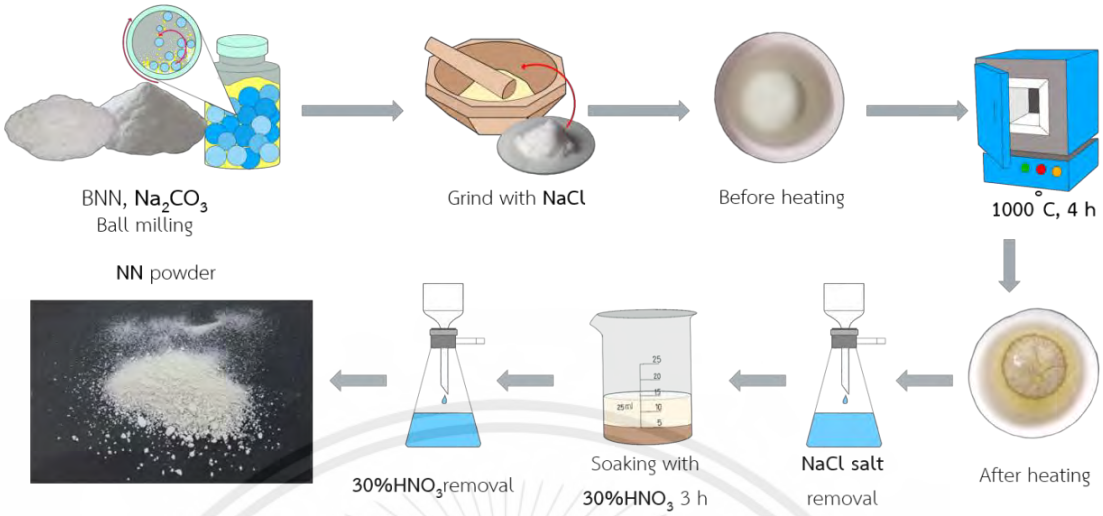

Figure 3.2 Experimental steps for synthesis of pure plate-like NN nanostructure via molten salt.

3.3 Synthesis of pure flower-like HA nanostructure via the hydrothermal method

3.3.1 Reagents

- Calcium chloride ($CaCl_2 2H_2O$), > Synthesis
- Ethylenediaminetetraacetic acid dissolution salt (EDTA), > CARLO ERBA reagents company, Ltd., U.S.A, 100.0% ± 1% purity.
- Di-potassium hydrogen phosphate anhydrous (K_2HPO_4), >, CARLO ERBA reagents company, Ltd., U.S.A, 99.0% purity.
- Potassium hydroxide pallets (KOH), > CARLO ERBA reagents company, Ltd., U.S.A, 98.0% purity.
- Distillated water.

3.3.2 Experimental procedure

3.3.2.1 Dissolved 0.012 mol of K_2HPO_4 and 0.012 mol of EDTA in 50 ml of distilled water.

3.3.2.2 The pH value was adjusted to 12 with the addition of KOH.

3.3.2.3 Heated and stirred the solution at 50 °C for 1.5 h.

3.3.2.4 Dissolved 0.02 mol of $CaCl_2 \cdot 2H_2O$ in 30 mL of distilled water.

3.3.2.5 Dropped the $CaCl_2 \cdot 2H_2O$ solution to the solution of K_2HPO_4 and EDTA and stirred for 15 min. (the resulted milky suspension)

3.3.2.6 Poured the suspension into a stainless steel Teflon-lined autoclave and heated in an oven at 200°C for 15 h, followed by natural cooling to room temperature.

3.3.2.7 Precipitates were filtered and washed several times with distillated water followed by ethanol. The experimental step are illustrated in Figure 3.3

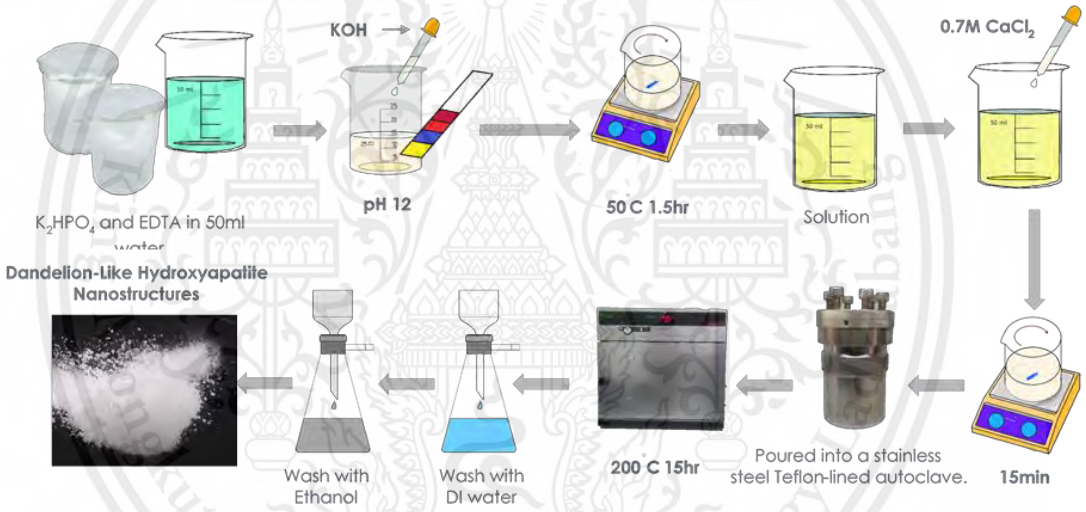

Figure 3.3 Experimental steps for obtaining pure flower-like HA nanostructure via hydrothermal method.

3.4 Synthesis of pure coral-like HA nanostructure via microwave irradiation

3.4.1 Reagents

- Calcium carbonate ($CaCO_3$), > Riedel-de Haen, France, 98.5% purity.
- Ethylenediaminetetraacetic acid dissolution salt (EDTA), > CARLO ERBA reagents company, Ltd., U.S.A, 100.0% ± 1% purity.

- Di-sodium hydrogen phosphate (Na_2HPO_4), >, CARLO ERBA reagents company, Ltd., U.S.A, 99.0% purity.
- Sodium hydroxide (NaOH), > CARLO ERBA reagents company, Ltd., U.S.A, 98.0% purity.
- Distillated water

3.4.2 Experimental procedure

3.4.2.1 Starting material, 1 g $CaCO_3$ powder was mixed with 0.1 mol/dm^3 of EDTA in water to form Ca-EDTA complex.

3.4.2.2 The 0.06 mol/dm^3 of Na_2HPO_3 solution was slowly added to the Ca- EDTA complex and stirred for 30 minutes (pH=8).

3.4.2.3 NaOH solution was added to adjust the solution pH to 13.

3.4.2.4 Then, the solution was transferred to a microwave oven (2.45 GHz, 600 W, LG, India) for 10 minutes.

3.4.2.5 The resulting white precipitate was washed with DI-water and dried at 110°C for 5 hours. The experimental step are illustrated in Figure 3.4.

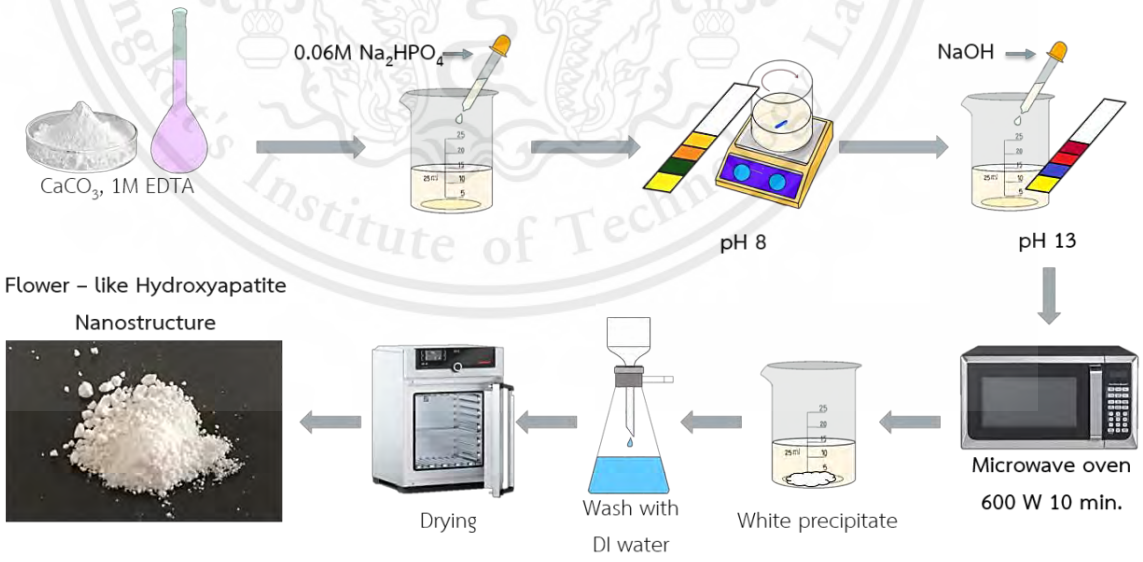

Figure 3.4 Experimental steps for obtaining pure coral-like HA nanostructure via microwave irradiation.

3.5 Fabrication of the oxide-PDMS piezoelectric composites nanogenerators

3.5.1 Reagents

- Polydimethylsiloxane (PDMS), > SYLGARD 184 Silicone Elastomer Kit, Ltd., U.S.A.
- Curing agent, > SYLGARD 184 Silicone Elastomer Kit, Ltd., U.S.A.
- Barium titanate ($BaTiO_3$, BT), > Inframat Advanced Materials Company, Ltd., U.S.A, 99.95% purity.
- Zinc oxide (ZnO), > Fluka company, Ltd., U.S.A. 99.0% purity.
- Pure plate-like $NaNbO_3$ nanostructure from molten salts method. ($NaNbO_3$, NN),> from step 3.2.
- Pure flower-like hydroxyapatite nanostructure via hydrothermal method. (HA),> from step 3.3.
- Pure coral-like hydroxyapatite nanostructure via microwave irradiation. (HA),> from step 3.4.

3.5.2 Experimental producers

3.5.2.1 We mixed the polydimethylsiloxane (PDMS) with curing agent in the ratio 10: 1 by weight.

3.5.2.2 Weighted viscous PDMS in the 30x30 mm a plastic mole ~1 g. Wait for 3, 4 and 5 hours for coagulation.

3.5.2.3 Dispersed BT, ZnO, NN flower-like HA or coral-like HA in the 30 x 30 mm a plastic mould.

3.5.2.4 Remove the composite from the plastic mould and wash it with water.

3.5.2.5 Weigh the composite

3.5.2.6 Complete a piezoelectric nanogenerator with copper sheets, copper wires and kapton tape. The experimental step are illustrated in Figure 3.5.

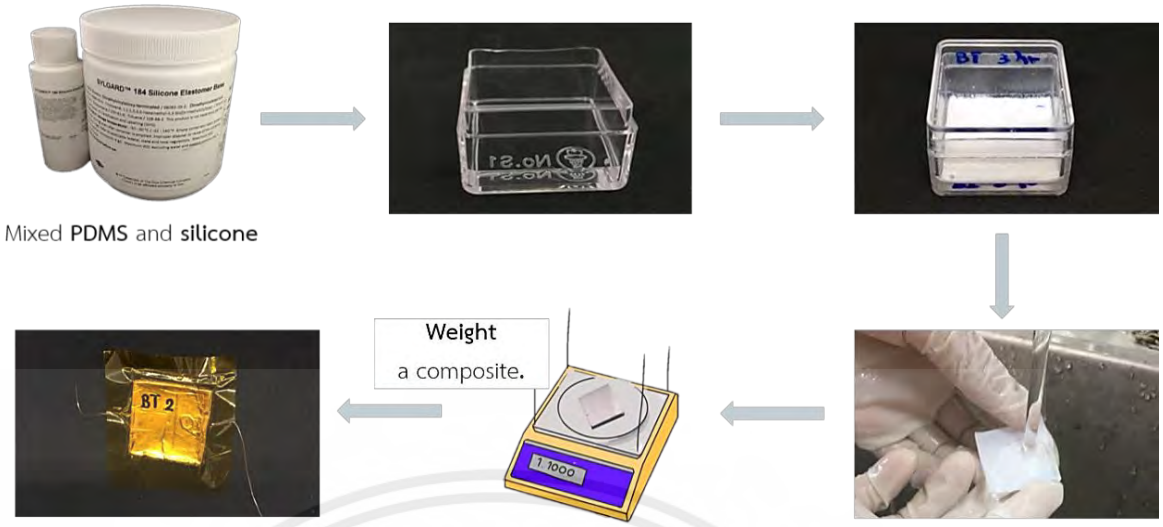

Figure 3.5 Experimental steps for fabrication of oxide-PDMS piezoelectric composites nanogenerators.

3.6 Characterization

3.6.1 X-Ray Diffractometer (XRD)

The purity powders was examined by X-Ray Diffractometer (XRD; Bruker AXS, D8 Advance) both in quality and quantity. Powder was grind to 2-10 μm and put in sample holder. BT and ZnO with a CuK_{α} radiation source in the 2Θ range of 20–120°, pure plate-like $NaNbO_3$ nanostructure from molten salt in the 2Θ range of 20–80°, pure flower-like hydroxyapatite nanostructure via hydrothermal method and pure coral-like hydroxyapatite via microwave irradiation in the 2Θ range of 20 – 60°. Then compared to the JCPDS database. [1-3]

Figure 3.6 X-Ray Diffractometer (XRD; Bruker AXS, D8 Advance) [21].

3.6.2 Fourier Transform Infrared Spectroscopy (FT-IR)

FT-IR can show the functional groups in the substance detect contaminants and non-crystalline. The phase identification was supported by the detecting of functional groups via Fourier Transform Infrared Spectroscopy (FT-IR; Spectrum GX). Thin solid pellets were prepared in potassium bromide (KBr). The FT-IR spectra were recorded from 4000 to 400 cm^{-1}. [5],[6].

Figure 3.7 Fourier Transform Infrared Spectroscopy (FT-IR; Spectrum GX) [20].

Figure 3.8 Manual Hydraulic Press for FT-IR [20].

3.6.3 Scanning electron microscope (SEM)

3.6.3.1 Powders

The morphological characterization was performed by field-emission scanning electron microscope (FE-SEM, Hitachi 54700 model). The powder was dispersed in ethanol and sonicated in an ultrasonic bath for 20 min before dropping onto the copper tape. All samples were then coated with a thin layer of gold for 120s to facilitate electrical conduction. Then the supports are placed inside the microscope which creates high vacuum and 5 keV of electron beam energy. [8],[9].

3.6.3.2 Piezoelectric composites

The morphological characterization was performed by field-emission scanning electron microscope (SEM; FEI, Quanta 250 model). The composites were soaked in liquid nitrogen and stuck on a stub. All samples were then coated with a thin layer of gold for 120s to facilitate electrical conduction. Then the supports are placed inside the microscope which creates high vacuum and 5 keV of electron beam energy.

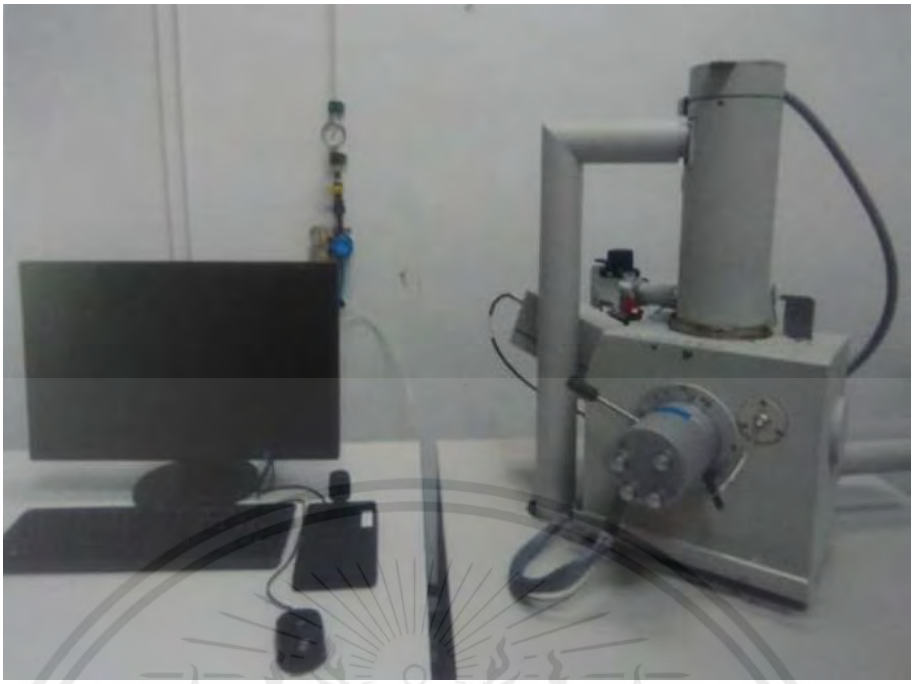

Figure 3.9 Scanning electron microscope (SEM; FEI, Quanta 250 model) [21].

3.7 Measurement of electrical properties

Measure the voltage, electrical and related properties of piezoelectric materials, in relation to the powder morphology and chemical composition, show a vital role in understanding the physical mechanism, as well as its practical benefit for device in nanoapplication, under the electrical properties of nonlinear dielectric or ferroelectric materials. We were concerned to study piezoelectric properties. We used an oscilloscope and digital multimeter (DM3058E, Rigol) installed in a home-made automatic pressing machine. A brief theoretical explanation of piezoelectric properties follows.

3.7.1 Piezoelectric nanogenerator

A piezoelectric nanogenerator was attached on blue stage of compression machine. Turn on switch for stamp it. Using a time base of 500 milliseconds and collecting data for 5 cycles, each 30s. Voltage and current output were shown in Oscilloscope. Then create a graph between voltage/current and time. [10-12].

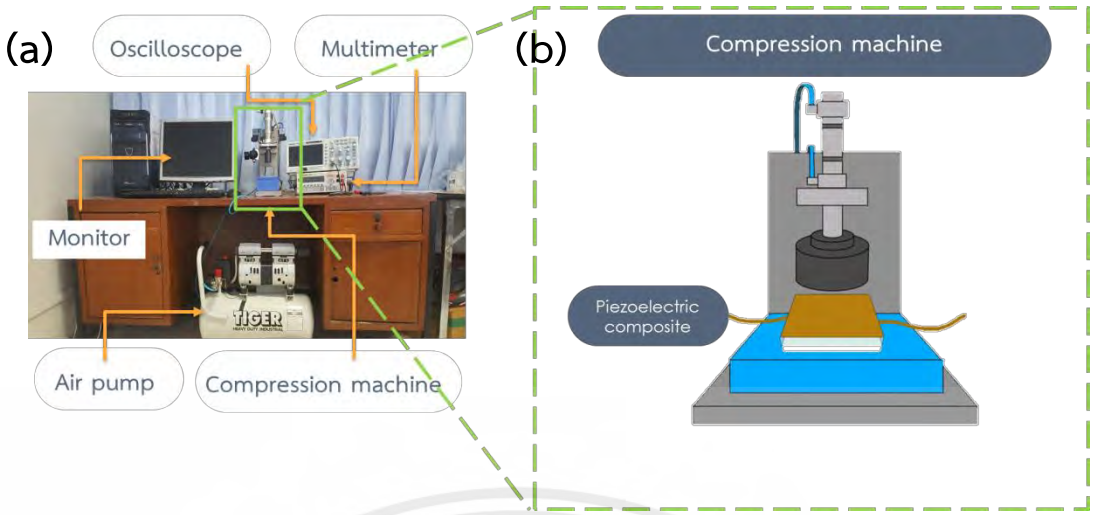

Figure 3.10 (a) Real picture of Electrical equipment series for piezoelectric materials. (b) Schematic illustration of the piezoelectric nanogenerator electrical measurement process.

3.8 REFERENCES

[1] ศุภฤกษ์ เห็นประเสริฐแท้, (2555). X-ray Diffraction. [Online]. Available: https://www2.mtec.or.th/th/e-magazine/admin/upload/268_12-18.pdf

[2] Synchrotron Light Research Institute, S. L. R. X-Ray Diffract meter (XRD) X-ray diffraction analyzer [Online]. Available: https://www.slri.or.th/bdd/th-x-ray-diffractometer-xrd.html.

[3] Barbara L Dutrow, L. S. U., Christine M. Clark, Eastern Michigan University (2019). X-ray Powder Diffraction (XRD). [Online]. Available: https://serc.carleton.edu/research_education/geochemsheets/techniques/XRD.html.

[4] Encyclopedia., K. (2019). "X-ray crystallography facts for kids." [Online]. Available: https://kids.kiddle.co/X-ray_crystallography.

[5] Synchrotron Light Research Institute, S. L. R. (2011). IR Spectroscopy and Imaging [Online]. Available: https://www.slri.or.th/th/beamline/bl41.html.

[6] อนุชิตโอฬาร, ว. (2546). "FT-IR Imaging." Materials Characterizations". [Online]. Available: https://www2.mtec.or.th/th/e-magazine/admin/upload/212_67-70.pdf.

[7] Synchrotron Light Research Institute, S. L. R. (2011). IR Spectroscopy and Imaging [Online]. Available: https://www.slri.or.th/th/beamline/bl41.html.

[8] ศรีอ่อน, อ. (2559). "หลักการทำงานของกล้องจุลทรรศน์อิเล็กตรอนแบบสแกนนิง." [Online]. Available: https://www2.mtec.or.th/th/e-magazine/admin/upload/299_77.pdf.

[9] Joshi, M. and A. Bhattacharyya (2008). Characterization techniques for nanotechnology applications in textiles.

[10] Garimella, R. C., Raghu Chandra, Garimella V.R.Sastry and Dr.Mohammed Shoeb Mohiuddin. (2015). "Piezo-Gen - An Approach to Generate Electricity from Vibrations." Procedia Earth and Planetary Science 11: 445-456.

[11] นูมหันต์, ว. (2560). เครื่องกำเนิดไฟฟ้านาโน Nanogenerator. [Online]. Available: http://www.productivityware.com/articles/arct148.php

[12] Woodford, C. (2018). Piezoelectricity. [Online]. Available: https://www.explainthatstuff.com/piezoelectricity.html.

[13] Lungu, M. (2004). "Electrical separation of plastic materials using the triboelectric effect." Minerals Engineering 17(1): 69-75.

[14] (2019). "Hamilton Beach 0.9 cu.ft. Microwave Oven, Stainless Steel." [Online]. Available: https://www.walmart.com/ip/Hamilton-Beach-0-9-cu-ft-Microwave-Oven-Stainless-Steel/55124372.

[15] (2019). "จำหน่ายอาหารเลี้ยงเชื้อสำเร็จรูป อุปกรณ์วิทยาศาสตร์ เครื่องแก้ว สารเคมี และอื่นๆ" [Online]. Available: https://www.mpimpex.co.th/product/192/incubator-53-l.

[16] ตึกปฏิบัติการเก่า คณะวิทยาศาสตร์ สถาบันเทคโนโลยีพระจอมเกล้าเจ้าคุณทหารลาดกระบัง.

[17] ศูนย์เครื่องมือ คณะวิทยาศาสตร์ สถาบันเทคโนโลยีพระจอมเกล้าเจ้าคุณทหารลาดกระบัง.

CHAPTER 4

RESULTS AND DISCUSSION

4.1 The synthesis of plate-like $NaNbO_3$ by molten salts

Plate-like sodium niobate ($NaNbO_3$; NN) was successfully synthesized by the molten salt method. After the synthesis, the phase identification of powder products were characterized by (1) Scanning electron microscope (SEM) investigated the morphology and filler phase distribution in piezoelectric composite, (2) X-ray diffraction (XRD) for the confirmations of phase purity and phase formation of NN powders, and (3) Fourier transform infrared (FT-IR) to study functional group in the powder.

4.1.1 Morphology

4.1.1.1 SEM of plate-like NN powder by molten salt method

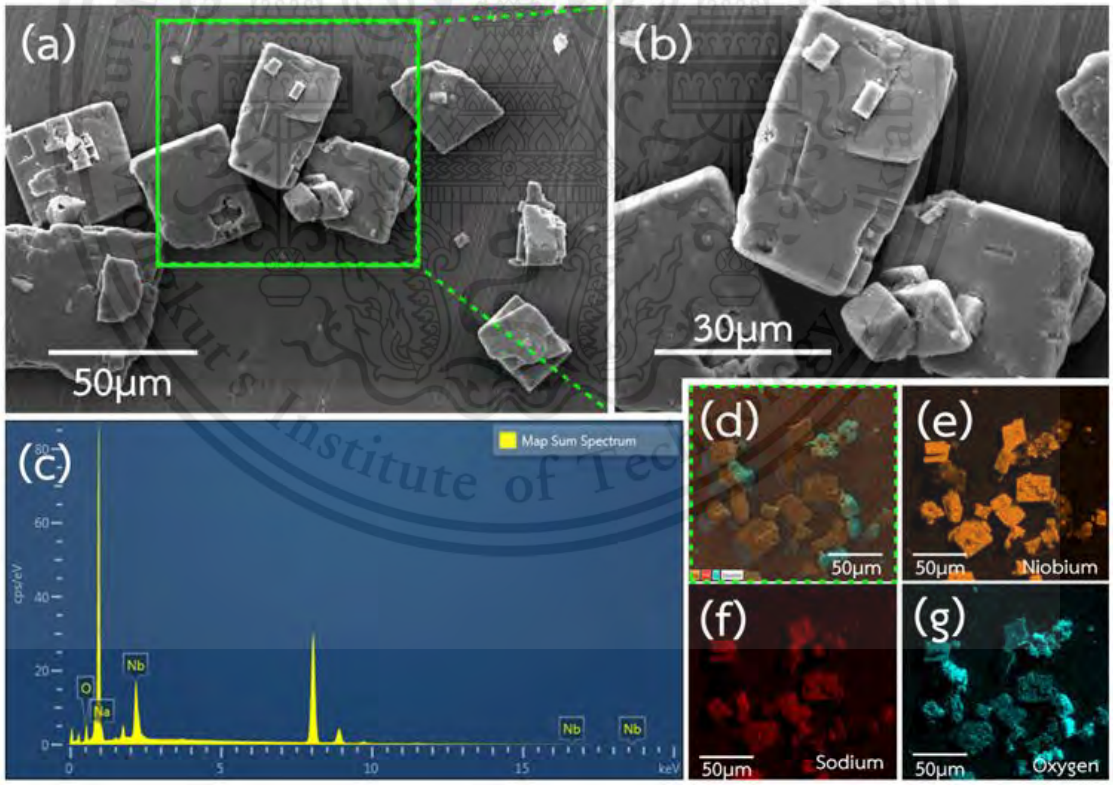

Figure 4.1 SEM images of NN powders in the different magnification of (a) 2000X, (b) 4000X, (c) EDX identifications for spectrum, and (d)-(g) The corresponded EDX matching of elements of NN powder presents the Na, Nb, and O.

According to Figure 4.1 (a) and (b), the NN powder shows plate-like shape with the aspect ratio of NN powder around 1.3 ± 0.4. The corresponding Energy-dispersive X-ray spectroscopy (EDX) matching elements of NN powder has taken presence Na, Nb, and O in obtained NN synthesized powder is shown in Figure 4.1 (c-g).

Table 4.1 The comparison of the aspect ratio for NN from this work with literatures

Sample	Research	Aspect ratio
NN powder	[3]	15-50
NN powder	This work	1.3 ± 0.3

4.1.2 Phase identification

4.1.2.1 X-ray diffraction (XRD) result of plate-like NN powder by molten salt method

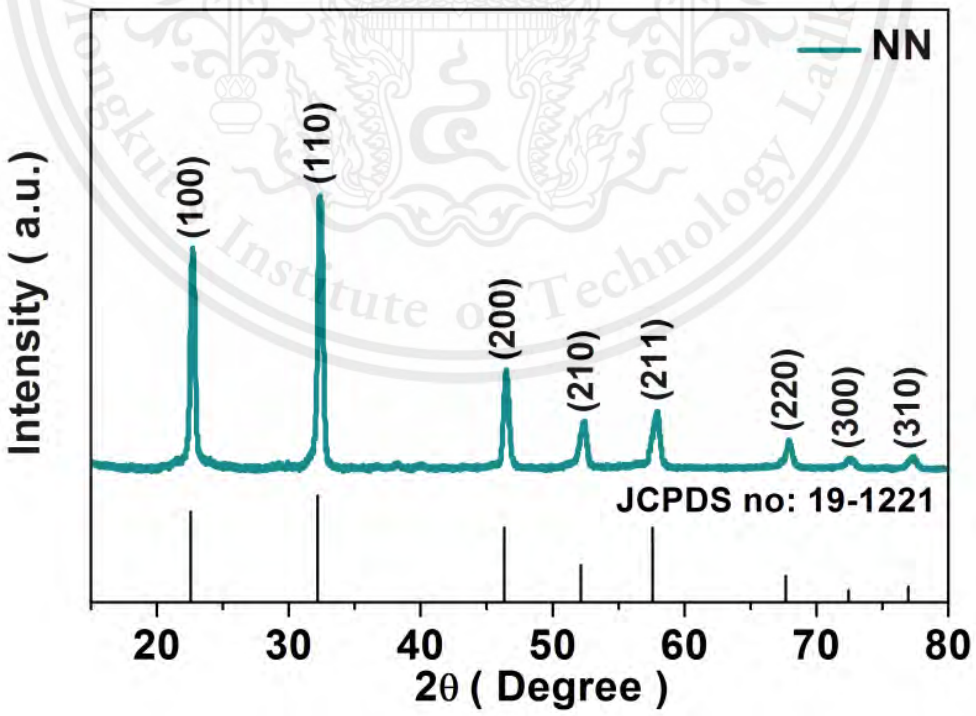

Figure 4.2 XRD pattern of NN powder product synthesized from molten-salt method.

According to Figure 4.2, the XRD pattern of the powder product (green line) shows a single phase of the cubic perovskite NN with no impurity or other secondary phase. The XRD peaks obtained from NN matched well with standard data JCPDF file no: 19-1221.

Table 4.2 Lattice parameter of NN synthesized powder.

Sample	JCPDS no.	Structure	Lattice parameter (Å)		
			a	b	c
NN	PDF no. 19-1221	cubic	3.910	-	-
NN	This work	cubic	3.912 ± 0.005	-	-

4.2.2.1 Fourier transforms infrared (FT-IR) result of plate-like NN powder by molten salt method

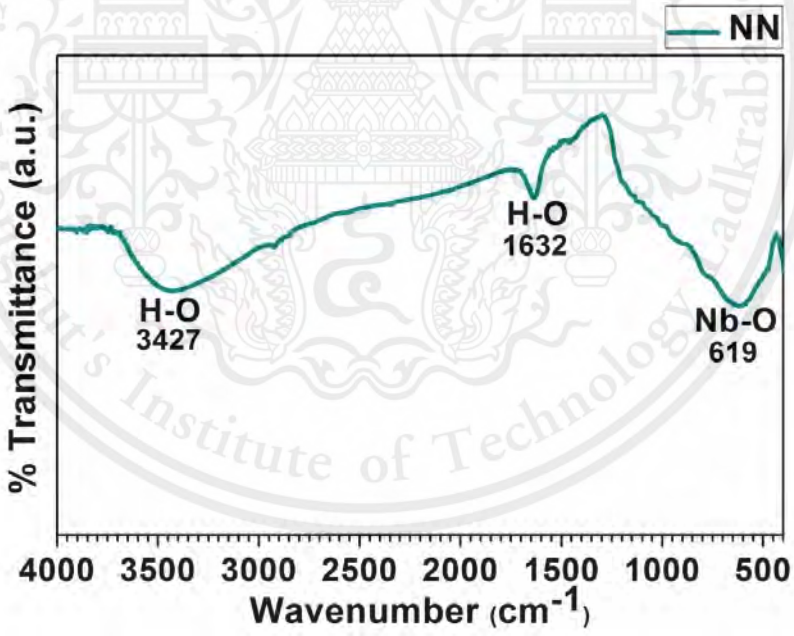

Figure 4.3 FT-IR spectrum of NN powder product synthesized from molten-salt method.

According to the FT-IR result in Figure 4.3, the board peak in the range of 2900-3500 cm^{-1} and 1655 cm^{-1} are attributed to the O-H stretching and O-H bending of the H_2O molecules. They could be come from the moisture in air. The peak at

670cm^{-1} was the characteristic of an asymmetric vibration of the Nb-O in the octahedral of NbO_6.

4.2 The synthesis of hydroxyapatite powder

4.2.1 The synthesis of flower-like hydroxyapatite powder by hydrothermal method

Flower-like hydroxyapatite ($Ca_5(PO_4)_3(OH)$; HA) was successfully synthesized by the hydrothermal method. After the synthesis, the phase identification of powder products were characterized by (1) Scanning electron microscope (SEM) investigated the morphology and filler phase distribution in piezoelectric composite, (2) X-ray diffraction (XRD) for the confirmations of phase purity and phase formation of HA powders, and (3) Fourier transform infrared (FT-IR) to study functional group in the powder

4.2.1.1 Morphology

4.2.1.1.1 SEM of flower-like HA powder synthesized by hydrothermal method

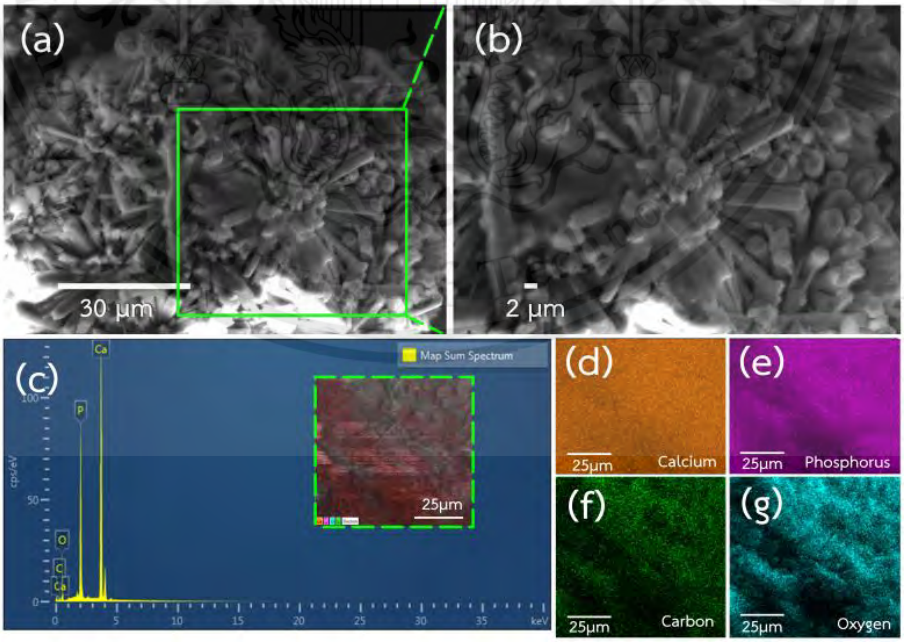

Figure 4.4 SEM images of flower-like HA powders in the different magnification of (a) 2000X, (b) 4000X, (c) EDX identifications for spectrum, and (d)-(g) The corresponded EDX matching of elements of flower-like HA powder presents the Ca, P, C, and O.

According to Figure 4.4 (a) and (b), the flower-like HA powder shows flower-like shape with the aspect ratio of flower-like HA powder around 14.2 ± 5.0. The corresponding EDX matching elements of flower-like HA powder has taken presence Ca, P, C, and O in obtained flower-like HA synthesized powder is shown in Figure 4.4 (c-g).

Table 4.3 The comparison of the aspect ratio for flower-like HA from this work with literatures

Sample	Research	Aspect ratio
Flower-like HA nanopowder	[4]	0.1
Flower-like HA nanopowder	This work	14.2 ± 5.0

4.2.1.2 Phase identification

4.2.1.2.1 X-ray diffraction (XRD) result of flower-like HA powder by hydrothermal method

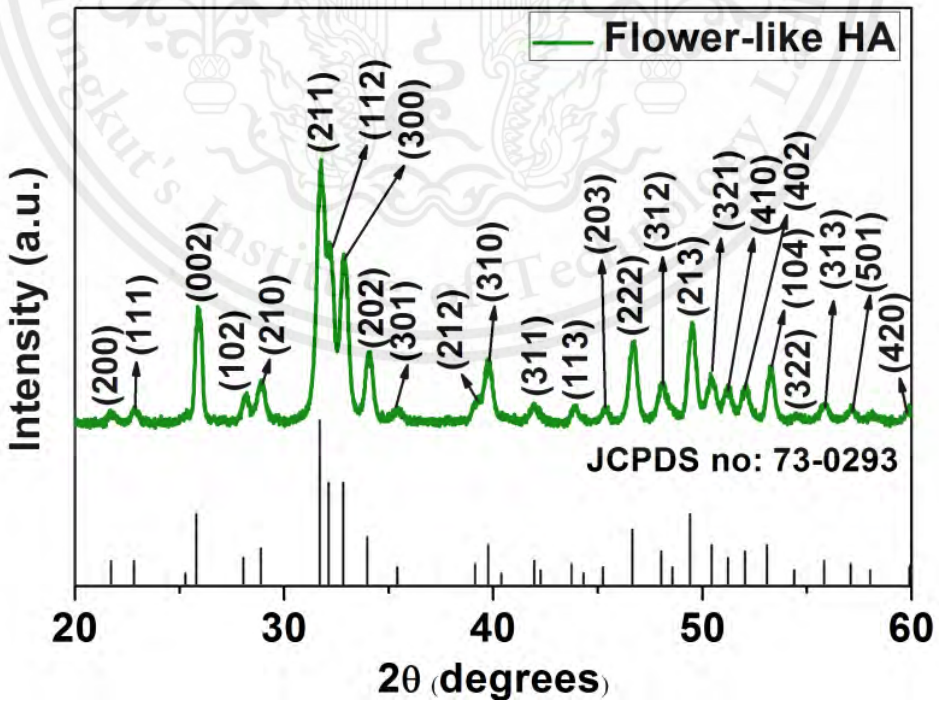

Figure 4.5 XRD pattern of flower-like HA powder product synthesized from hydrothermal method. [5]

According to Figure 4.5, the XRD pattern of the powder product (green line) shows a single phase of the hexagonal HA with no impurity or other secondary phase. The XRD peaks obtained from HA matched well with standard data JCPDF file no: 73-0293.

Table 4.4 Lattice parameter of flower-like HA synthesized powder.

Sample	JCPDS no.	Structure	Lattice parameter (Å)		
			a	b	c
Flower-like HA	PDF no. 709-0432	hexagonal	9.418	-	6.883
Flower-like HA	This work	hexagonal	9.440 ± 0.004	-	6.873 ± 0.004

4.2.1.2.2 Fourier transform infrared (FT-IR) result of flower-like HA powder by hydrothermal method

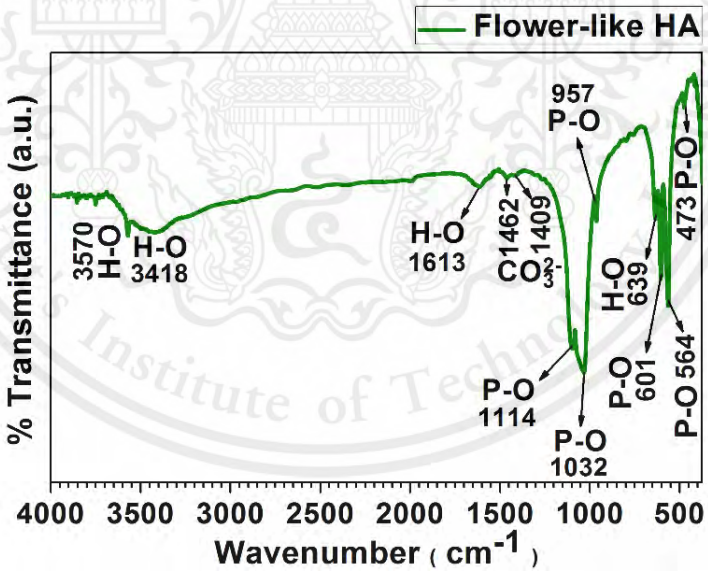

Figure 4.6 FT-IR spectrum of flower-like HA powder product synthesized from hydrothermal method.

Figure 4.6 shows the FT-IR spectrum of the hydroxyapatite powder synthesized via hydrothermal method. The peak at 466 cm^{-1} appeared the phosphate stretching peak. The band at 564 and 601 cm^{-1} are P-O bending and the

symmetric P-O stretching peak appeared at 957 cm^{-1}. The peaks at 1032 and 1114 cm^{-1} are the P-O asymmetric stretching. The O-H stretching peak appeared at 3415 cm^{-1} and O-H bending peak appeared at 639 and 1613 cm^{-1}. The absorption band at 1409-1462 cm^{-1} are presented the carbonate group in HA particles. The crystallinity of HA can be derived from intensities of both the O-H peak and the P-O stretching peak at 957 cm^{-1}.

4.2.2 The synthesis of coral-like hydroxyapatite powder by microwave irradiation method

Coral-like hydroxyapatite ($Ca_5(PO_4)_3(OH)$; HA) was successfully synthesized by the microwave irradiation method. After the synthesis, the phase identification of powder products were characterized by (1) Scanning electron microscope (SEM) investigated the morphology and filler phase distribution in piezoelectric composite, (2) X-ray diffraction (XRD) for the confirmations of phase purity and phase formation of HA powders, and (3) Fourier transform infrared (FT-IR) to study functional group in the powder.

4.2.2.1 Morphology

4.2.2.1.1 SEM of coral-like HA powder by hydrothermal method

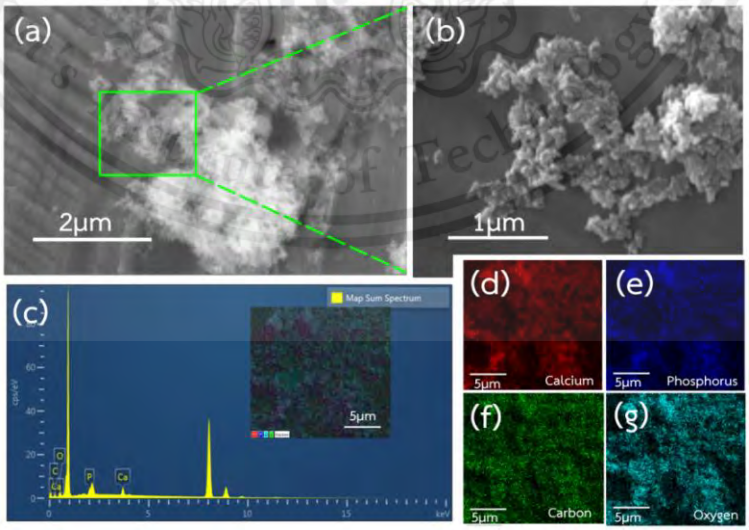

Figure 4.7 SEM images of coral-like powders in the different magnification of (a) 2000X, (b) 4000X, (c) EDX identifications for spectrum, and (d)-(g) The corresponded EDX matching of elements of coral-like HA powder presents the Ca, P, C, and O.

According to Figure 4.7 (a) and (b), the coral-like HA powder shows coral-like shape with the aspect ratio of coral-like HA powder around 14.2 ± 5.0. The corresponding EDX matching elements of flower-like HA powder has taken presence Ca, P, C, and O in obtained coral-like HA synthesized powder is shown in Figure 4.7 (c-g).

Table 4.5 The comparison of the aspect ratio for coral-like HA from this work with literatures.

Sample	Research	Aspect ratio
Coral-like HA nanopowder	[6]	0.200
Coral-like HA nanopowder	This work	3.858 ± 1.190

4.2.2.2 Phase identification

4.2.2.2.1 X-ray diffraction (XRD) result of coral-like HA nanopowder by microwave irradiation method

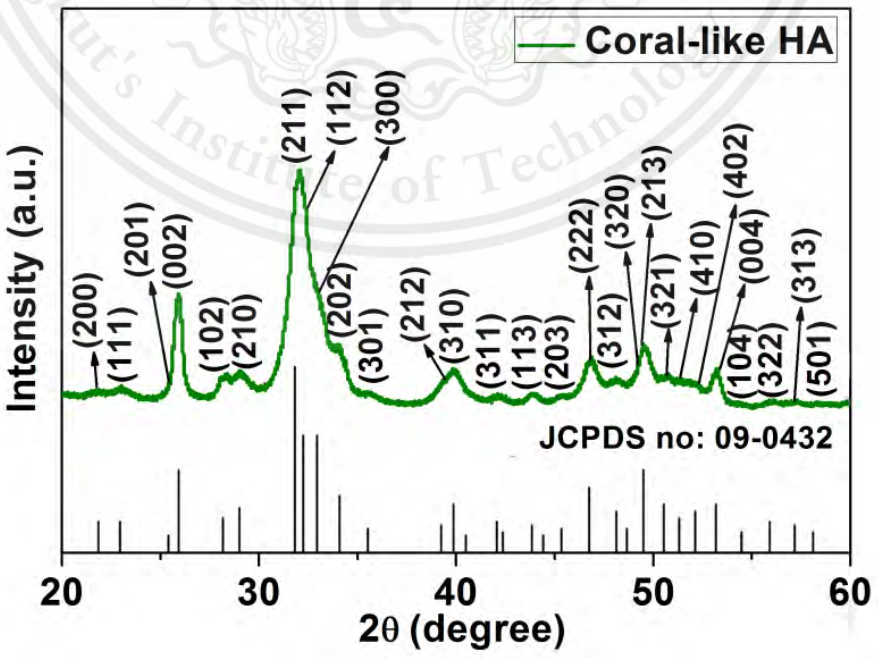

Figure 4.8 FT-IR spectrum of ZnO commercial grade powder.

According to Figure 4.8, the XRD pattern of the powder product (green line) shows a single phase of the hexagonal HA with no impurity or other secondary phase. The XRD peaks obtained from HA matched well with standard data JCPDF file no: 09-0432.

Table 4.6 Lattice parameter of coral-like HA synthesized powder.

Sample	JCPDS no.	Structure	Lattice parameter (Å)		
			a	b	c
Coral-like HA	PDF no. 73-0293	hexagonal	9.418	-	6.883
Coral-like HA	This work	hexagonal	9.497 ± 0.079	-	6.841 ± 0.037

4.2.2.2.2 Fourier transform infrared (FT-IR) result of flower-like HA nanopowder by microwave irradiation method

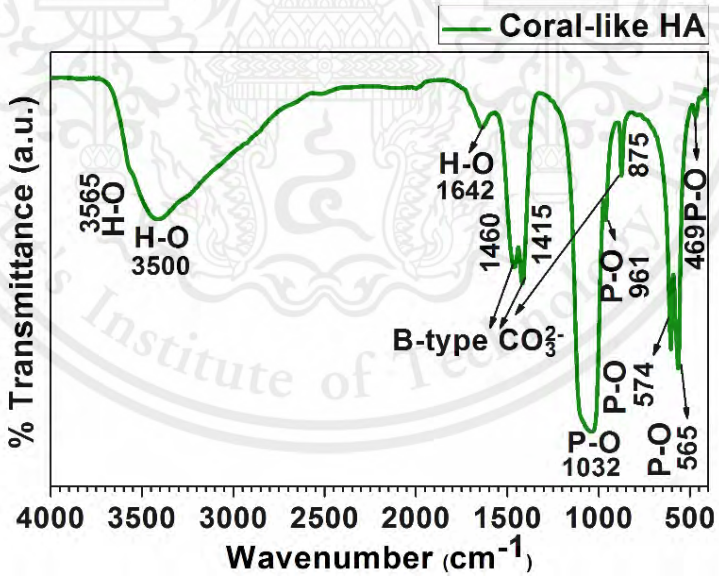

Figure 4.9 FT-IR spectrum of coral-like HA powder product synthesized from microwave irradiation method.

The FT-IR spectrum of the coral-like hydroxyapatite nanopowder is shown in Figure 4.9. The characteristic vibrations of HA appeared phosphate groups at 565 and

574 cm^{-1} along with other phosphate peaks at 469, 961 and 1032 cm^{-1} respectively. The wavenumber at around 3500 cm^{-1} is the broad of the characteristic O-H stretching of HA. The board band expanding from 2500 to 3800 cm^{-1} is stretching mode of the H_2O molecules. The band at 1642 cm^{-1} is bending mode of the H_2O molecules. Moreover, its result showed additional peaks at region 875, 1415 and 1460 cm^{-1} are indicate the formation of b-type carbonate group of HA.

4.3 The $BaTiO_3$ commercial grade nanopowder 99.95% purity

Barium titanate ($BaTiO_3$; BT) commercial grade nanopowder, the phase identification of powder were characterized by (1) Scanning electron microscope (SEM) investigated the morphology and filler phase distribution in piezoelectric composite, (2) X-ray diffraction (XRD) for the confirmations of phase purity and phase formation of BT powders, and (3) Fourier transform infrared (FT-IR) to study functional group in the powder.

4.3.1 Morphology

4.3.1.1 SEM of barium titanate commercial grade nanopowder

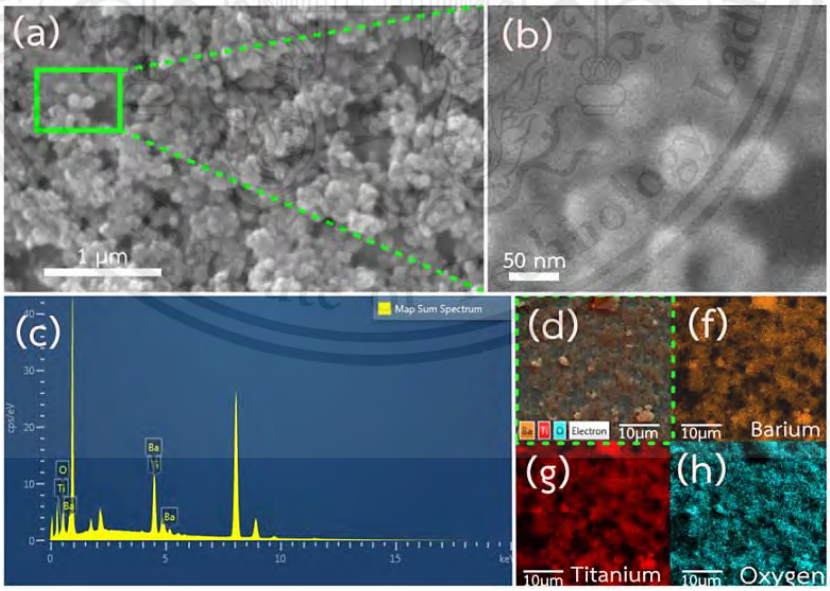

Figure 4.10 SEM images of BT powders in the different magnification of (a) 2000X, (b) 4000X, (c) EDX identifications for spectrum, and (d)-(h) The corresponded EDX matching of elements of BT powder presents the Ba, Ti, and O.

According to Figure 4.10 (a) and (b), the BT powder shows spherical shape with an approximate average size around 105 ± 19.8 nm. The corresponding EDX matching elements of BT powder has taken presence Ba, Ti, and O in BT powder is shown in Figure 4.10 (c-h).

Table 4.7 The comparison of the average particle size for BT nanopowder from this work with literatures.

Sample	Research	Average particle size (nm)
BT nanopowder	[1]	15 - 255
BT nanopowder	This work	105 ± 19.8

4.3.2 Phase identification

4.3.2.1 X-ray diffraction (XRD) result of BT commercial grade nanopowder

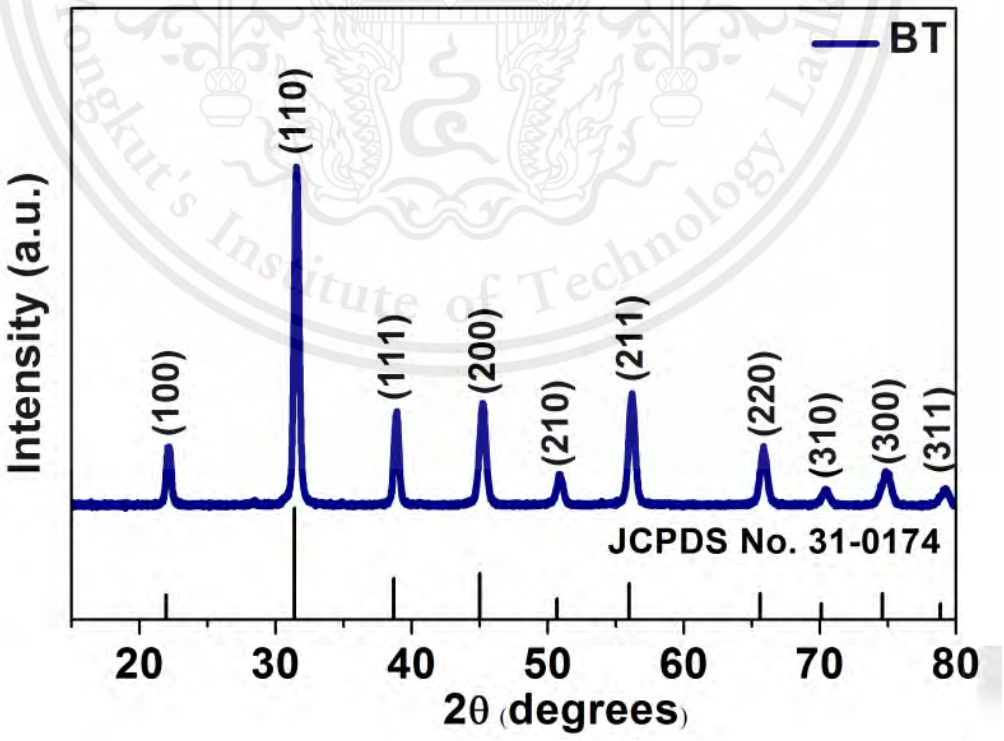

Figure 4.11 XRD pattern of BT commercial grade nanopowder.

According to Figure 4.11, the XRD pattern of the powder product (blue line) shows a single phase of the cubic BT with no impurity or other secondary phase. The XRD peaks obtained from BT matched well with standard data JCPDF file no: 31-0174.

Table 4.8 Lattice parameter of BT nanopowder.

Sample	JCPDS No.	Structure	Lattice parameter (Å)		
			a	b	c
BT	PDF no 31-0174	cubic	4.031	-	-
BT	This work	cubic	4.630 ± 0.006	-	-

4.3.2.2 Fourier transform infrared (FT-IR) result of BT commercial grade nanopowder

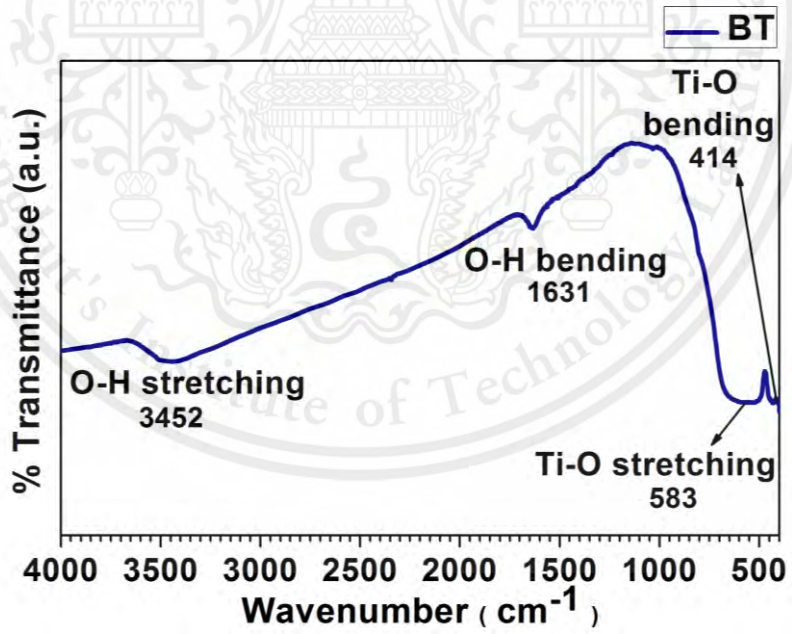

Figure 4.12 FT-IR spectrum of BT commercial grade powder.

The FT-IR spectrum of BT commercial grade nanopowder is shown in Figure 4.12. The broad peak at 3452 and 1631 cm^{-1} are indicated to the O-H stretching and

O-H bending of the H_2O molecules. The peak at 583 and 414 cm^{-1} represents the characteristic of stretching and asymmetric vibration of the Ti-O.

4.4 The ZnO commercial grade nanopowder

Zinc oxide (ZnO) commercial grade nanopowder, the phase identification of powder were characterized by (1) Scanning electron microscope (SEM) investigated the morphology and filler phase distribution in piezoelectric composite, (2) X-ray diffraction (XRD) for the confirmations of phase purity and phase formation of ZnO powders, and (3) Fourier transform infrared (FT-IR) to study functional group in the powder.

4.4.1 Morphology

4.4.1.1 SEM of ZnO commercial grade nanopowder

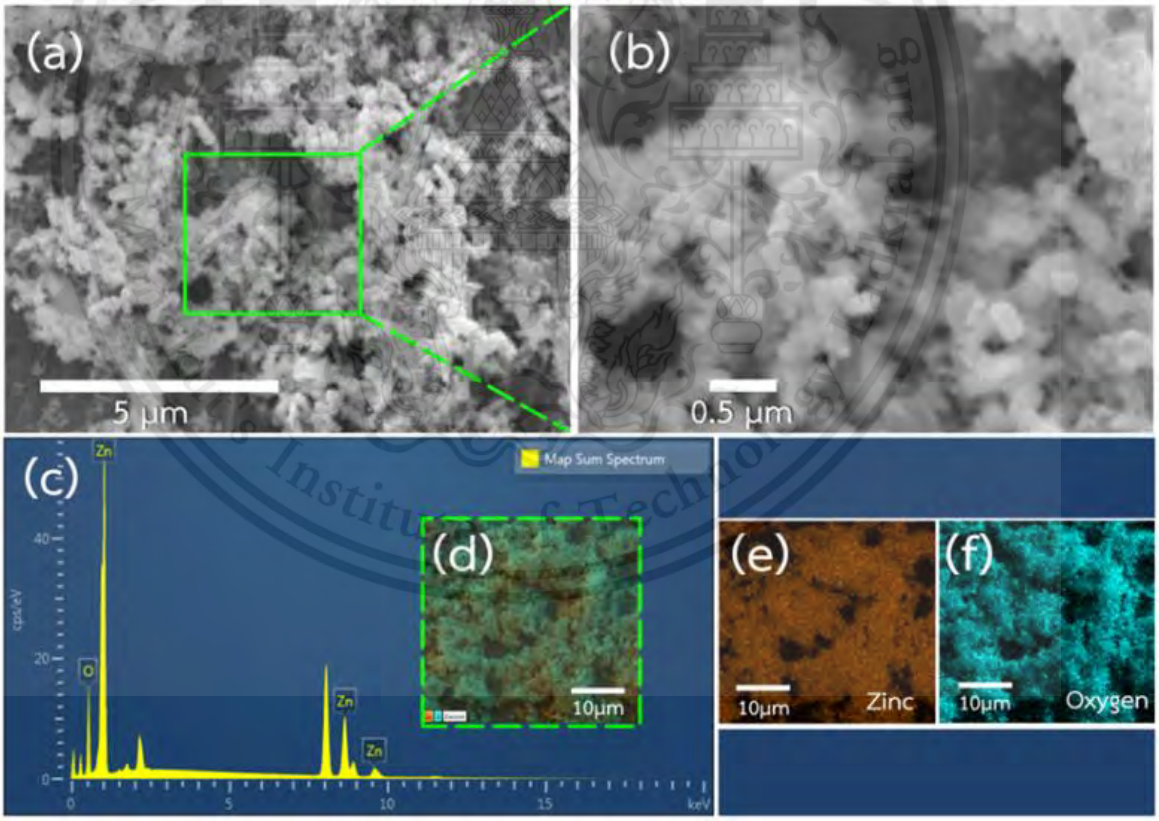

Figure 4.13 SEM images of ZnO powders in the different magnification of (a) 2000X, (b) 4000X, (c) EDX identifications for spectrum, and (d)-(h) the corresponded EDX matching of elements of ZnO powder presents the Zn and O.

According to Figure 4.13 (a) and (b), the ZnO powder shows nearly spherical shape with an approximate average size around 64 ± 26.2 nm. The corresponding EDX matching elements of ZnO powder has taken presence Zn and O in ZnO is shown in Figure 4.13 (c-f).

Table 4.9 The comparison of the average particle size for ZnO nanopowder from this work with literatures.

Sample	Research	Average particle size (nm)
ZnO nanopowder	[2]	159
ZnO nanopowder	This work	64 ± 26.2

4.4.2 Phase identification

4.4.2.1 X-ray diffraction (XRD) result of ZnO commercial grade nanopowder

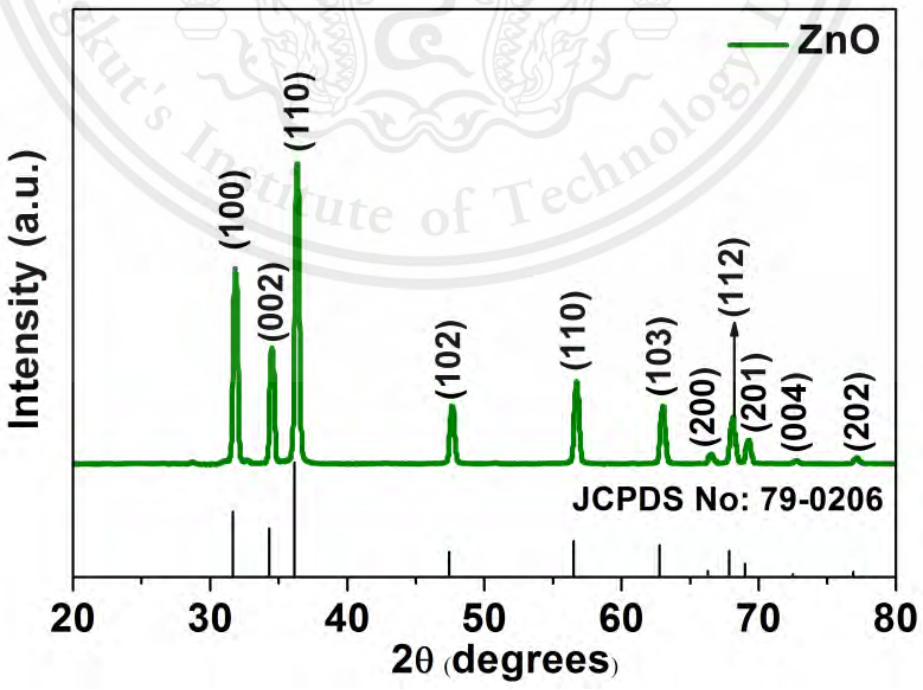

Figure 4.14 XRD pattern of ZnO commercial grade nanopowder.

According to Figure 4.14, the XRD pattern of the powder product (green line) shows a single phase of the hexagonal ZnO with no impurity or other secondary phase. The XRD peaks obtained from ZnO matched well with standard data JCPDF file no: 79-0206.

Table 4.10 Lattice parameter of ZnO nanopowder.

Sample	JCPDS No.	Structure	Lattice parameter (Å)		
			a	b	c
ZnO	PDF no. 79-0206	hexagonal	3.250	-	5.207
ZnO	This work	hexagonal	3.245 ± 0.001	-	5.200 ± 0.000

4.4.2.2 Fourier transform infrared (FT-IR) result of ZnO commercial grade nanopowder

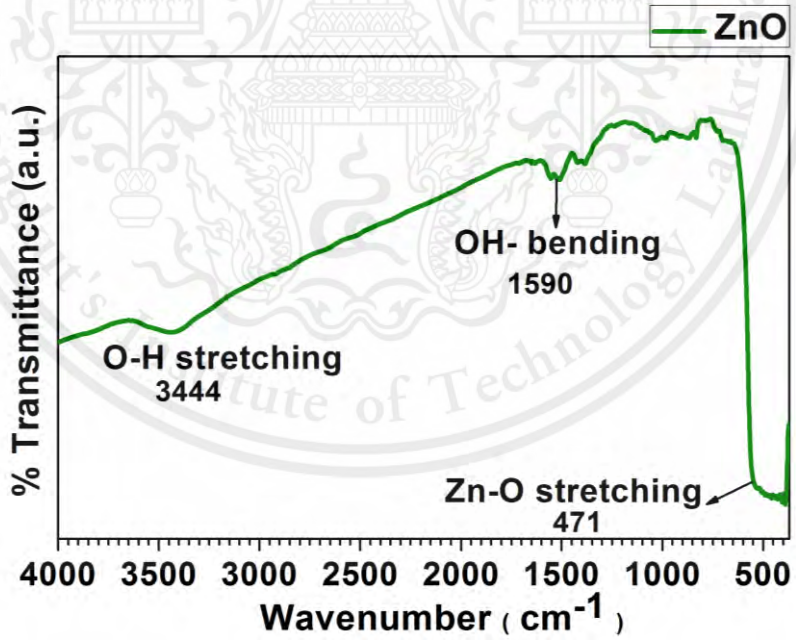

Figure 4.15 FT-IR spectrum of ZnO commercial grade powder.

The FT-IR spectrum of ZnO commercial grade nanopowder is shown in Figure 4.15. The broad peaks at 3444 cm^{-1} correspond to the O-H stretching vibrations. The stretching vibrations of C=O and the stretching vibrations of Zn-OH are observed at

1590 and 900 cm^{-1}. The characteristic absorptions band of Zn-O stretching vibrations represent at 471 cm^{-1}.

4.5 The piezoelectric composite

4.5.1 NN/PDMS composite

4.5.1.1 Morphology

4.5.1.1.1 Scanning electron microscope (SEM)

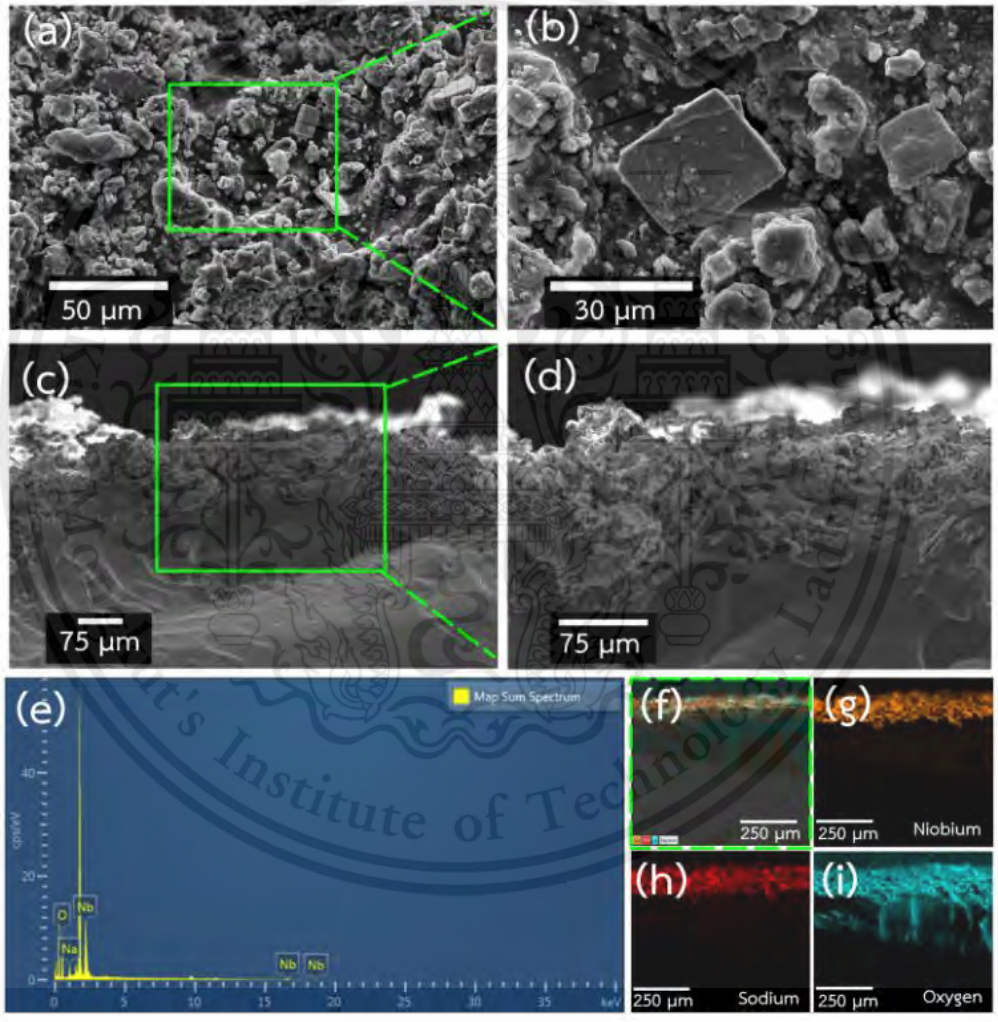

Figure 4.16 SEM images showing (a) and (b) the surface area with different magnification (2000X and 4000X), (c) and (d) the cross-section of composite film with different magnification (500X and 1000X). (e) EDX identifications of spectrum and (f)-(i) element mapping forms of NN/PDMS piezoelectric composite at curing time 3 hr.

The SEM images of NN/PDMS composite are different magnification shows the surface areas are shown in Figure 4.16 (a) and (b). The top area of composite has powder distribute all over, there is no space and NN powder is agglomerate. And the cross-section of NN/PDMS composite with different magnification are shown in Figure 4.16 (c) and (d). The corresponding EDX matching elements of NN/PDMS composite indicated the presence of Na, Nb, and O is shown in Figure 4.16 (e-i).

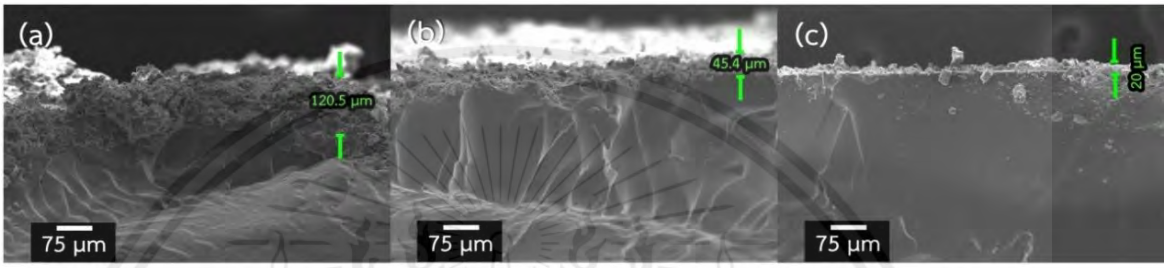

Figure 4.17 Cross section of NN/PDMS composite with difference curing time 3, 4 and 5 hr.

Figure 4.17 shows the cross section of NN/PDMS composite; (a) cross section at curing time 3 hr., the composite has a thickness around 3.990 ± 1.062 µm, (b) cross section at curing time 4 hr., the composite has a thickness around 1.506 ± 0.621 µm, and (c) cross section at curing time 5 hr., the composite has a thickness around 0.663 ± 0.440 µm.

4.5.1.2 Electrical output of NN/PDMS composite

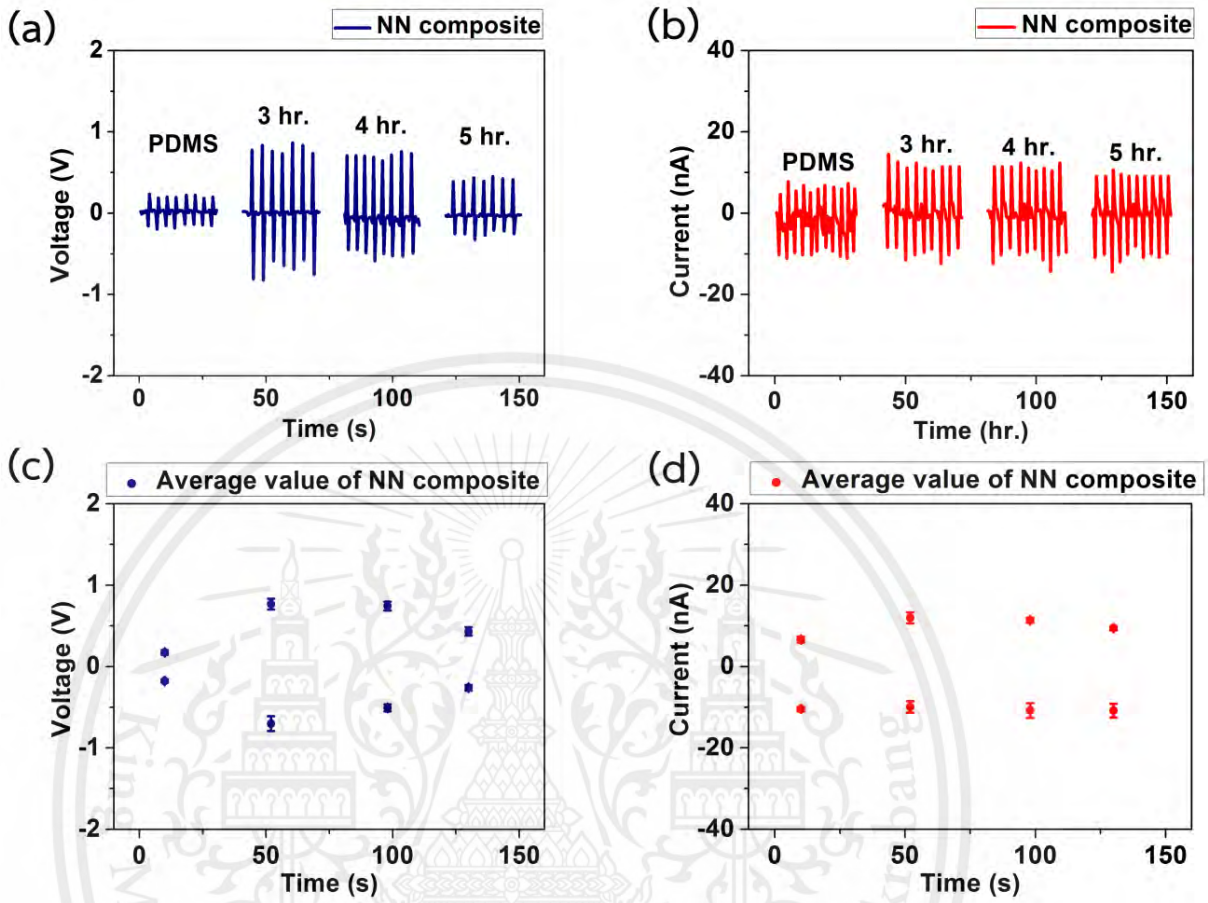

Figure 4.18 Electrical output: (a) The output voltage; (b) The output current; (c) Average positive-negative value of the output voltage; (d) Average positive-negative value of the output current for NN/PDMS piezoelectric composite with different curing time at 3, 4 and 5 hr.

The output voltage and average output voltage of NN/PDMS composite are shown in Figure 4.18 (a) and (c). The output voltage at curing time 3 hr. around 0.768 ± 0.067 V, at curing time 4 hr. around 0.743 ± 0.055 V and at curing time 5 hr. around 0.4312 ± 0.051 V, respectively. And the output current and average output current of NN/PDMS composite are shown in Figure 4.18 (b) and (d). of NN/PDMS composite at curing time 3 hr. around 11.935 ± 1.160 nA, at curing time 4 hr. around 11.396 ± 0.683 nA and at curing time 5 hr. around 9.425 ± 0.453 nA, respectively.

4.5.1.3 The effect of curing time of NN/PDMS composite

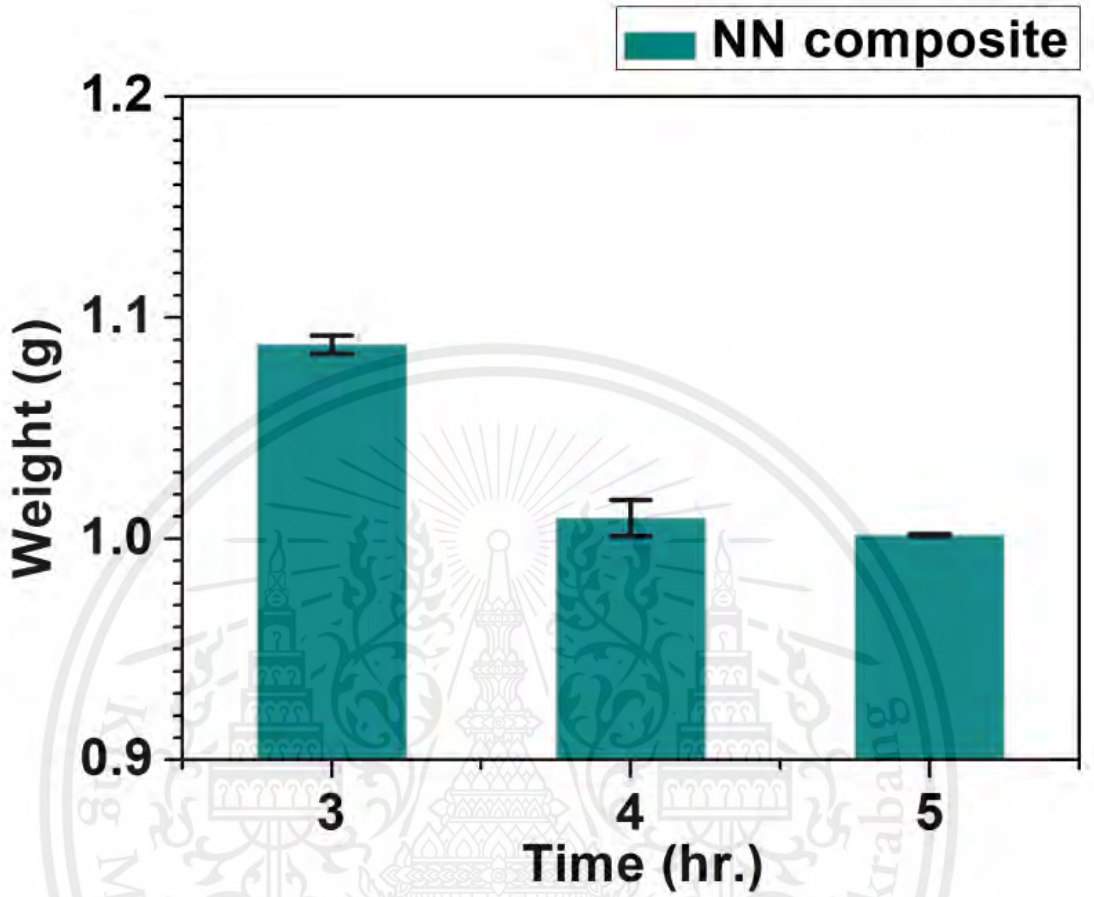

Figure 4.19 Relative between different curing time 3, 4 and 5 hr. and amount of piezoelectric powder that embedded in PDMS matrix for NN/PDMS piezoelectric.

The effect of curing time makes the amount of oxide powder embedded in the composite have different. In Figure 4.19 show the NN/PDMS composite at curing time 3 hr. has the highest amount of powder and it has a weight around 1.088 ± 0.004 g. In part of NN/PDMS composite at curing time 4 and 5 hr. have weight of around 1.009 ± 0.008 g and 1.002 ± 0.001 g, respectively.

4.5.2 HA /PDMS composite

4.5.2.1 Flower-like HA /PDMS composite

4.5.2.1.1 Morphology

4.5.2.1.1.1 Scanning electron microscope (SEM)

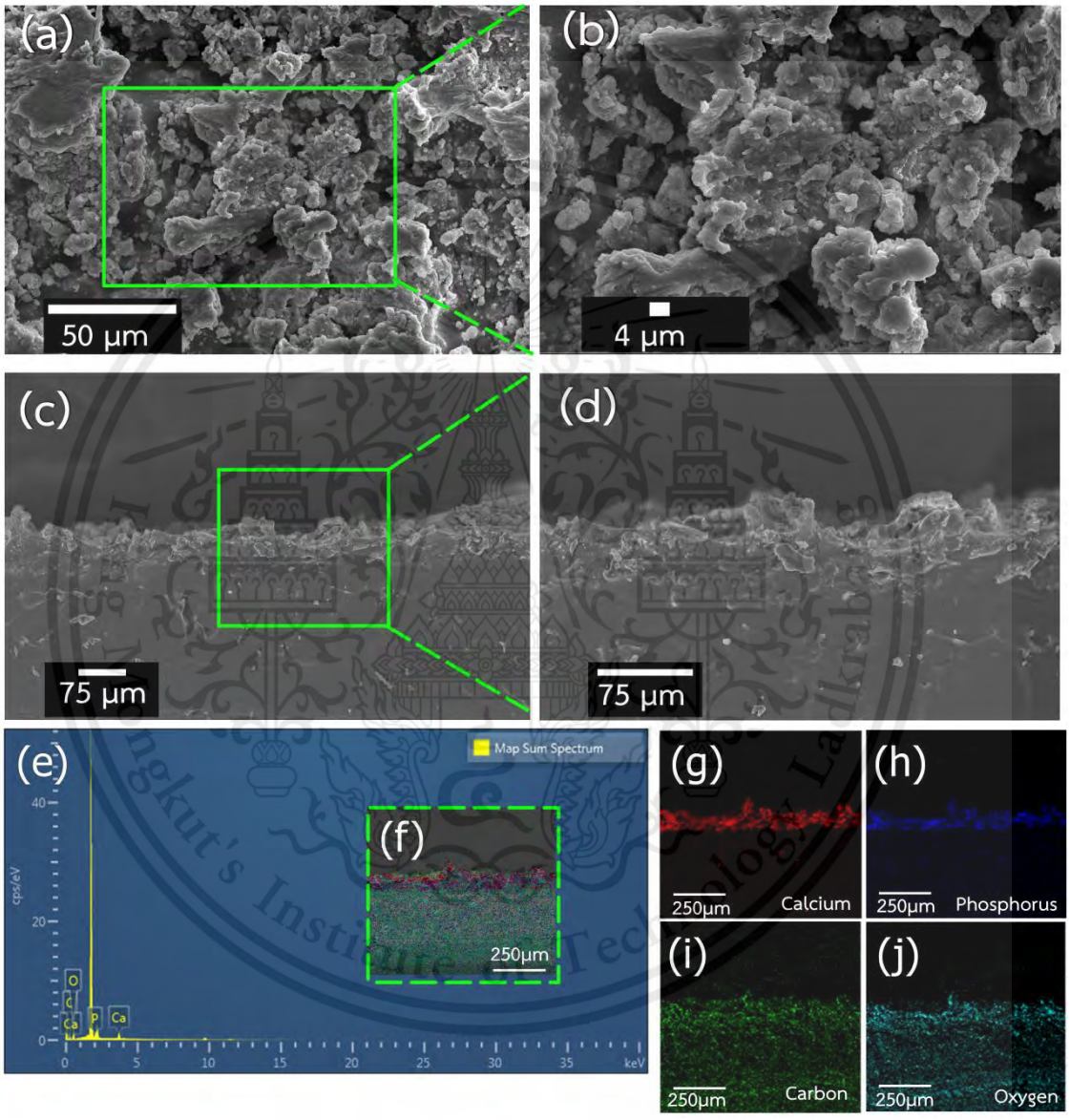

Figure 4.20 SEM images showing (a) and (b) the surface area with different magnification (2000X and 4000X), (c) and (d) the cross-section of composite film with different magnification (500X and 1000X). (e) EDX identifications of spectrum and (f)-(i) element mapping forms of flower-like HA/PDMS piezoelectric composite at curing time 3 hr.

The SEM image of flower-like HA/PDMS composite are different magnification shows the surface areas are shown in Figure 4.20 (a) and (b). The top area of composite has powder distribute all over, there is no space and flower-like HA powder is agglomerate. And the cross-section of flower-like /PDMS composite with different magnification are shown in Figure 4.20 (c) and (d). The corresponding EDX matching elements of flower-like HA/PDMS composite indicated the presence of Ca, P, C and O is shown in Figure 4.20 (e-j).

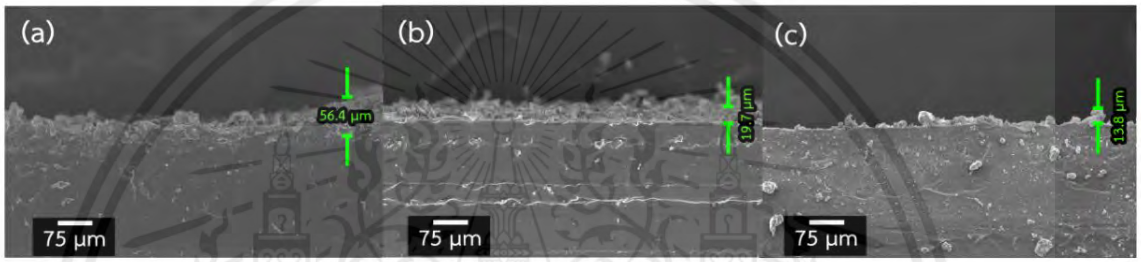

Figure 4.21 Cross section of HA (flower-like)/PDMS composite with difference curing time 3, 4 and 5 hr.

Figure 4.21 shows the cross section of flower-like HA /PDMS composite; (a) cross section at curing time 3 hr., the composite has a thickness around 56.4 ± 0.7 µm, (b) cross section at curing time 4 hr., the composite has a thickness around 19.6 ± 0.7 µm, and (c) cross section at curing time 5 hr., the composite has a thickness around 13.8 ± 0.9 µm.

4.5.2.1.2 Electrical output of flower-like HA /PDMS composite

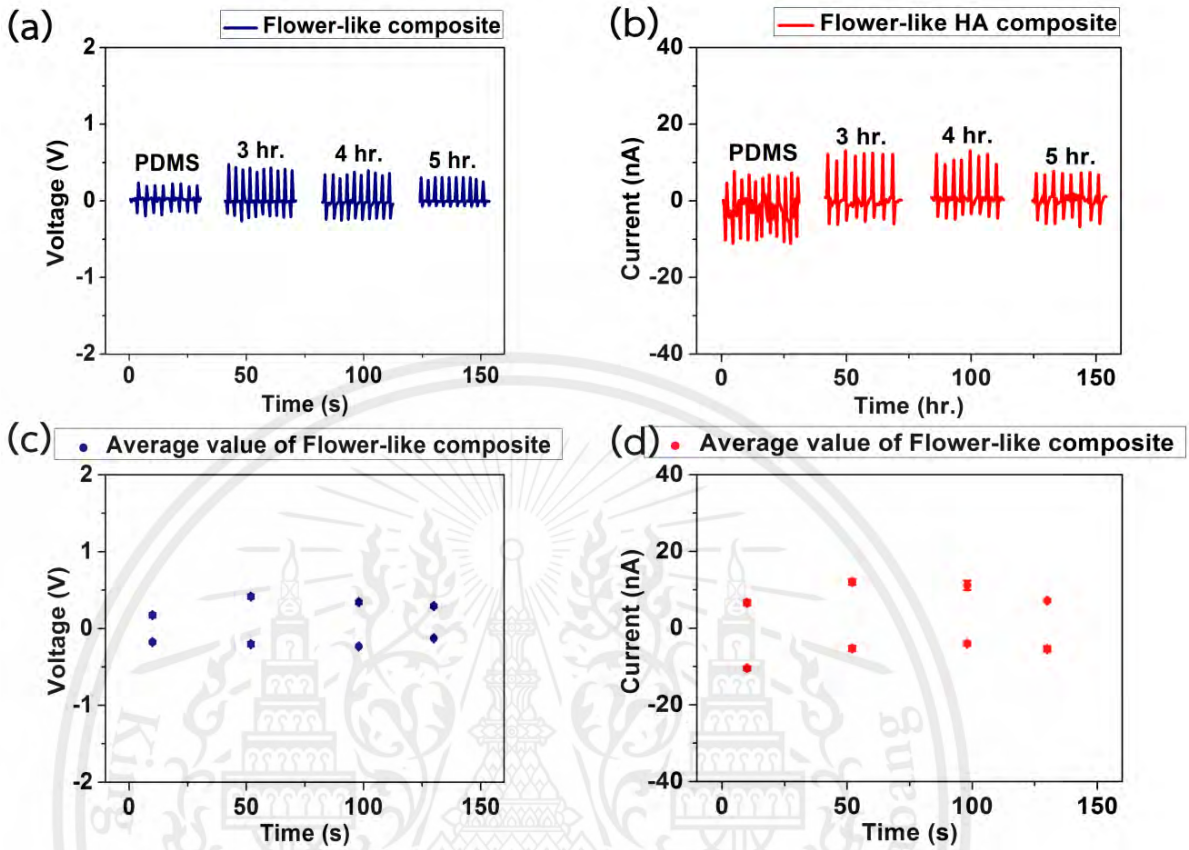

Figure 4.22 Relative between different curing time 3, 4 and 5 hr. and amount of piezoelectric powder that embedded in PDMS matrix for flower-like HA /PDMS piezoelectric.

The output voltage and average output voltage of flower-like HA /PDMS composite are shown in Figure 4.22 (a) and (c). The output voltage of NN/PDMS composite at curing time 3 hr. around 0.416 ± 0.027 V, at curing time 4 hr. around 0.344 ± 0.026 and at curing time 5 hr. around 0.292 ± 0.018 V, respectively. And the output current and average output current flower-like HA /PDMS composite are shown in Figure 4.22 (b) and (d), the output current at curing time 3 hr. around 12.035 ± 0.707 nA, at curing time 4 hr. around 11.171 ± 1.214 nA and at curing time 5 hr. around 7.185 ± 0.313 nA, respectively.

4.5.2.1.3 The effect of curing time of flower-like HA/PDMS composite

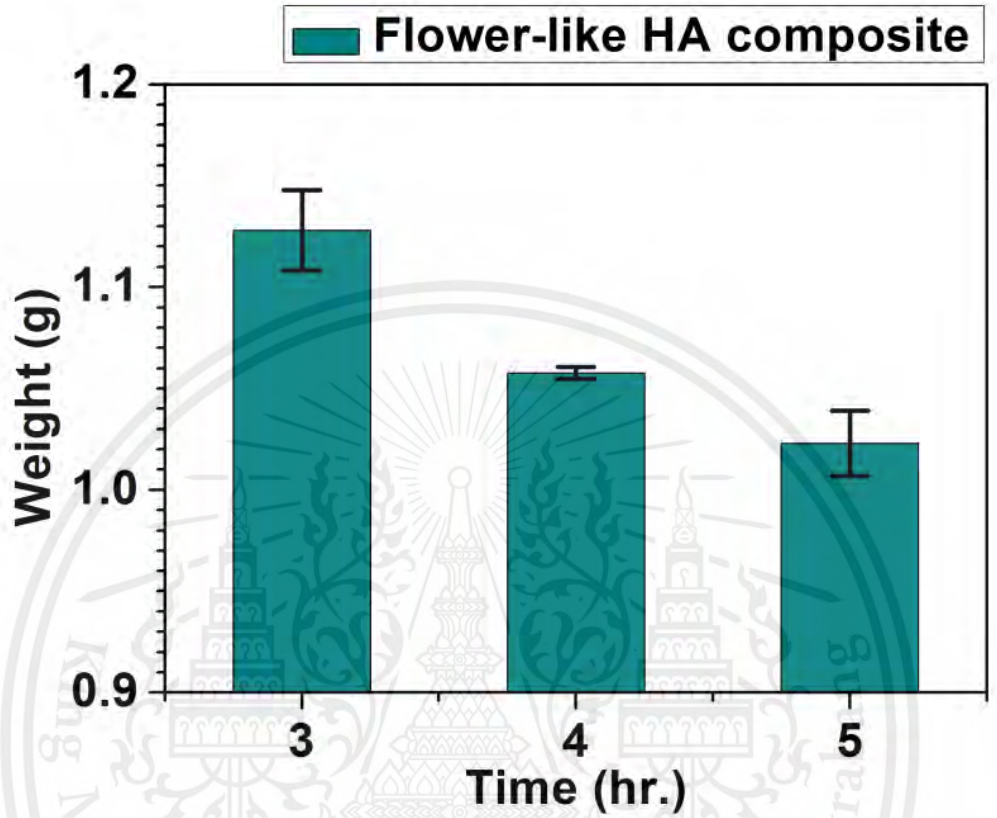

Figure 4.23 Relative between different curing time 3, 4 and 5 hr. and amount of piezoelectric powder that embedded in PDMS matrix for flower-like HA /PDMS piezoelectric.

The effect of curing time makes the amount of oxide powder embedded in the composite have different when the curing time is different. In Figure 4.23 the flower-like HA /PDMS composite at curing time 3 hr. It has the highest amount of powder and it has a weight around 1.128 ± 0.020 g. In part of flower-like HA/PDMS composite at curing time 4 and 5 hr. have weight around 1.058 ± 0.005 g and 1.023 ± 0.016 g, respectively.

4.5.2.2 Coral-like HA /PDMS composite

4.5.2.2.1 Morphology

4.5.2.2.1.1 Scanning electron microscope (SEM)

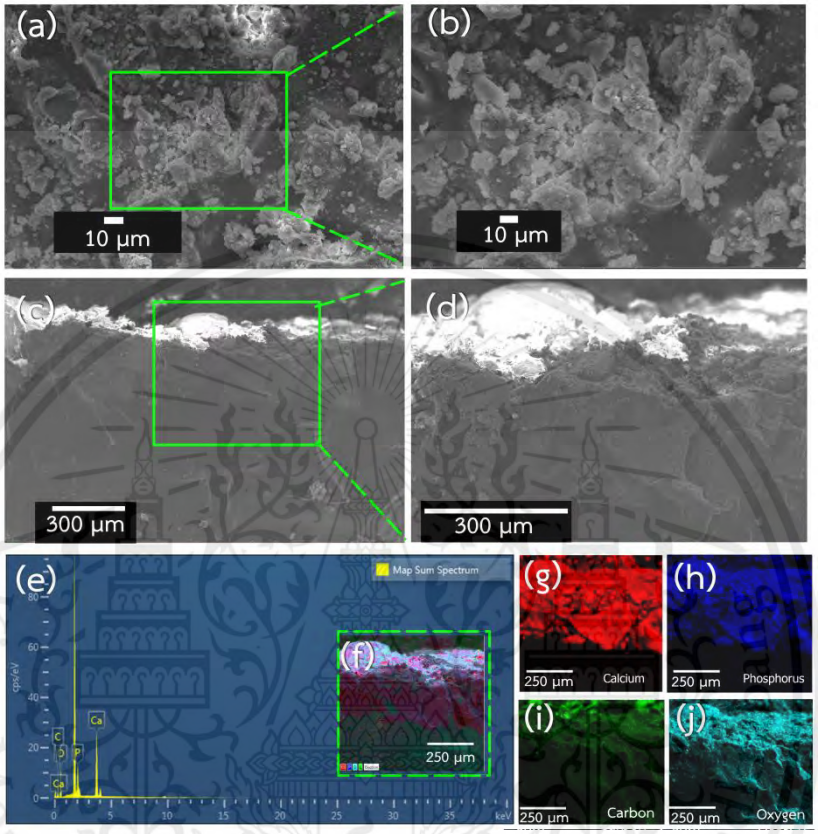

Figure 4.24 SEM images showing (a) and (b) the surface area with different magnification (2000X and 4000X), (c) and (d) the cross-section of composite film with different magnification (200X and 500X). (e) EDX identifications of spectrum and (f)-(i) element mapping forms of coral-like HA/PDMS piezoelectric composite at curing time 3 hr.

The SEM image of coral-like HA/PDMS composite are different magnification shows the surface areas are shown in Figure 4.24 (a) and (b). The top area of composite has powder distribute all over, there is no space and coral-like HA powder is agglomerate. And the cross-section of coral-like HA/PDMS composite with different magnification are shown in Figure 4.24 (c) and (d). The corresponding EDX matching elements of coral-like HA/PDMS composite indicated the presence of Ca, P, C and O is shown in Figure 4.24 (e-j).

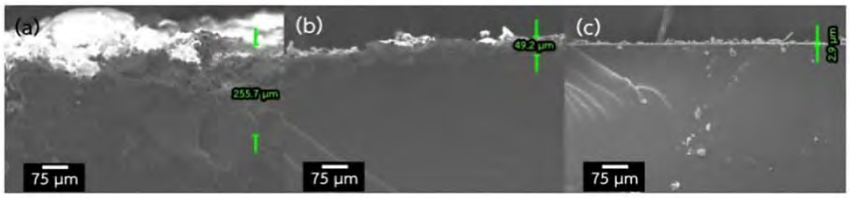

Figure 4.25 Cross section of coral-like HA/PDMS composite with difference curing time 3, 4 and 5 hr.

Figure 4.25 shows the cross section of coral-like HA/PDMS composite; (a) cross section at curing time 3 hr., the composite has a thickness around 8.447 ± 1.546 µm, (b) cross section at curing time 4 hr., the composite has a thickness around 1.626 ± 0.477 µm, and (c) cross section at curing time 5 hr., the composite has a thickness around 0.095 ± 0.072 µm.

4.5.2.2.2 Electrical output of coral-like HA/PDMS composites

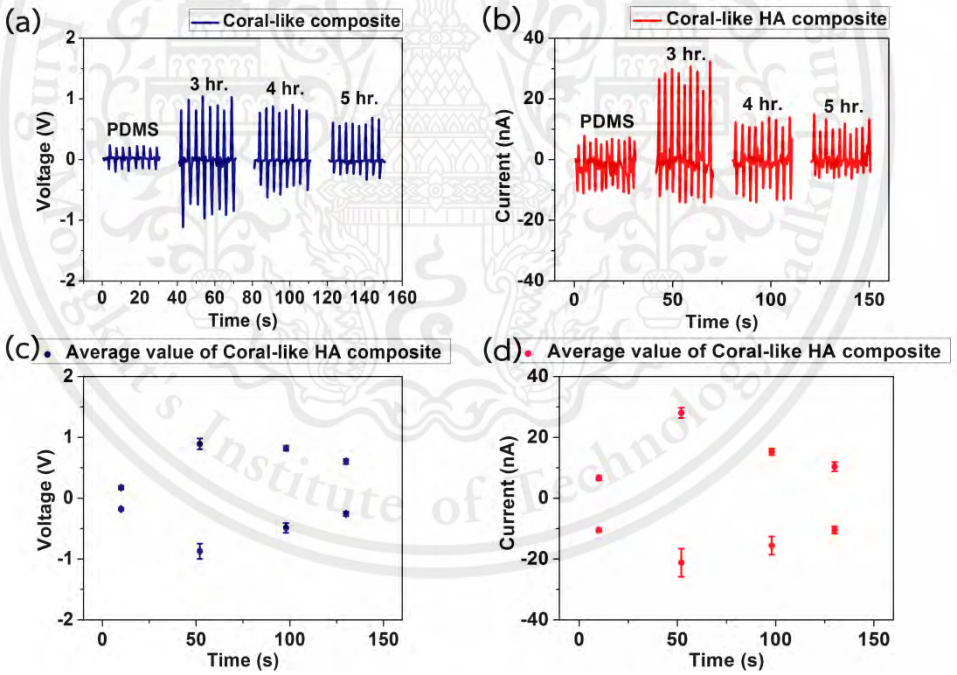

Figure 4.26 Relative between different curing time 3, 4 and 5 hr. and amount of piezoelectric powder that embedded in PDMS matrix for coral-like HA/PDMS piezoelectric.

The output voltage and average output voltage of coral-like HA/PDMS composite are shown in Figure 4.26 (a) and (c). The output voltage at curing time 3 hr. around 0.892 ± 0.089 V, at curing time 4 hr. around 0.823 ± 0.042 V and at curing

time 5 hr. around 0.605 ± 0.0413 V, respectively. And the output current and average output current of coral-like HA/PDMS composite are shown in Figure 4.26 (b) and (d)., the output at curing time 3 hr. around 26.031 ± 2.675 nA, at curing time 4 hr. around 11.868 ± 1.621 nA and at curing time 5 hr. around 4.979 ± 0.791 nA, respectively.

4.5.2.2.3 The effect of curing time of coral-like HA/PDMS composite

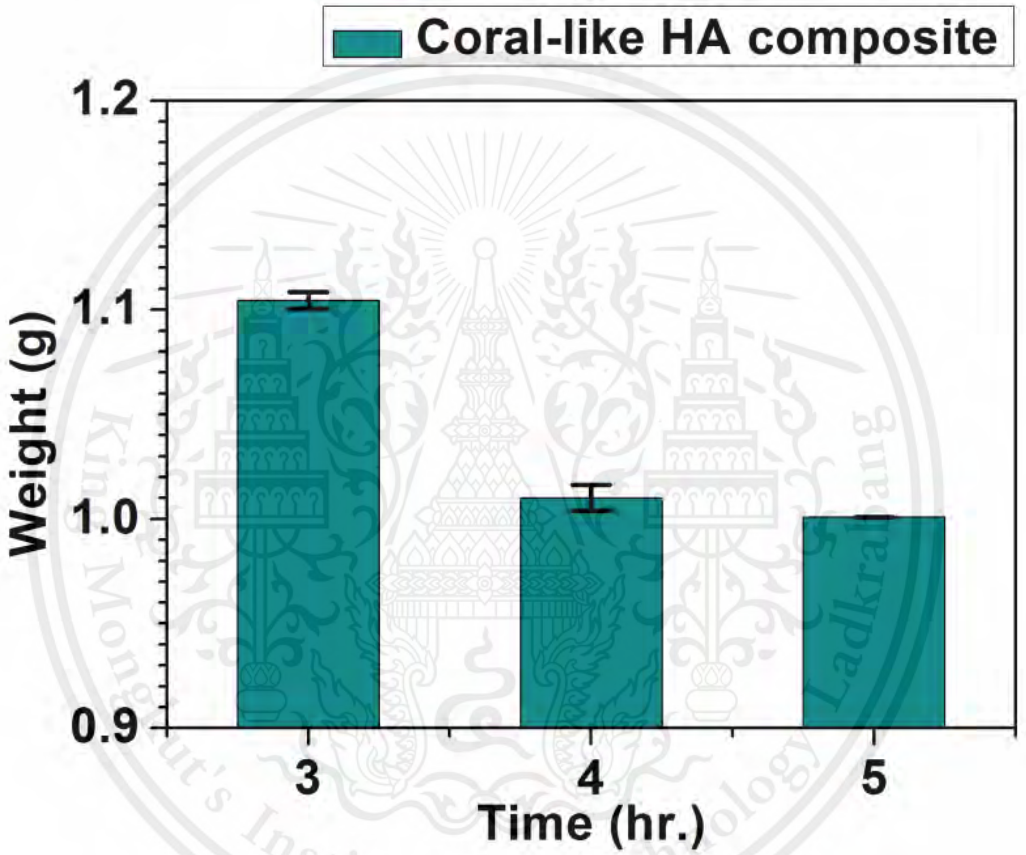

Figure 4.27 Relative between different curing time 3, 4 and 5 hr. and amount of piezoelectric powder that embedded in PDMS matrix for coral-like/PDMS piezoelectric.

In Figure 4.27 shows the coral-like HA /PDMS composite at curing time 3 hr. it has the highest amount of powder and it has weight around 1.105 ± 0.004 g. In part of coral-like HA/PDMS composite at curing time 4 and 5 hr. have weight around 1.010 ± 0.006 g and 1.000 ± 0.001 g, respectively.

4.5.3 BT/PDMS composite

4.5.3.1 Morphology

4.5.3.1.1 Scanning electron microscope (SEM)

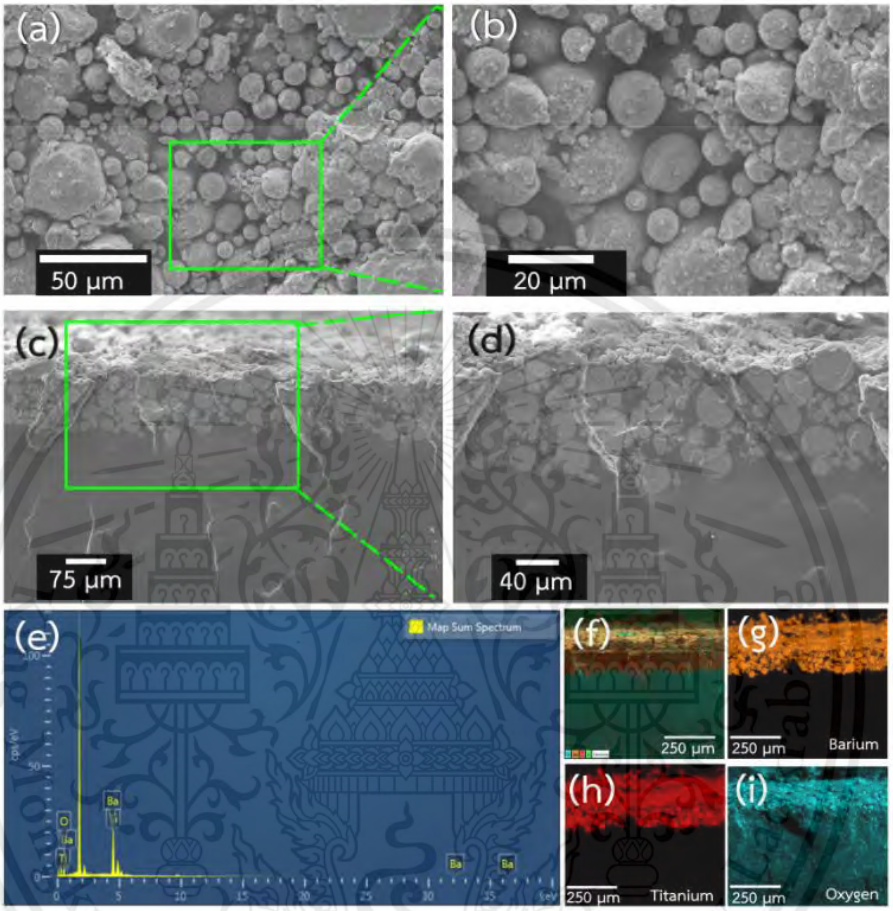

Figure 4.28 SEM images showing (a) and (b) the surface area with different magnification (2000X and 4000X), (c) and (d) the cross-section of composite film with different magnification (500X and 1000X). (e) EDX identifications of spectrum and (f)-(i) element mapping forms of BT/PDMS piezoelectric composite at curing time 3 hr.

The SEM images of BT/PDMS composite are different magnification shows the surface areas are shown in Figure 4.28 (a) and (b). The top area of composite has powder distribute all over, there is no space and BT powder is agglomerate. And the cross-section of BT/PDMS composite with different magnification are shown in Figure 4.28 (c) and (d). The corresponding EDX matching elements of BT/PDMS composite indicated the presence of Ba, Ti, and O is shown in Figure 4.28 (e-j).

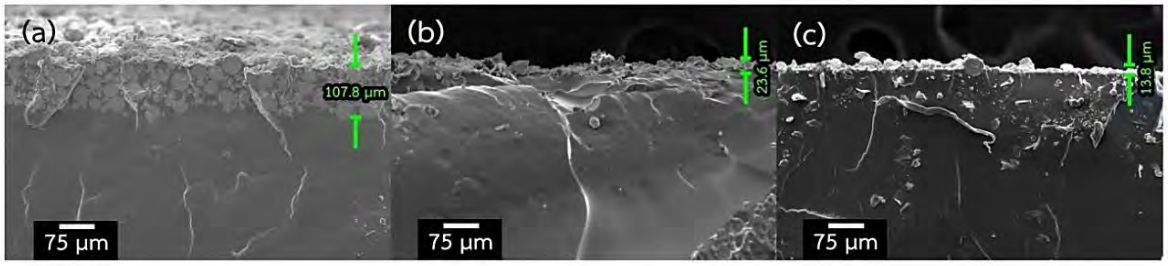

Figure 4.29 Cross section of BT/PDMS composite with difference curing time 3, 4 and 5 hr.

Figure 4.29 shows the cross section of BT/PDMS composite; (a) cross section at curing time 3 hr., the composite has a thickness around 3.568 ± 0.491 µm, (b) cross section at curing time 4 hr., the composite has a thickness around 0.781 ± 0.282 µm, and (c) cross section at curing time 5 hr., the composite has a thickness around 0.456 ± 0.290 µm.

4.5.3.2 Electrical output of BT/PDMS composite

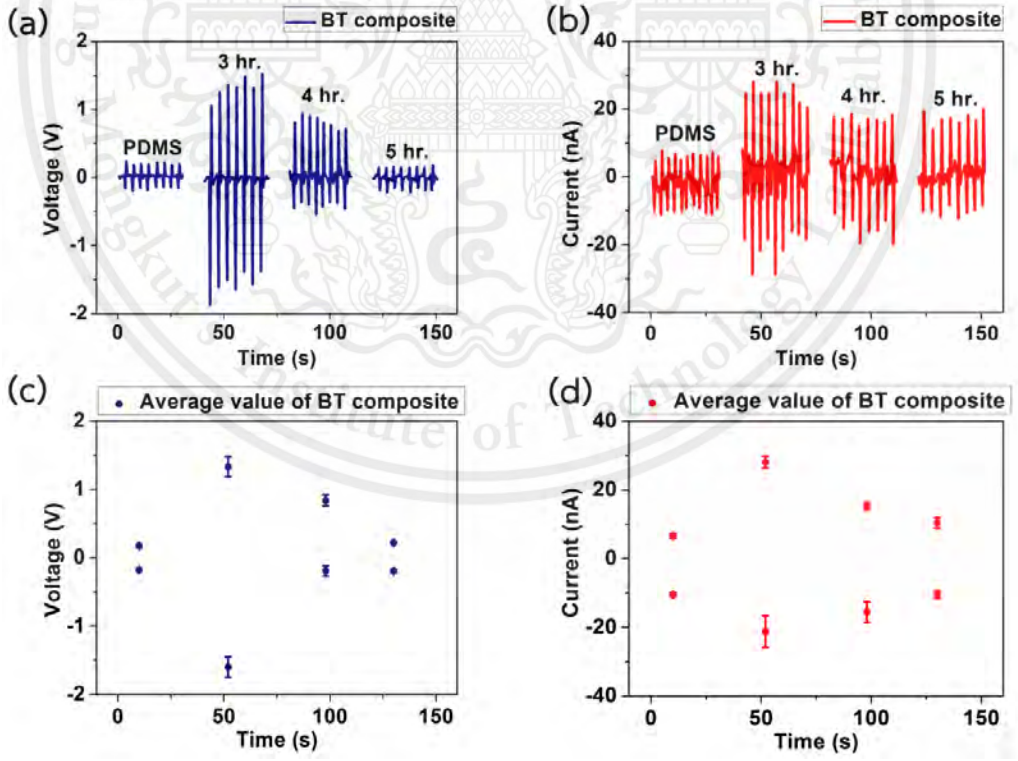

Figure 4.30 Relative between different curing time 3, 4 and 5 hr. and amount of piezoelectric powder that embedded in PDMS matrix for BT/PDMS piezoelectric.

The output voltage and average output voltage of BT/PDMS composite are shown in Figure 4.30 (a) and (c). The output voltage at curing time 3 hr. around 1.330 ± 0.146 V, at curing time 4 hr. around 0.837 ± 0.0078 V and at curing time 5 hr. around 0.201 ± 0.009 V, respectively. And the output current and average output current of BT/PDMS composite are shown in Figure 4.30 (b) and (d)., the output current at curing time 3 hr. around 28.072 ± 1.674 nA, at curing time 4 hr. around 15.278 ± 1.0713 nA and at curing time 5 hr. around 10.377 ± 0.791 nA, respectively.

4.5.3.3 The effect of curing time of BT/PDMS composite

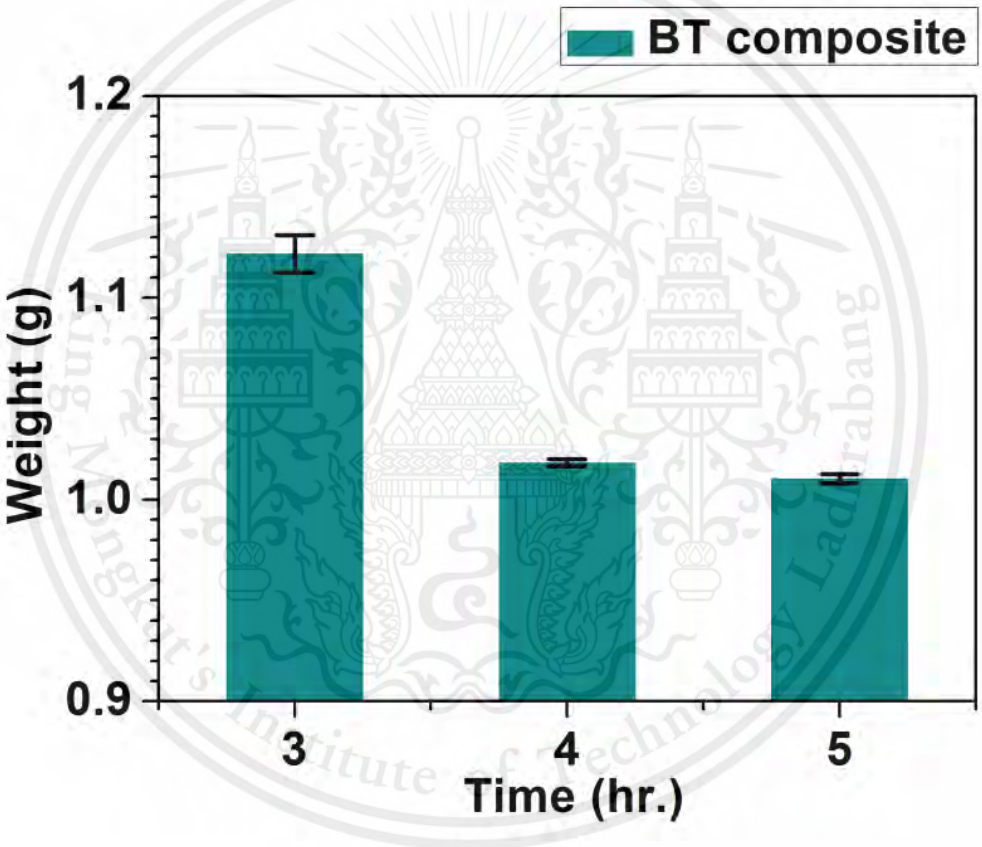

Figure 4.31 Relative between different curing time 3, 4 and 5 hr. and amount of piezoelectric powder that embedded in PDMS matrix for BT/PDMS piezoelectric.

In Figure 4.31 show BT/PDMS composite at curing time 3 hr. It has a weight around 1.123 ± 0.009 g. In part of BT/PDMS composite at curing time 4 and 5 hr. have weight around 1.018 ± 0.001 g and 1.010 ± 0.002 g, respectively.

4.5.4 ZnO/PDMS composite

4.5.4.1 Morphology

4.5.4.1.1 SEM of ZnO/PDMS composite

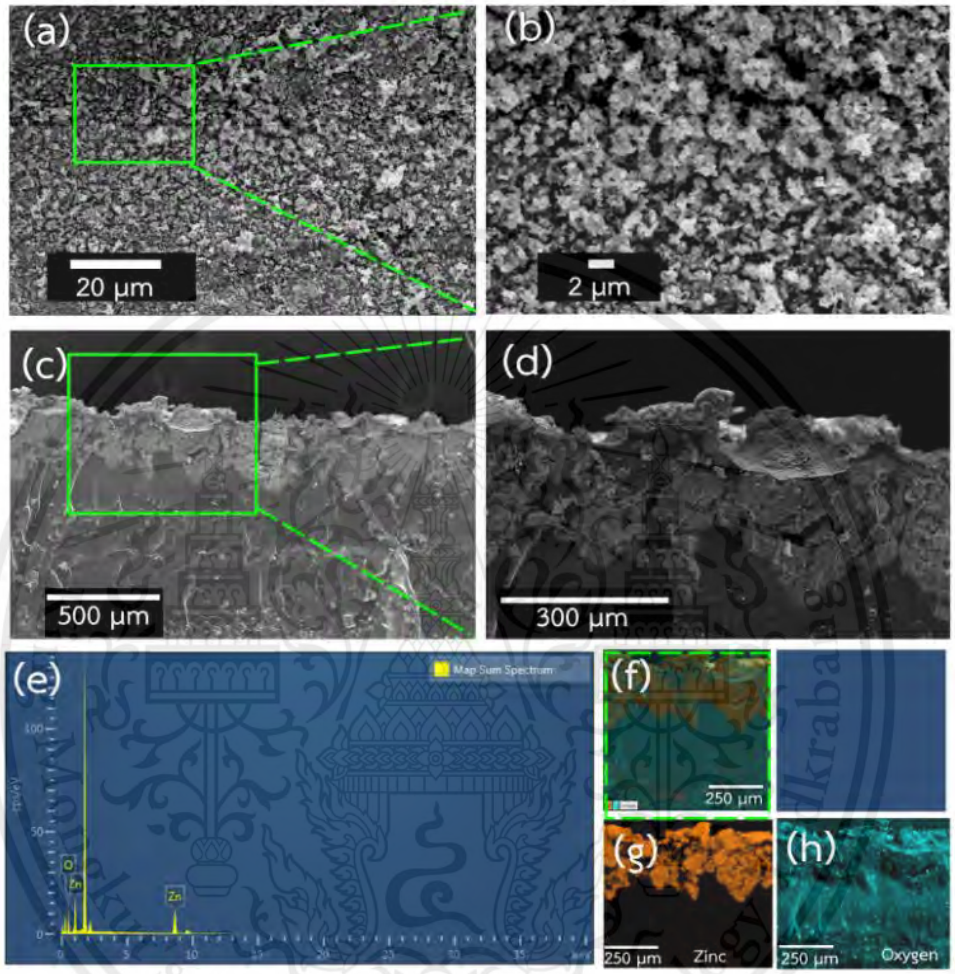

Figure 4.32 SEM images showing (a) and (b) the surface area with different magnification (2000X and 4000X), (c) and (d) the cross-section of composite film with different magnification (200X and 500X). (e) EDX identifications of spectrum and (f)-(i) element mapping forms of ZnO/PDMS piezoelectric composite at curing time 3 hr.

The SEM images of ZnO/PDMS composite are different magnification shows the surface areas are shown in Figure 4.32 (a) and (b). The top area of composite has powder distribute all over, there is no space and ZnO powder is agglomerate. And the cross-section of ZnO/PDMS composite with different magnification is shown in

Figure 4.32 (c) and (d). The corresponding EDX matching elements of ZnO/PDMS composite indicated the presence of Zn and O is shown in Figure 4.32 (e-h).

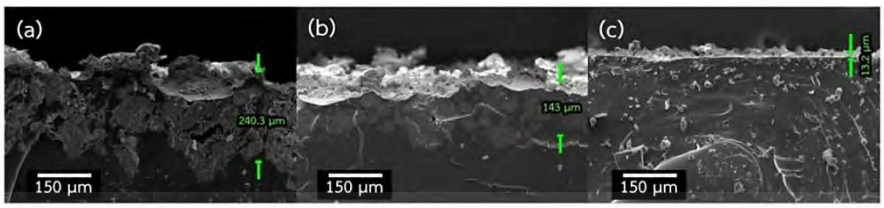

Figure 4.33 Cross section of ZnO/PDMS composite with difference curing time 3, 4 and 5 hr.

Figure 4.33 shows the cross section of ZnO/PDMS composite; (a) cross section at curing time 3 hr., the composite has a thickness around 7.954 ± 1.713 µm, (b) cross section at curing time 4 hr., the composite has a thickness around 4.732 ± 0.723 µm, and (c) cross section at curing time 5 hr., the composite has a thickness around 0.435 ± 0.270 µm.

4.5.4.2 Electrical output of ZnO/PDMS composite

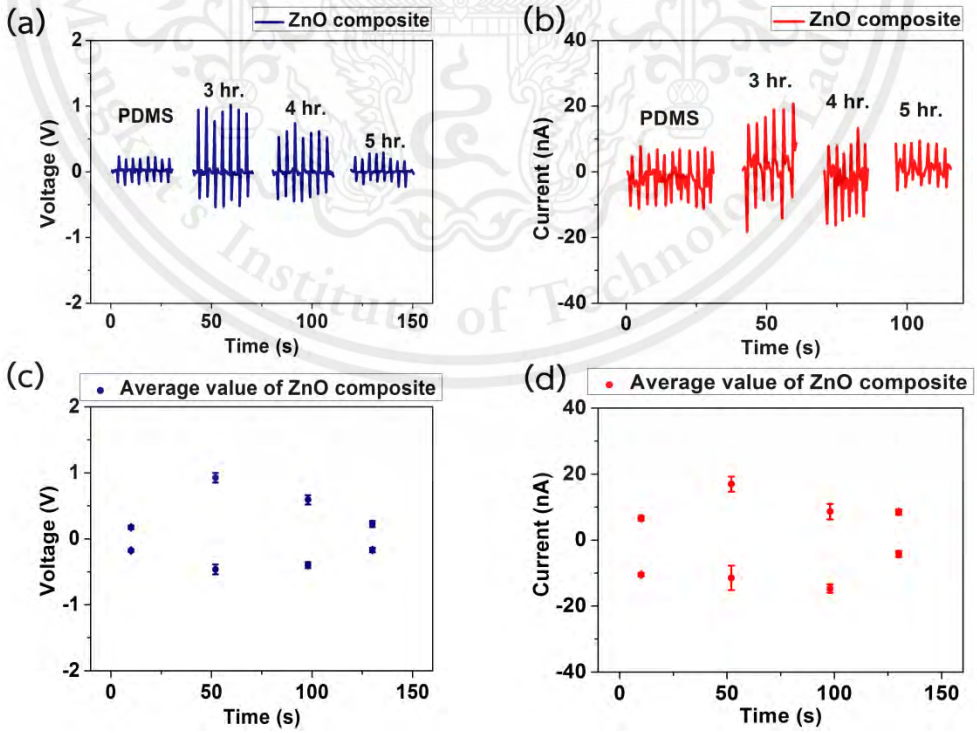

Figure 4.34 Relative between different curing time 3, 4 and 5 hr. and amount of piezoelectric powder that embedded in PDMS matrix for ZnO/PDMS piezoelectric.

The output voltage and average output voltage of ZnO/PDMS composite are shown in Figure 4.34 (a) and (c). The output voltage at curing time 3 hr. around 0.092 ± 0.014 V, at curing time 4 hr. around 0.077 ± 0.005 V and at curing time 5 hr. around 0.053 ± 0.004 V, respectively. And the output current and average output current of ZnO/PDMS composite are shown in Figure 4.34 (b) and (d)., the output current at curing time 3 hr. around 16.986 ± 2.294 nA, at curing time 4 hr. around 8.638 ± 2.318 nA and at curing time 5 hr. around 8.520 ± 0.799 nA, respectively.

4.5.4.3 The effect of curing time of ZnO/PDMS composite

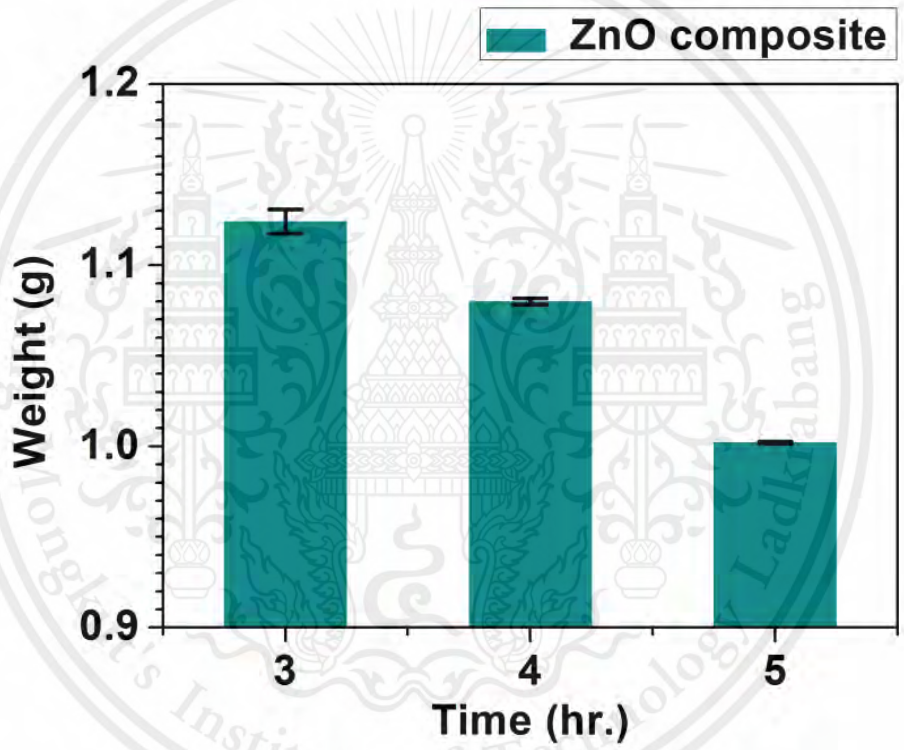

Figure 4.35 Relative between different curing time 3, 4 and 5 hr. and amount of piezoelectric powder that embedded in PDMS matrix. for ZnO/PDMS piezoelectric.

Figure 4.35 shows ZnO/PDMS composite at curing time 3 hr. has weight around 1.124 ± 0.006 g. In part of ZnO/PDMS composite at curing time 4 and 5 hr. have weight around 1.080 ± 0.002 g and 1.002 ± 0.001 g, respectively.

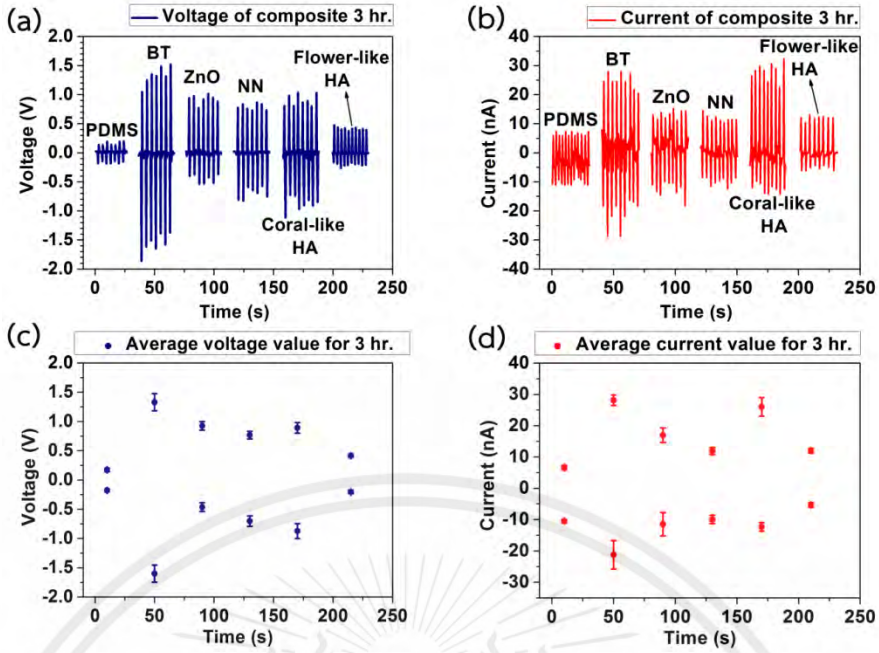

Figure 4.36 The electrical output of pure PDMS, BT, ZnO, NN, HA/PDMS piezoelectric composite with different curing time: (a) The output voltage; (b) The output current; (c) Average positive-negative value of the output voltage; (d) Average positive-negative value of the output current of piezoelectric composite at curing time 3 hr.

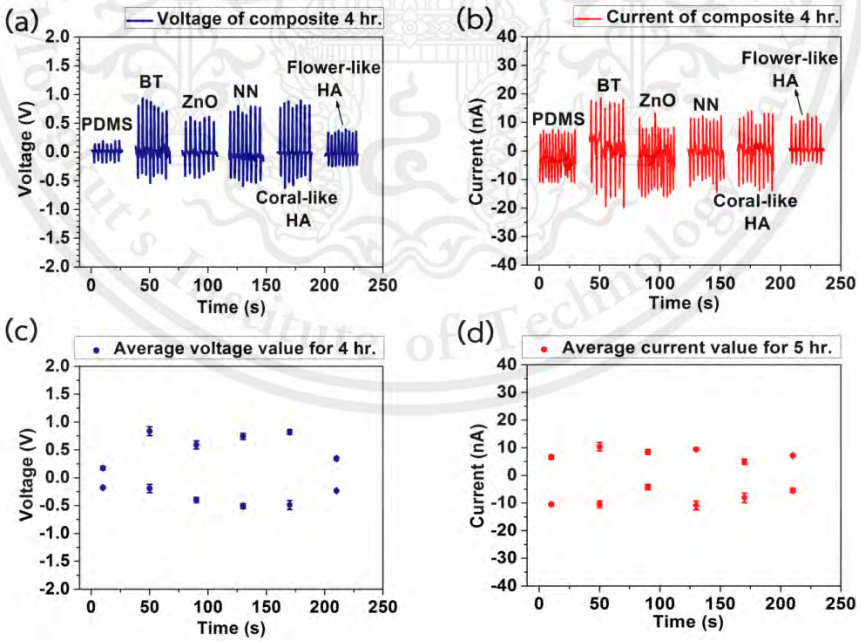

Figure 4.37 The electrical output of pure PDMS, BT, ZnO, NN, HA/PDMS piezoelectric composite with different curing time: (a) The output voltage; (b) The output current; (c) Average positive-negative value of the output voltage; (d) Average positive-negative value of the output current of piezoelectric composite at curing time 4 hr.

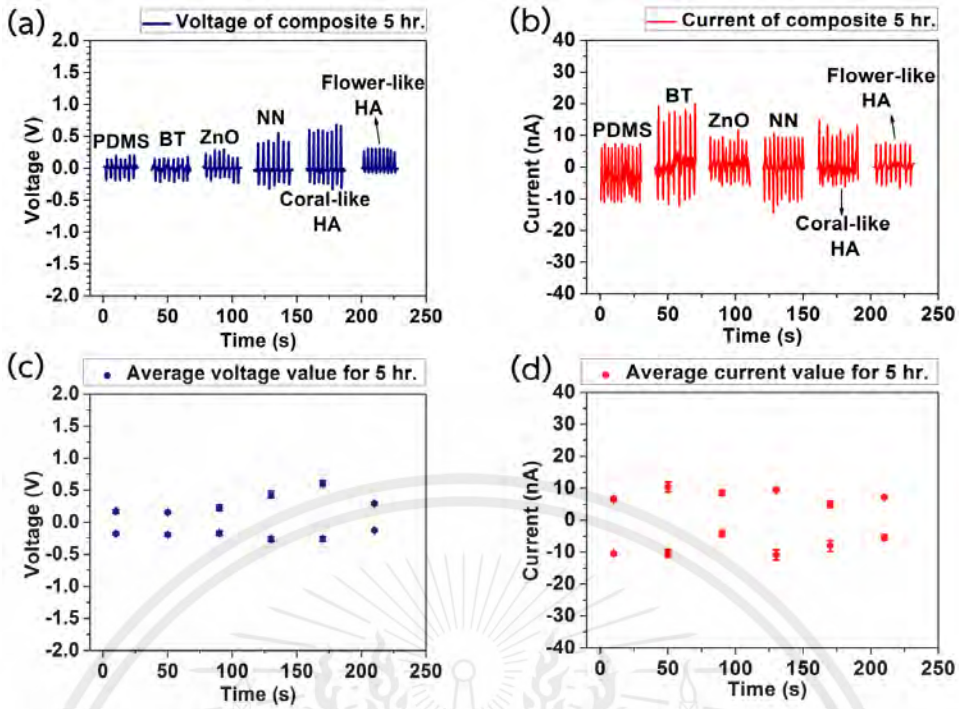

Figure 4.38 The electrical output of pure PDMS, BT, ZnO, NN, HA/PDMS piezoelectric composite with different curing time: (a) The output voltage; (b) The output current; (c) Average positive-negative value of the output voltage; (d) Average positive-negative value of the output current of piezoelectric composite at curing time 5 hr.

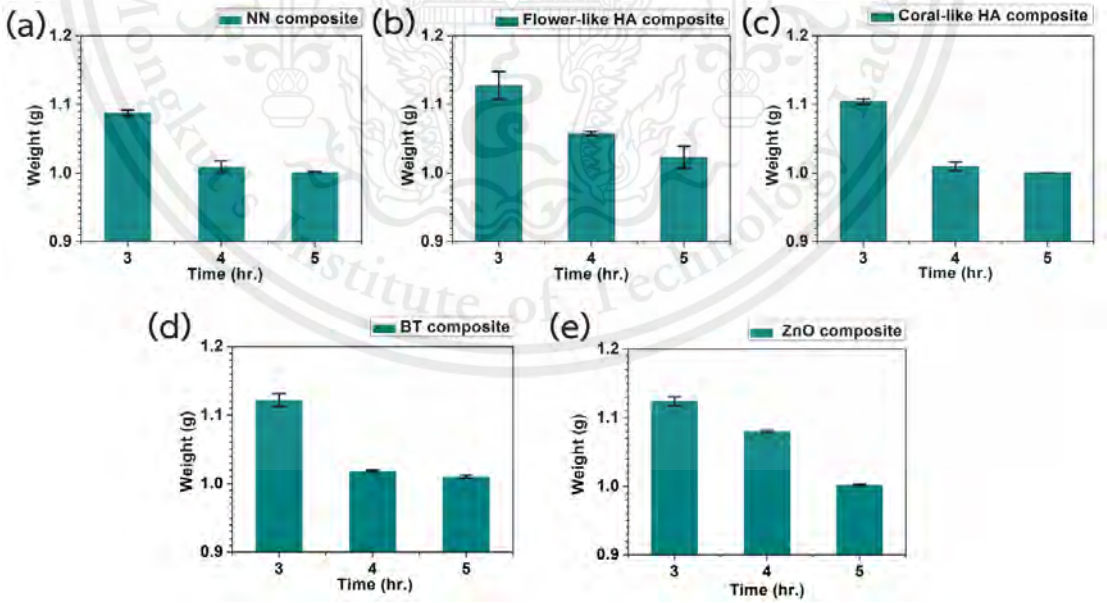

Figure 4.39 relative between different curing time 3, 4 and 5 hr. and amount of piezoelectric powder that embedded in PDMS matrix for piezoelectric composite: (a) NN/PDMS, (b) flower-like HA/PDMS, (c) coral-like HA/PDMS, (d) BT/PDMS, and (e) ZnO/PDMS piezoelectric composite.

From the overall results, it was found that NN, flower-like HA, coral-like-HA, BT, and ZnO are decreasing trend of V and I according to the increase of curing time is 3, 4 and 5 hr. Due to the amount of powder embedded in PDMS matrix is less. When the curing time increases, PDMS is highly viscous. Therefore, the powder is less embedded. The amount of powder embedded within the composite plays a role fundamental effect term of piezoelectric properties which affects the electrical output value.

The electrical output was generated from the NN, flower-like HA, coral-like HA, BT, and ZnO/PDMS piezoelectric composite. Due to the NN, flower-like HA, coral-like HA, BT, and ZnO powder have piezoelectric properties, it has asymmetry structure. When the piezoelectric composite obtained external mechanical force, the piezoelectric potential has produced between electrodes because it formed dipole within the piezoelectric composite and PDMS layer is insulator layer, electrons can flow all over the external circuit to balance charge and accumulated at the surface of the top electrode. And when without external mechanical force, the piezoelectric properties disappear due to the structure is symmetrical. This behavior generates electrical output i.e. voltage and current.

From 5 system of piezoelectric material, including NN, HA (flower-like), HA (coral-like), BT, and ZnO with all 5 systems having conditions 3, 4 and 5 hr. To measure the electrical output i.e. voltage (V) and electric current (I) under external periodical force by compression machine. The results from all 4 systems are shown in Figure 4.36, 4.37, and 4.38, respectively.

4.6 REFERENCE

[1] Erdem, Emre Boettcher, R.Gläsel, Hans-Jürgen Hartmann, E.Klotzsche, G.Michel, Dieter. (2005).Size effects in $BaTiO_3$ nanopowders studied by EPR and NMR.

[2] Boumezoued, A.Guergouri, K.Barille, R.Rechem, D.Zaabat, M.Rasheed, M. (2019). "ZnO nanopowders doped with bismuth oxide, from synthesis to electrical application." Journal of Alloys and Compounds 791: 550-558.

[3] Zhang, Miaohua Fan, Huiqing Chen, Lei Yang, C. (2009). Synthesis and Formation Mechanisms of High Aspect Ratio Plate-Like $NaNbO_3$ Particles by Topochemical Microcrystal Conversion.

[4] Lak, Aidin Mazloumi, Mahyar Mohajerani, Matin Sadat Kajbafvala, A. Zanganeh, Saeid Arami, Hamed Sadrnezhaad, S. K. (2008). Self-Assembly of Dandelion-Like Hydroxyapatite Nanostructures Via Hydrothermal Method.

[5] Yushi Yang, Min Wang, Qingzhi Wu, Jia Long (2014). “Hydrothermal Synthesis of Hydroxyapatite with Different Morphologies: Influence of Supersaturation of the Reaction System” Crystal Growth & Design 14(9):4864-4871.

[6] Kumar, G. Suresh Thamizhavel, A. Girija, E. K. (2012). "Microwave conversion of eggshells into flower-like hydroxyapatite nanostructure for biomedical applications." Materials Letters 76: 198-200.

[7] Hicham EL Boujaady, El Rhilassi Abdelhadi, M. Mourabet, M. Bennani-Ziatni (2016). “Adsorption of a textile dye on synthesized calcium deficient hydroxyapatite (CDHAp): Kinetic and thermodynamic studies” Mater. Environ. Sci. 7 (11) (2016) 4049-4063.

CHAPTER 5

CONCLUSION

This thesis presents (1) synthesis of piezoelectric powder plate-like NN powder via molten salt method, flower-like hydroxyapatite powder via hydrothermal method, and flower-like hydroxyapatite powder via microwave irradiation method, (2) the dispersion of all powder on 5 systems, and (3) the influence of curing time on all 5 systems are NN, flower-like HA, coral-like HA, BT, and ZnO/PDMS piezoelectric composite and study electrical output.

5.1 Synthesis of oxide powders

5.1.1 The synthesis of plate-like NN powder by molten salts

In this topic, plate-like NN powders were synthesized successfully via the molten salt method. The result of the SEM image illustrates the morphology of the NN powders, we found the NN powders showed a plate-like shape with an aspect ratio of approximately 1.312 ± 0.350. For the results of the crystal structure that characterized with XRD technique, we found the NN powder matched well the standard data JCPDF file no: 19-1221, it exhibited the hexagonal structure with the lattice parameters of a = b = c = 3.912 ± 0.005 A°, and it without the additional impurity phases. And the FT-IR spectrum of NN, we found the broad peak expanding in range of 2900 to 3500 cm^{-1} is indicated of O-H group. The wavenumber at 1655 and 1088 cm^{-1} indicate stretching and bending of O-H. The peak at 670 cm^{-1} is the characteristic for asymmetric enlargement of the Nb-O band. By the peaks mentioned above have functional group corresponding with the NN spectrum.

5.1.2 The synthesis of flower-like HA nanopowder by hydrothermal method

In this topic, flower-like HA powders were synthesized successfully via the hydrothermal method. The result of the SEM image illustrates the

morphology of the flower-like HA powders, we found the flower-like HA powders showed a flower-like shape with an aspect ratio of approximately 14.187 ± 5.036. For the results of the crystal structure that characterized with XRD technique, we found the flower-like HA matched well the standard data JCPDF file no: 73-0293, it exhibited the cubic structure with the lattice parameters of a = b ≠ c; a = 9.440 ± 0.004 and c = 6.873 ± 0.004 Å, and it without the additional impurity phases. And the FT-IR spectrum of flower-like HA, we found the peak at 466 cm^{-1} appeared the phosphate stretching peak. The peaks at 564 and 601 cm^{-1} are P-O bendings and the symmetric P-O stretching peak appeared at 957 cm^{-1}. The peaks at 1032 and 1114 cm^{-1} are the P-O asymmetric stretching. The O-H stretching peak appeared at 3415 cm^{-1} and O-H bending peak appeared at 639 and 1613 cm^{-1}. The absorption peak at 1409-1462 cm^{-1} has presented the carbonate group in flower-like HA particles. The crystallinity of flower-like HA derived from intensities of both the O-H peak and the P-O stretching peak at 957 cm^{-1}.

5.1.3 The synthesis of coral-like hydroxyapatite nanopowder by microwave irradiation method

In this topic, coral-like HA powders were synthesized successfully via the microwave irradiation method. The result of the SEM image illustrates the morphology of the coral-like HA powders, we found the coral-like HA powders showed a coral-like shape with an aspect ratio of approximately 3.858 ± 1.190. For the results of the crystal structure that characterized with XRD technique, we found the coral-like HA matched well the standard data JCPDF file no: 09-0432, it exhibited the hexagonal structure with the lattice parameters of a = b ≠ c; a = 9.497 ± 0.079 and c = 6.841 ± 0.037 Å, and it without the additional impurity phases. And the FT-IR spectrum of coral-like HA, we found the characteristic vibrations of HA appeared phosphate groups at 565 and 574 cm^{-1} along with other phosphate peaks at 469, 961 and 1032 cm^{-1} respectively. The wavenumber at 3500 cm^{-1} is the broad of the characteristic O-H stretching of HA. The board band expanding from 2500 to 3800 cm^{-}

^{1} is stretching mode of the H_2O molecules. The band at 1642 cm^{-1} is bending mode of the H_2O molecules. Moreover, its result showed additional peaks at region 875, 1415 and 1460 cm^{-1} are indicate the formation of b-type carbonate group of HA.

5.2 Commercial oxide powder

5.2.1 BT commercial grade nanopowder

In this topic, BT commercial grade nanopowders were characterized by SEM, XRD, and FT-IR techniques. The result of the SEM image illustrates the morphology of the BT nanopowders, we found the BT nanopowders showed a spherical shape an approximate average size around 105 ± 19.750 nm. For the results of the crystal structure that characterized with XRD technique, we found the BT matched well the standard data JCPDF file no: 31-0174, it exhibited the cubic structure with the lattice parameters of a = b = c = 4.630 ± 0.006 A°, and it without the additional impurity phases. And the FT-IR spectrum of BT, we found the broad peak at 3500 and 1631 cm^{-1} are indicated to the O-H stretching and O-H bending of the H_2O molecules. The peak at 583 and 414 cm^{-1} represents the characteristic of stretching and asymmetric vibration of the Ti-O.

5.2.2 ZnO commercial grade nanopowder

In this topic, ZnO commercial grade nanopowders were characterized by SEM, XRD, and FT-IR techniques. The result of the SEM image illustrates the morphology of the ZnO nanopowders, we found the ZnO nanopowders showed a nearly spherical shape an approximate average size around 64 ± 26.230 nm. For the results of the crystal structure that characterized with XRD technique, we found the ZnO matched well the standard data JCPDF file no: 79-0206, it exhibited the hexagonal structure with the lattice parameters of a = b ≠ c; a = 3.245 ± 0.001 and c = 5.200 ± 0.000 A°, and it without the additional impurity phases. And the FT-IR spectrum of ZnO, we found the broad peaks at 3500 cm^{-1} correspond to the O-H stretching vibrations. The stretching vibrations of C=O and the stretching vibrations of

Zn-OH are observed at 1590 and 900 cm^{-1}. The characteristic absorptions band of Zn-O stretching vibrations indicated at 471 cm^{-1}.

5.3 The dispersion of oxide powders on PDMS and measure output voltages and currents from piezoelectric composite

5.3.1 The piezoelectric composite

From the study for dispersion of oxide powder in piezoelectric composite, we found oxide powders disperse throughout of surface. But these oxide powders have high agglomerate because the oxide powder used in this research is nano-scale. It has high surface area, the powder then agglomerate together. Therefore, resulting the output values is less.

5.4 The influence of curing time on these systems.

Normally, the thickness of the oxide powder layer depends on curing time. We found the piezoelectric composite at curing time 3 hr. has the highest thickness of oxide powder because at curing time 3 hr., PDMS has a low viscosity. Therefore, the oxide powder can good embedded in PDMS. And at curing time 4 and 5 hr. have a higher viscosity, when the curing times increase. Therefore, resulting in the piezoelectric composite at curing time 4 and 5 hr. have less amount of embedded oxide powder when the curing time is highest. If the curing time is more than 5 hr., the amount of powder embedded on the composite does not differ significantly with curing time 5 hr.

In summary, we successfully fabricate the piezoelectric composites based on oxide powder. PDMS was casting in the mold and the oxide powder are sprinkle on PDMS to enhance the charge on the surface for prepare piezoelectric composite (30 × 30 mm). Under provided periodical force, the electrical output was generated from piezoelectric composite and its output and the output value has enhanced

from the addition of oxide powder. In all system, the piezoelectric from synthesis, coral-like HA /PDMS piezoelectric composite provide the highest electrical output. It provides output voltage around 0.892 ± 0.089 V and outputs current around 28.172 ± 2.956 nA. It has less output value than the composite based on BT commercial powder. Our piezoelectric composite has high flexibility, it can be bent for use in applications and also non-toxic with the environment.

APPENDIX

APPENDIX A

JCPDS File no. 31-0174

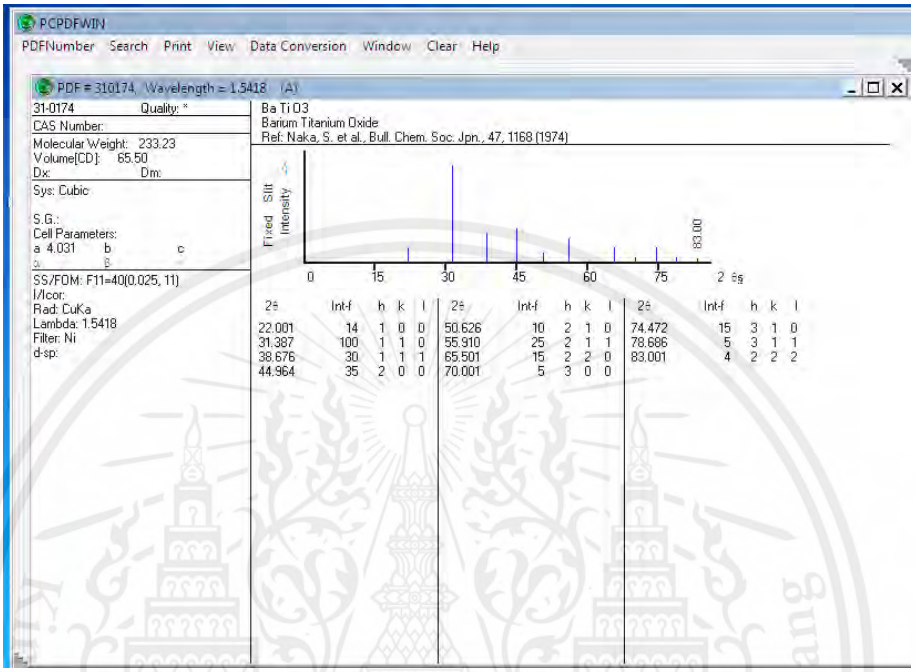

JCPDS File no. 19-1221

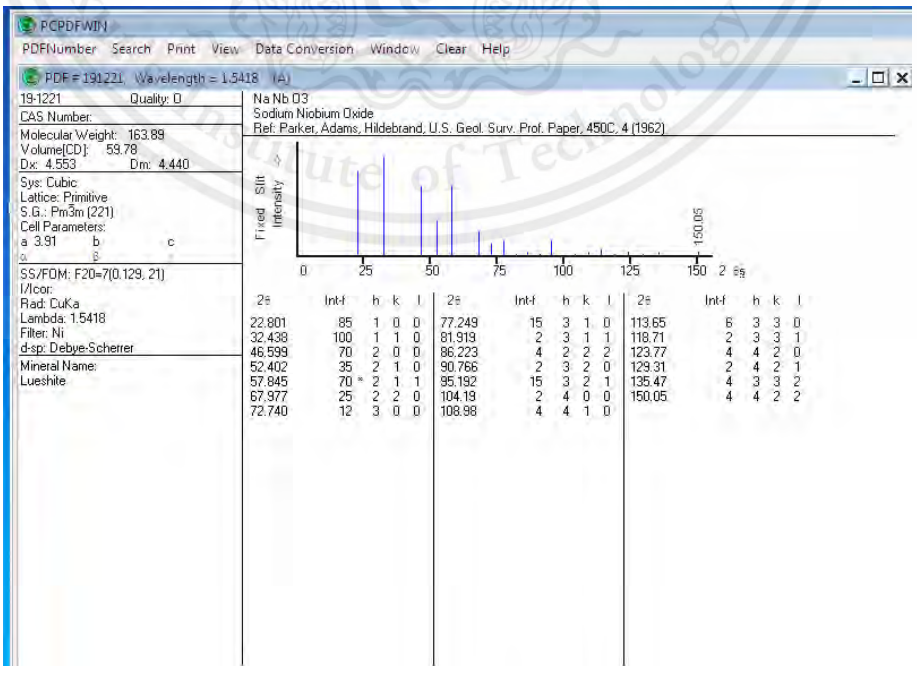

APPENDIX A

(Continued)

JCPDS File no. 79-2205

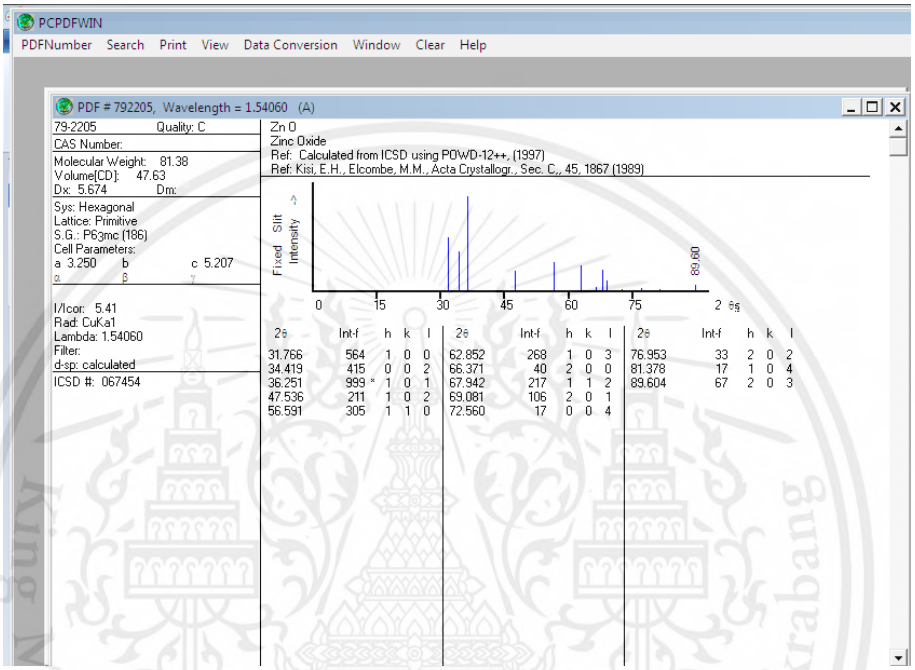

APPENDIX B

Calculation lattice parameters of $NaNbO_3$ and $BaTiO_3$

It can be calculated by use Bragg's Law as follows.

$$\frac{1}{d^2} = \frac{h^2 + k^2 + l^2}{a^2}$$

By h, k, l are plane of crystal

a is Lattice parameters with a cubic structure

d is Distance between planes

λ is The wavelength is equal to 1.5418 Å

n is The integer number is equal to 1

Where d is calculated from

$$2dsin\,\Theta = n\lambda\,; d = \frac{\lambda}{2dsin\,\Theta}$$

APPENDIX B

(Continued)

Calculation lattice parameters of ZnO and $Ca_5(PO_3)_4(OH)$

It can be calculated by use Bragg's Law as follows.

$$\frac{1}{d^2} = \frac{h^2 + k^2 + l^2}{a^2}$$

By h, k, l are plane of crystal

a is Lattice parameters with a hexagonal structure

d is Distance between planes

λ is The wavelength is equal to 1.5418 Å

n is The integer number is equal to 1

Where d is calculated from

$$2dsin\,\Theta = n\lambda\,;d = \frac{\lambda}{2dsin\,\Theta}$$